Master Thesis, c960861

Dispersion in Electrokinetically and Pressure Driven Microflows

Flemming Rytter Hansen

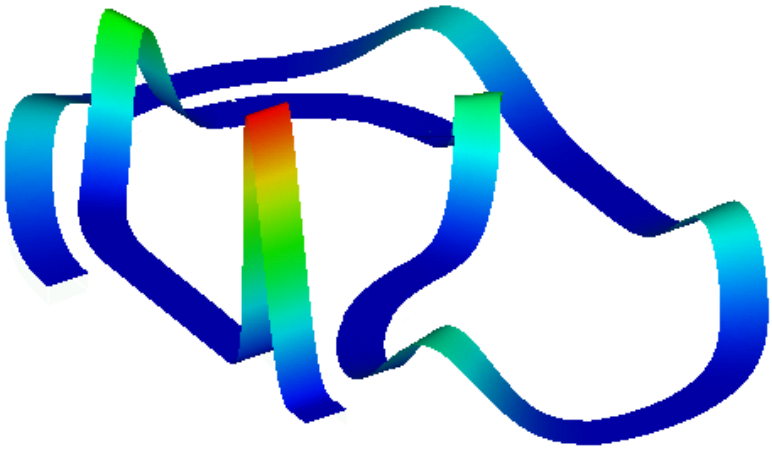

Supervisors: Henrik Bruus and Goran Goranović

Mikroelektronik Centret - MIC

28th June 2002

Abstract

Dispersion of samples driven in microflows may be either wanted or unwanted. For example, the mixing of one chemical into the other may be wanted for faster chemical reactions. Dispersion may be undesired when, for example, measuring the concentration of a florescent species, since too much dispersion yields low concentrations, which makes it difficult to obtain accurate detection measurements.

We have considered three different effects causing dispersion of samples in microflows: diffusion, velocity gradients of the flow profile, and finally geometrical effects, such as the "race track" effect observed when a sample flows through a turn. The dispersion has been investigated theoretically and by means of computational fluid dynamics (CFD). The theoretical findings have been compared with CFD simulations. With respect to flows in cylindrical geometries, the so-called Taylor dispersion has been studied, and a general formula for finding Taylor's effective dispersion coefficient has been derived. Investigations have been made as to whether the dispersion in a turn can be diminished by short circuiting the electric field in the turn. Using CFD we have concluded that the short circuiting worsened the dispersion caused by the turn. To minimize the dispersion induced by turns with flows driven electrokinetically, we have suggested changes of the electroosmotic mobility. CFD simulations demonstrate the correctness of the suggestions. Moreover, a novel method for controlling dispersion is suggested, and the steady state situation is studied.

Resumé

Dispersion af væskeprøver drevet i strømninger i mikrokanaler kan være både ønsket og uønsket. For eksempel kan blandning af et kemikalie i et andet være ønsket for at opnå hurtigere kemiske reaktioner. Dispersion kan være uønsket i tilfælde hvor koncentrationen af et flourecerende stof skal måles, idet dispersion giver lave koncentrationer, hvilket medfører problemer med at opnå præcise målinger.

Tre forskellige effekter som giver anledning til dispersion i mikrokanaler er blevet undersøgt: Diffusion, gradienter i hastigheds profiler og geometriske effekter, som for eksempel "race-track"-effekten, der opstår når en væskeprøve sendes igennem et sving. Dispersionen er blevet undersøgt teoretisk og ved hjælp af kommercielt software, CFD. Teorien er blevet sammenlignet med CFD simuleringerne. Med hensyn til strømninger i cylinderformede geometrier er den såkaldte Taylor dispersion studeret, og en generel formel til bestemmelse af Taylor's effektive dispersionskoefficient er udledt. Desuden er det blevet undersøgt om dispersionen i et sving kunne mindskes ved at kortslutte det elektriske felt. Ved hjælp af CFD er det blevet fastslået at kortslutningen øger dispersionen, så idéen må forkastes. Til mindskning af dispersionen forårsaget af sving i mikrokanaler er ændringer til den elektroosmotiske mobilitet foreslået. CFD simuleringer cementerer rigtigheden af de foreslåede ændringer. Ydermere er en metode til at kontrollere dispersionen af en væskeprøve ved hjælp af elektriske felter blevet foreslået, og "steady-state" tilstanden er blevet undersøgt.

Preface

This master thesis is made at Mikroelektronik Centret, MIC in the period from the 10th of September 2001 to the 1st of May 2002, 7 months and 3 weeks. It is the final project of my education at the Technical University of Denmark, DTU, and a degree of cand.polyt. is obtained when the project is defended the 24th of May 2002.

The project is made in a very new group at MIC, the Microfluidic Theory and Simulation Group. This thesis is thus among the very first master theses to be finished in the group. We, as members of this group, among the first in Denmark to study the field of theory and simulation of microfluidic systems.

I would like to thank my supervisor, Henrik Bruus, for patiently trying to extend my understanding of theoretical physics and for excellent supervision. I would also like to thank Goran Goranović, firstly for convincing me to make my master thesis at MIC, secondly for being an excellent supervisor throughout the entire period.

During this project I have been working together with: Lennart Bitsch, Anders Brask, and Mads Jakob Jensen. We all began our master thesises at the same time, and are all going to hand them in the 1st of May 2002. We have made each our own projects, but all within the field of microfluidics. I would like to thank these fine men for many valuable discussions and for keeping a good spirit in our daily work.

Finally I would like to thank the Coventor Support group in Amsterdam for their advice in the use of the Coventor software and their dedicated effort to answer questions about it.

A comment should be made regarding the typesetting of this document. Throughout this thesis I have tried to use the Physical Review standard of writing scientific work. I have pursued to do this consistently, except for the following two cases: Instead of writing 'Eq. (x)' when referring to equations, I have written 'equation (x)'. Instead of writing 'Fig. x' when referring to figures, I have written 'Figure x'.

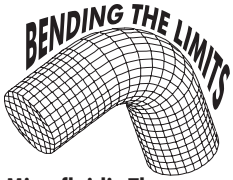

Microfluidic Theory and Simulation Group

Contents

1 Introduction **1**

2 Basic Physics **3**
2.1 Fluid Flow . . . 3
2.2 Diffusion . . . 4
2.2.1 Temperature Dependence of Viscosity and the Diffusion Coefficient . . . 5
2.3 Electrical Phenomena . . . 6
2.4 Transport of Charged Species . . . 7

3 Electrokinetically Driven Flows **9**
3.1 Electrophoresis . . . 9
3.2 Electroosmosis . . . 10
3.2.1 Electroosmosis in a Circular Capillary . . . 10
3.2.2 The Debye Length . . . 11

4 Pressure Driven Flows **15**
4.1 Steady Flow in a Cylindrical Tube . . . 15
4.2 Velocity Profile in a Turn . . . 16

5 Dispersion **23**
5.1 Taylor Dispersion . . . 23
5.1.1 Taylor Dispersion . . . 23
5.2 Geometry Effects . . . 33
5.2.1 The Race Track Effect . . . 33
5.2.2 Electrokinetically Driven Fluids. . . . 34

6 Dispersion Control by Electric Fields **39**
6.1 Practical Considerations . . . 39
6.2 Dispersion Control in a 1D channel . . . 40
6.3 Dispersion Control in a 3D Tube . . . 42
6.4 Numerical Solution . . . 48

7 CFD Applied to Dispersion Problems **53**
7.1 Measuring the Dispersion . . . 54
7.2 Parametric Studies . . . 55
7.2.1 Pressure Driven Flow in a Turn . . . 55
7.2.2 Diffusion in a Straight Channel . . . 57
7.3 Dispersion in a Turn, Part 1 . . . 59

7.3.1 Simulations 64
7.3.2 3D Simulations 67
7.4 Dispersion in a Turn, Part 2 68
7.4.1 Simulations 68
7.5 Spirals 75
7.5.1 Simulations 76

8 Conclusion **83**

Bibliography **85**

A MatLab Code **87**
A.1 ODE-solver 87
A.2 System ODE Setup 87

B Fourier Coefficients **88**

C MatLab Code for Ions in a Tube **89**

D Coventor Support Q&A **92**

E Curve Fitting **99**

F Grid Dependency Analysis **100**

G MatLab Code for Velocity Profile in a Turn **103**

List of Figures

2.1 Viscosity, μ, and the self diffusion coefficient, D, as function of temperature of water. The points are table values and the curves are fittings to these table values. The viscosity and self diffusion coefficients are fitted as, $\mu = A_1 \exp(B_1/T)$ and $D = A_2 T \exp(B_2/T)$, where (A_1, A_2, B_1, B_2) are constants adjusted to obtain the best fitting. 6

3.1 The dimensionless potential, ϕ', for varying dimensionless Debye lengths, $\lambda' = \lambda_D/a$. The dimensionless zeta potential, ζ', at the wall has been chosen to be 2.79. We notice that λ' can be regarded as a screening length. 13

4.1 Geometry of the domain where the solution is found with system of coordinates. Be aware that the angular coordinate θ is defined from the y-axis. . . 17
4.2 Velocity profile. 20
4.3 Contour of velocity profile. Notice the asymmetry. The peak of the profile is closer to the inner wall than the outer wall. 21

5.1 The figure shows the dispersion of a sample in a tube with and without diffusion present at the initial stage, $t = 0$, and at two later stages $t_1 > 0$ and $t_2 > t_1$. The gray scale represent the density of species. 24
5.2 Two Gaussian curves with different characteristic length scales L are given. Notice that L_1, which is shorter than L_2, has larger concentration gradients. σ_1 and σ_2 are the standard deviations for the two Gaussians. 26
5.3 Visualization of regions where different approximations can be made regarding the problem of sample broadening in a capillary tube. (From Probstein (1994), after A.A. Sonin). 29
5.4 Concentration profiles for different times. $\frac{n_0}{\pi a^2} = 0.5$, $U = 2$, $D_{\text{eff}} = 0.05$. . . 30
5.5 Figure (a) shows the velocity profile for $n = 2$, $n = 6$ and $n = 12$. Figure (b) shows α_T as a function of n. 32
5.6 Channel with a U-turn. 33
5.7 Relative error between E_c and E_{av}. 35
5.8 $\Delta\ell$ as function of t_D/t_t. 38

6.1 Sketch of the separation idea. A number of electrodes are imagined placed along a channel. Varying the voltages in time it is possible to transport the ions along the channel. 40
6.2 Left figure: Distribution of positive and negative ions given as dimensionless concentration. Right figure: Dimensionless applied, intrinsic and total potential. The applied potential is for this example given as: $\phi'_a = 6x'^2$, and $L = 500\,\mu$m. 42

6.3 Splitting of the boundary value problem into two cases, which are easier solved. Finding ϕ_1 and ϕ_2 the solution is given as: $\phi'_{tot} = \phi_1 + \phi_2$. 45
6.4 Splitting of the boundary value problem into three cases, which are easier solved. Finding ϕ_{1a}, ϕ_{1b} and ϕ_{1c} we obtain: $\phi_1 = \phi_{1a} + \phi_{1b} + \phi_{1c}$. 45
6.5 Flow chart sketching the pseudo code. 49
6.6 Flow chart sketching the pseudo code. 50
6.7 Distribution of positive and negative ions. Panels (a) and (b) show how the positive ions have been driven into the middle of the tube. Panels (c) and (d) show how the negative ions have been driven out to the ends of the tube. 51
6.8 Distribution of positive and negative ions. Panels (a) and (b) show how the positive ions have been driven into the middle of the tube. Panels (c) and (d) show how the negative ions have been driven out to the ends of the tube. 52

7.1 Sketch of the grid and the geometry used in the numerical simulation of flow taking a 180° turn. 54
7.2 Sketch of the grid and the geometry used in the numerical simulation of flow taking a 180° turn. 55
7.3 Contour plot of the velocity profile in the cross section of a 180° turn. The pressure drop from turn inlet to turn outlet is 1×10^{-6} MPa. The contour plot is obtained with the MatLab code in Appendix G. 56
7.4 Sketch of two straight channels connected by a 180° turn. 59
7.5 Sketch of the two straight channels connected by a 180° turn. The 2D flow profiles are sketched to illustrate that short circuiting the turn affects the profiles in the electroosmotic flow in the straight channels. 61
7.6 The velocity profiles for the system shown in Figure 7.5. The profiles u_1 and u_3 are equal because the boundary velocities u_1^* and u_3^* are equal. 62
7.7 Results extracted from Mathematica. *u1new* corresponds to the u_1 and u_3 velocity profiles. *u2new* corresponds to the u_2 velocity profile. *deltaP* corresponds to equation (7.12). 63
7.8 The velocity profile for a slice plane placed at the z-value equal to half the depth of the channel. A pressure drop from inlet to outlet has removed the velocity gradients in the straight channels. 63
7.9 Figures (a) and (d) are examples of the short circuited turn made with an applied pressure to remove velocity gradients in the straights. Figures (b) and (e) are made with all walls, also the turn, having the same electroosmotic mobility. Figures (c) and (f) are made with optimised electroosmotic mobilities in the turn according to equations (5.79) and (5.80). 66
7.10 Simulation results for a 3D simulation of a sample travelling through a turn connecting two straight channels. 67
7.11 Visualization of the procedure to find the peak concentration in Coventor's simulation Visualizer. The lower bound is raised until only the peak is visible. 69
7.12 Simulation with a parabolic velocity profile in the turn. A pressure drop has been added to remove velocity gradients in the straight channels. The diffusion coefficient for the simulation is: $D = 2260\ \mu\text{m}^2\ \text{s}^{-1}$. 70
7.13 The sample at the times: $t = 0$, $t = 2$, $t = 4$, $t = 6$. The lower bound was set to 0.15 and the upper bound was 1, meaning that only concentrations in that range are visualized. 71
7.14 Simulation with all walls having the same electroosmotic mobility. The diffusion coefficient for the simulation is: $D = 565\ \mu\text{m}^2\ \text{s}^{-1}$. 72

7.15 Simulation with all walls having the same electroosmotic mobility. The diffusion coefficient for the simulation is: $D = 2260\ \mu\mathrm{m}^2\ \mathrm{s}^{-1}$. 72
7.16 Simulation with the walls of the straight channel having the same electroosmotic mobility and modified electroosmotic mobilities on the walls in the turn. The diffusion coefficient for the simulation is: $D = 2260\ \mu\mathrm{m}^2\ \mathrm{s}^{-1}$. . . . 73
7.17 Simulation with the walls of the straight channel having the same electroosmotic mobility and modified electroosmotic mobilities of the walls in the turn The diffusion coefficient for the simulation is: $D = 226\ \mu\mathrm{m}^2\ \mathrm{s}^{-1}$. 74
7.18 Sketch of a spiral. 75
7.19 Sketch of a spiral. 76
7.20 The channel geometry is composed of five parts. The first and the fourth parts are straight channels. The second and the third parts are turns bending an angle of, $180^o + 79.19^o$, and the radius of curvature at the centerline is $r = 200\mu$m. The fifth part is a turn bending 180^o, and the radius of curvature at the centerline is $r + d = 275\ \mu$m. 77
7.21 Simulation results from a sample travelling through a spiral. 78
7.22 Simulation results from a sample travelling through a spiral. 79
7.23 2D Simulation of a sample travelling through a spiral. Notice that the distortion of the sample caused by the first turn is corrected to some degree in the following turn. 79
7.24 Simulation results from a sample travelling through a spiral. 80
7.25 The plug as function of time. 80

E.1 Linear regression to table values. 99

F.1 Excell. 101
F.2 Excell. 102

List of Symbols

Symbol	Description	Unit
B	Magnetic field	T=V s m^{-2}
c	Concentration	mol m^{-3}
D_{heat}	Heat diffusion coefficient	
D_{mass}	Mass diffusion coefficient	m^2 s^{-1}
e	Elementary charge	C=A s
E	Electric field	V m^{-1}
F	Faradays constant	9.6485×10^4
g	Gravity constant	9.80665 m s^{-2}
N_A	Avogadros number	6.02214×10^{23} mol^{-1}
Pe	Pechlet number	
r_i	Inner radius	m
r_o	Outer radius	m
r_c	Center radius	m
R	Gas constant	8.31451 J K^{-1} mol^{-1}
Re	Reynolds number	
Res	Resolution	
T	Temperature	K
u	Velocity	m s^{-1}
u_∞	Helmholtz velocity	m s^{-1}
U	Potential drop	V
w	Channel width	m
z	Number of charges	
α	Mobility	m^2 V^{-1} s^{-1}
δ	Stern layer thickness	m
ϵ	Dielectric constant	C^2 J^{-1} m^{-1}
ϵ_r	Relative permittivity	
ϵ_0	Vacuum permittivity	C^2 J^{-1} m^{-1}
ζ	Zeta-potential	V
λ_D	Debye length	m
μ	Dynamic viscosity	kg s^{-1} m^{-1}
ν	Kinematic viscosity	m^2 s^{-1}
ρ	Mass density	kg m^{-3}
ρ_e	Charge density	C m^{-3}
σ	Standard deviation	
σ^2	Variance	

Chapter 1

Introduction

Microtechnology has within the last decade given birth to systems for analysing fluids on micrometer scale, the so-called Micro Total Analysis Systems, μ-TAS, which has been developing with considerable success. Applications of μ-TAS are e.g. found in pollution detection and medicine research. In this context it is natural also to mention the Lab-on-a-Chip concept. The idea behind Lab-on-a-Chip is to make a system on the micrometer scale[1], which can perform all the necessary steps in a specific analysis process. No user interaction is needed except at the initial input stage. Advantages of making such a system on a micrometer scale are that it becomes very portable, many systems could be made easy to mass produce, and the quantities needed to make the analysis are measured in nanograms rather than several grams. Especially the pharmaceutical industry has shown interest in the Lab-on-a-Chip concept, because of the request for fast analysis. The ability to speed up the analysis process is important, because of issues such as patents and intellectual properties, IP, which only run for a limited period of time.

In this thesis we will be concerned with the dispersion or spreading of a chemical substance, a sample. This dispersion takes place in microchannels, which form the basis of μ-TAS or Lab-on-a-Chip technology. We will not concern ourselves with the actual chemical reactions. In order to account for the dispersion of samples a thorough understanding is needed of the constitutive physical relations governing fluid dynamics, diffusion, and electromagnetism. Applying mathematics to fluid dynamics naturally leads to computational fluid dynamics, CFD, which is one of the most important tools for solving μ-TAS problems without making real experiments. We will not claim that CFD can replace experimental work. CFD is rather a supplement to the work of experimentalists. Procedures such as sensitivity analysis on a whole range of parameters can be made easier applying CFD. CFD can also present solutions visually giving us the possibility of studying parameters almost continuously through time. A feature which could prove to be very valuable in the search of novel designs.

Thus, during this project we will study the dispersion of samples in microflows both from a theoretical point of view and through CFD simulations. The CFD simulations will be made using the commercial software Coventor.

[1] Compare these microfluidic systems with a human hair, which is roughly 200μm wide.

Chapter Review

After this introductory chapter we will in Chapter 2 lay out the basic physics needed throughout the thesis. The basic physics include equations for conservation of mass, momentum and energy, equations for diffusion and convection of a sample, and a transport equation for a sample influenced by diffusional, convectional, and electrical forces.

In Chapter 3 we will consider the possibilities of driving liquids electrokinetically. Here the understanding of the basic principles behind electrophoresis and electroosmosis are key issues.

A more common way of driving fluids is by means of pressure gradients. In Chapter 4 velocity profiles obtained in pressure driven flows are found using an analytical approach.

Now that the fundamentals of driving flows have been accounted for we will in Chapter 5 consider the dispersion of a sample placed in such a flow. Different effects contributing to the dispersion of a sample are discussed, such as Taylor dispersion and the *race track* effect. Possible ways of counteracting dispersion are proposed. The theory presented closely follow the work by Probstein (1994).

A novel technique for dispersion control is presented in Chapter 6. Shortly, the possibility of applying electric fields to obtain a separation of oppositely charged ions is studied. When a separation is obtained a spacial translation of the electric field will drag along the separated ions and keep them separated.

In Chapter 7 the commercially available CFD software, Coventor, will be applied to investigate the dispersion of an electrokinetically driven sample travelling through a turn. Different approaches will be taken toward minimizing the dispersion. The advantages of applying CFD simulations for such studies will become apparent.

Finally, in Chapter 8 conclusions and outlook are presented. We will sum up the important findings and experiences gathered throughout this project, and give an overview of the further work, which lies as a natural continuation of this master thesis.

Chapter 2

Basic Physics

In the following the basic physical relations needed throughout this thesis will be presented. Theory in the following chapters is thus solely based on the fundamental physical principles described below.

Definition of a fluid: "A fluid can be defined as a material that deforms continuously and permanently under the application of a shearing stress, no matter how small." This definition is quite common and can be found in many textbooks. Applying a shear stress, if it is not too large, will deform a solid to some degree, but the solid deforms only while the shear stress is applied and regains its original shape when it is relieved.

2.1 Fluid Flow

The governing equations for fluid flow concerns mass, momentum, and energy. Mass is dealt with through the continuity equation. Momentum is dealt with through Newton's second law, and energy is dealt with through the thermal diffusion equation. Newton's second law is in the case of fluid flow most conveniently written in the form of the Navier-Stokes equation

$$\frac{\partial \mathbf{u}}{\partial t} + (\mathbf{u} \cdot \boldsymbol{\nabla})\mathbf{u} = -\frac{1}{\rho}\boldsymbol{\nabla} p + \nu \boldsymbol{\nabla}^2 \mathbf{u} + \mathbf{f}, \tag{2.1}$$

where $\mathbf{u}$ is the fluid velocity, t is time, ρ is mass density, ν is the kinematic viscosity and $\mathbf{f}$ is body forces acting on the fluid such as gravity or electrical forces. The first term on the right-hand side governs the change in momentum caused by the pressure gradient, whereas the second term governs the diffusion of momentum, and the kinematic viscosity can as such be considered as a diffusion constant for momentum. We will later on consider mass and thermal diffusion. Often we will refer to the dynamic viscosity (μ) instead of the kinematic viscosity. This is given as

$$\mu = \nu\rho. \tag{2.2}$$

The Navier-Stokes equation governs the flow of momentum. Correspondingly the conservation of mass is governed by the continuity equation for fluid flow,

which generally is given as

$$\frac{\partial \rho}{\partial t} + \boldsymbol{\nabla} \cdot (\rho \mathbf{u}) = 0 \tag{2.3}$$

In many cases fluids can be considered incompressible, ρ constant, and indeed we will assume this throughout this thesis. This assumption simplifies the continuity equation as follows

$$\nabla \cdot \mathbf{u} = 0. \tag{2.4}$$

Besides the governing equations two dimensionless quantities are worth mentioning as they are traditionally important for fluid flows. The Reynolds number and Peclet number respectively defined as

$$Re = \frac{\text{momentum transported by convection}}{\text{momentum transported by viscous diffusion}} = \frac{UL}{\nu}, \tag{2.5}$$

$$Pe = \frac{\text{mass transported by convection}}{\text{mass transported by diffusion}} = \frac{UL}{D}, \tag{2.6}$$

where U is a characteristic velocity (e.g. the mean velocity), L is the characteristic length (e.g. the radius of a tube), ν is the kinematic viscosity and D is the diffusion coefficient. The Peclet number defined above is also known as the diffusion Peclet number. A thermal Peclet number can be defined similarly just replacing mass with heat. We will mainly be concerned with the diffusion Peclet number.

2.2 Diffusion

The governing equation for diffusion of particles is given by Fick's law, which states that the particle current density given by

$$\mathbf{J} = \mathbf{u}c, \tag{2.7}$$

is proportional to the concentration gradient

$$\mathbf{J} = -D\boldsymbol{\nabla} c, \tag{2.8}$$

where D is the diffusion coefficient. D is thus a measure of how easy it is for a particle to diffuse given a specific concentration gradient. The equation for the conservation of species is given by

$$\frac{\partial c}{\partial t} + \boldsymbol{\nabla} \cdot (\mathbf{u}c) = 0. \tag{2.9}$$

Often in a microfluidic system a species is also transported by convection as well as diffusion, i.e.

$$\mathbf{J} = -D\nabla^2 c + \mathbf{u}c. \tag{2.10}$$

Combining equations (2.8) and (2.10) yields the convection diffusion equation

$$\frac{\partial c}{\partial t} + \boldsymbol{\nabla} \cdot (\mathbf{u}c) = D\nabla^2 c, \tag{2.11}$$

Assuming the fluid to be incompressible we arrive at

$$\frac{\partial c}{\partial t} + (\mathbf{u} \cdot \boldsymbol{\nabla})c = D\nabla^2 c. \tag{2.12}$$

A similar equation exists for the transfer of heat (Fourier's law), where a heat diffusion coefficient appears instead of D and c is replaced by temperature, T,

$$\frac{\partial T}{\partial t} + (\mathbf{u} \cdot \nabla)T = \alpha_{\text{temp}} \nabla^2 T, \tag{2.13}$$

where α_{temp} is the thermal diffusivity. We have thus presented the equations for conservation of mass together with the transport equations for momentum, species and thermal energy.

2.2.1 Temperature Dependence of Viscosity and the Diffusion Coefficient

We will consider a model for the temperature dependence of the viscosity, or diffusion coefficient of momentum. Next we will use a coupling between the dynamic viscosity and the diffusion coefficient, to obtain a relation between D and temperature.

The velocity gradient in the flow direction, $\frac{\partial u}{\partial y}$ is proportional to the product of the shear stress τ_{yx} and the exponential factor $\exp(-\Delta G/RT)$ (Probstein, 1994),

$$\frac{\partial u}{\partial y} \propto \tau_{yx} \exp\left(\frac{-\Delta G}{RT}\right), \tag{2.14}$$

ΔG is the minimum energy required for a molecule to escape from its neighboring molecules in the liquid, R is the gas constant, and T is the temperature. The connection between shear stress and the velocity gradient for Newtonian fluids,

$$\tau_{yx} = \mu \frac{\partial u}{\partial y}, \tag{2.15}$$

then yields

$$\mu \propto \exp\left(\frac{\Delta G}{RT}\right), \tag{2.16}$$

relating temperature and dynamic viscosity. The connection between the viscosity and the diffusion coefficient is found from Stokes' law and the Stoke-Einstein equation, respectively

$$f = 6\pi a \mu, \tag{2.17}$$

$$f = \frac{RT}{N_A D}, \tag{2.18}$$

where f is the frictional force. Eliminating f we obtain

$$D = \frac{RT}{6\pi N_A a \mu}. \tag{2.19}$$

Inserting the temperature dependence on the viscosity yield

$$D \propto \frac{RT}{6\pi N_A a} \exp\left(\frac{\Delta G}{RT}\right). \tag{2.20}$$

Hence we have found, $\mu = A_1 \exp(B_1/T)$ and $D = A_2 T \exp(B_2/T)$, where (A_1, A_2, B_1, B_2) are constants. Below an example is given for water. Table values for the self diffusion coefficient and the viscosity at different temperatures have been found on the internet[1]. Figure 2.1 shows the Table values as, $*$. The curves are fittings to the Table values, where (A_1, A_2, B_1, B_2) are adjusted to obtain the best fitting. Details on the fitting are given in Appendix E. We notice that it is indeed possible to make a reasonably good fit from the relations, $\mu = A_1 \exp(B_1/T)$ and $D = A_2 T \exp(B_2/T)$, indicating that the above theory can be trusted.

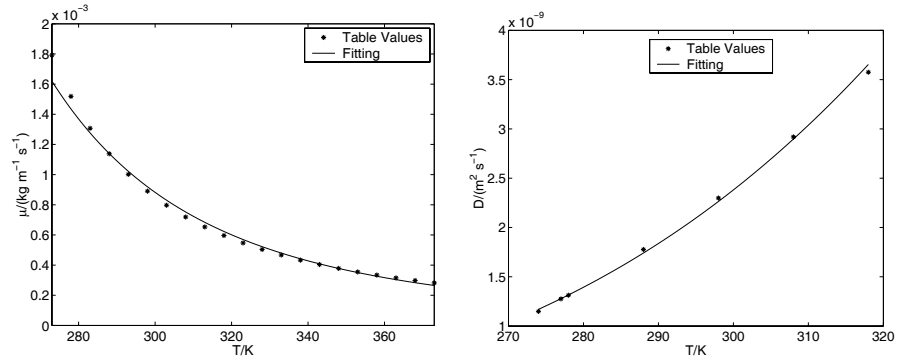

(a) (b)

Figure 2.1: Viscosity, μ, and the self diffusion coefficient, D, as function of temperature of water. The points are table values and the curves are fittings to these table values. The viscosity and self diffusion coefficients are fitted as, $\mu = A_1 \exp(B_1/T)$ and $D = A_2 T \exp(B_2/T)$, where (A_1, A_2, B_1, B_2) are constants adjusted to obtain the best fitting.

2.3 Electrical Phenomena

The macroscopic Maxwell equations form the basis of the theory of electromagnetism. Governing the electrical potential we have

$$\nabla \cdot \mathbf{D} = \rho_e, \tag{2.21}$$

where $\mathbf{D}$ is the electric displacement and ρ_e is the free charge density. The connection between the electric displacement and the electric field $\mathbf{E}$ is for a linear material per definition $\mathbf{D} = \boldsymbol{\epsilon}\mathbf{E}$, where $\boldsymbol{\epsilon}$ in general is a tensor. We will assume the dielectric constant to be isotropic. The electric potential ϕ is defined from the equation

$$\mathbf{E} = -\nabla\phi \tag{2.22}$$

[1] http://www.nmr-relaxation.com/handbook/general/water.htm

Combining equations (2.21) and (2.22) gives the Poisson equation relating the electrical potential and the charge density.

$$\nabla^2\phi = -\frac{1}{\epsilon}\rho_e. \tag{2.23}$$

We mentioned earlier that a body force could be present in the Navier-Stokes equation, e.g. electrical forces. In the case of a fluid particle, with charge q, the body force is given by the Lorentz force

$$\mathbf{F}_e = q(\mathbf{E} + \mathbf{u} \times \mathbf{B}), \tag{2.24}$$

where $\mathbf{B}$ is the magnetic field. In the cases considered in this thesis magnetic fields are disregarded ($\mathbf{B} = 0$). In order to make the Lorentz force applicable to the Navier-Stokes equation in the form it is presented in equation (2.1) we divide by a unit volume to obtain

$$\mathbf{f}_e = \rho_e\mathbf{E} = -\rho_e\nabla\phi. \tag{2.25}$$

2.4 Transport of Charged Species

Consider a dilute solution of charged species. To obtain the total flux of species the contribution from electromigration must be added to equation (2.10). This yields the Nernst-Planck equation (Probstein, 1994) for the total flux ($\mathbf{J}_i$) of the $i'th$ particle

$$\mathbf{J}_i = -\alpha_i^* z_i F c_i \bar{\boldsymbol{\nabla}}\phi - D_i\bar{\boldsymbol{\nabla}}c_i + c_i\mathbf{u} \tag{2.26}$$

where α_i^* is a mobility, z_i is the charge, c is concentration, ϕ is electric potential, D_i is the mass diffusion coefficient and $\mathbf{u}$ is the velocity. The mobility is related to the diffusion coefficient by the Nernst-Einstein equation: $D_i = RT\alpha_i^*$. Notice that the first term on the right-hand side is the flux caused by the Lorentz force. The mobility is thus regarded as a measure of how mobile the charges are in the electric field.

Chapter 3

Electrokinetically Driven Flows

Before we can begin to consider the dispersion of some species in a microflow, we need to understand what drives the actual flows. In this chapter we will study how liquids can be driven electrokinetically. When referring to flows driven electrokinetically we think of electrophoresis and electroosmosis, which can be defined as

- **Electrophoresis**: Consider a charged material suspended or dissolved in a liquid. Applying an electric field to the system results in a movement of the charged material. This is electrophoresis. In case the charged material is able to move without any applied electric field, e.g. by sedimentation, an electric field is created. This electrokinetic phenomenon is known as the *sedimentation potential* and can be regarded as the opposite of electrophoresis.
- **Electroosmosis**: Consider a liquid in contact with a charged surface. Moving the liquid with an applied electric field we obtain electroosmosis. In case liquid in contact with a charged surface is moved by another source than an electric field, e.g. by pressure, an electric field is created. This electrokinetic phenomenon is known as the streaming potential and can be regarded as the opposite of electroosmosis.

3.1 Electrophoresis

For practical purposes electrophoresis has been used as a powerful tool for separation of ionized chemical mixtures. This is possible because different charged molecules are mobile to a different degree. E.g. large molecules will experience more resistance when dragged through a fluid than a smaller molecule with the same charge. We will not go into detail on these matters here, but just stress the important empirical relation between the electric field and the velocity of the charged particle.

$$\mathbf{u} = \alpha_{ep}\mathbf{E} = -\alpha_{ep}\boldsymbol{\nabla}\phi, \tag{3.1}$$

where α_{ep} is the electrophoretic mobility. This relation will form the basis on everything concerning electrophoresis throughout this thesis. We will hence neglect any sedimentation potentials, which might be present in any of the discussed cases.

3.2 Electroosmosis

The handling of electroosmosis in Coventor is very simple, since only an electroosmotic mobility needs to be specified at the wall. This gives a velocity boundary condition at the wall, which is the local electric field times the electroosmotic mobility. In the following we will consider an example with electroosmosis in a circular capillary, and with this example justify the manner velocity boundary conditions are specified in Coventor.

3.2.1 Electroosmosis in a Circular Capillary

We consider an infinitely long circular capillary, i.e. we neglect the special cases at the ends of the capillary. The inner surface of the capillary is assumed to be negatively charged and placed in an electric field parallel to the symmetry axis of the capillary. The force on an ion of charge q is given by the Lorentz equation. The force per unit volume is

$$\mathbf{f}_e = \rho_e \mathbf{E} \tag{3.2}$$

The momentum equations for the flow is given by the Navier-Stokes equation. Assuming the flow to be inertia free, $\rho\frac{D\mathbf{u}}{Dt} = 0$, without pressure gradients, $\nabla p = 0$, and neglecting the gravitational force, $\rho\mathbf{g} = 0$, we obtain a balance between the viscous force and the electric force

$$\mu\nabla^2\mathbf{u} + \rho_e\mathbf{E} = 0. \tag{3.3}$$

From the definition of the Reynolds number: $Re = \frac{\text{inertial force}}{\text{viscous force}} = \frac{\rho U^2/L}{\mu U/L^2}$, we see that neglecting the inertia is equivalent to assuming $Re = 0$. In the direction of the symmetry axis equation (3.3) becomes

$$\mu\left[\frac{1}{r}\frac{\partial u}{\partial r} + \frac{\partial^2 u}{\partial r^2} + \frac{1}{r^2}\frac{\partial^2 u}{\partial \theta^2} + \frac{\partial^2 u}{\partial z^2}\right] + \rho_e\mathbf{E} = 0. \tag{3.4}$$

We assume rotational symmetry, $\partial/\partial\theta = 0$, uniform conditions in the axis of symmetry, $\partial/\partial z = 0$. Furthermore assuming $\lambda_D \ll a$ (a being the radius of the capillary, and λ_D is the Debye length, which is defined later) we can neglect the curvature term, giving an equation corresponding to a plane case (notice r has been replaced by y to indicate the plane case situation)

$$\mu\frac{\partial^2 u}{\partial y^2} = -\rho_E E_x = \epsilon\frac{\partial^2\phi}{\partial y^2}E_x \tag{3.5}$$

where we have used Poisson's equation. Integrating (3.5) we obtain

$$\mu\frac{\partial u}{\partial y} = \epsilon\frac{\partial\phi}{\partial y}E_x + \text{constant} \tag{3.6}$$

At the edge of the diffuse layer ($y \to \infty$) we set the velocity u and the electric potential ϕ to be constant, hence

$$\frac{\partial u}{\partial y} = 0 \quad \text{for} \quad y \to \infty, \tag{3.7}$$

$$\frac{\partial \phi}{\partial y} = 0 \quad \text{for} \quad y \to \infty, \tag{3.8}$$

which means that the constant in equation (3.6) must be zero. Integrating (3.6) and setting $\phi = \zeta$ for $u = 0$ we obtain the Helmholtz-Smoluchowski equation

$$U_\infty = -\frac{\epsilon \zeta E_x}{\mu}. \tag{3.9}$$

From the above equation the earlier claimed linear relation between the electric field and the velocity at the wall is found. The electroosmotic mobility is thus

$$\alpha_{eo} = -\frac{\epsilon \zeta}{\mu}. \tag{3.10}$$

Example: Electric field: $E_x = 2.5 \times 10^3$ V/m. Zeta potential: $\zeta = 0.1$ V. With the dielectric constant and dynamic viscosity for water, the velocity becomes: $U_\infty = 200\ \mu$m/s.

3.2.2 The Debye Length

In the previous subsection we mentioned a length scale called the Debye length. This length scale will be defined in the following example. We will consider the interior of a tube with a fixed potential at the wall, the zeta potential. When assuming no convection and no total flux, the Nernst-Planck equation gives a balance between the diffusion and the electromigration, which can be integrated to give the Boltzmann distribution for the concentration of positive and negative ions respectively

$$-\alpha_\pm z_\pm F c_\pm \frac{d\phi}{dr} = D_\pm \frac{dc_\pm}{dr} \tag{3.11}$$

where $D_\pm = RT\alpha_\pm$. Rearranging and integrating gives

$$-\int d\phi = \frac{RT}{z_\pm F} \int \frac{dc}{c_\pm} \tag{3.12}$$

yielding

$$c_\pm(x, r) = c_0(x) \exp\left(\mp \frac{zF\phi(r)}{RT}\right). \tag{3.13}$$

Notice that $z_\pm = \pm z$. Poisson's equation gives

$$\frac{1}{r}\frac{\partial}{\partial r}\left(r\frac{\partial \phi}{\partial r}\right) = -\frac{Fz}{\epsilon}(c_+ - c_-) \tag{3.14}$$

Inserting (3.13) into (3.14) gives a non-linear second order ODE

$$\frac{\lambda'^2}{r'}\frac{\partial}{\partial r'}\left(r'\frac{\partial \phi'}{\partial r'}\right) = \sinh\phi' \tag{3.15}$$

The differential equation has been made non-dimensional in the following manner

$$r' = r/a \qquad \lambda' = \lambda_D/a \qquad \phi' = zF\phi/RT \tag{3.16}$$

Above we have introduced the Debye length, λ_D ,which from the non-dimensionalizing is found to be

$$\lambda_D = \left(\frac{\epsilon RT}{2F^2z^2c}\right)^{1/2}. \tag{3.17}$$

Example: Temperature: $T = 25^o$C. Dielectric constant for water: $\epsilon = 78.3\epsilon_0$. Concentration: $10^2\frac{\text{mol}}{\text{m}^3}$ (0.1M). These values gives a Debye length of: $\lambda_D = 2$nm.

Equation (3.15) has been solved numerically using symmetry boundary conditions at $r' = 0$ and Dirichlet boundary conditions at $r' = 1$ at the surface

$$\frac{\partial \phi'}{\partial r'} = 0 \quad \text{at} \quad r' = 0, \tag{3.18}$$

$$\phi' = \zeta' \quad \text{at} \quad r' = 1. \tag{3.19}$$

Using the MatLab Code given in Appendix A the curves given in Figure 3.1 have been obtained. The curves give a clear picture of the meaning of the Debye length. Ions which exist a certain number of non dimensional Debye lengths from the wall are screened from the zeta potential. The Debye length can hence be regarded as a measure of the screening length. When λ' becomes larger than 1 we notice that the screening is very poor, because all of the interior of the tube is closer than 1 Debye length from the wall.

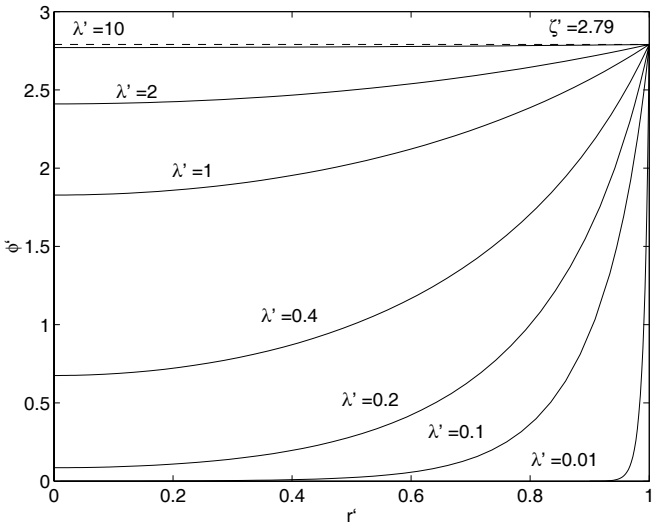

Figure 3.1: The dimensionless potential, ϕ', for varying dimensionless Debye lengths, $\lambda' = \lambda_D/a$. The dimensionless zeta potential, ζ', at the wall has been chosen to be 2.79. We notice that λ' can be regarded as a screening length.

Chapter 4

Pressure Driven Flows

In this chapter solutions of different types of flow problems are presented, i.e. velocity profiles given by the Navier-Stokes equation in either two or three dimensions with some given boundary conditions. The velocity profile gradients are important in respect to the dispersion. This becomes evident in the theory on Taylor dispersion presented in the next chapter. Moreover, the analytically calculated profiles can be used to verify the simulation software, and to obtain an estimate of the grid dependency.

4.1 Steady Flow in a Cylindrical Tube

At first we consider a two dimensional steady flow in a straight channel. The velocity distribution of such a problem is found to be the shape of a parabola

$$u(y) = u_{\max}\left(1 - \frac{y^2}{h^2}\right). \tag{4.1}$$

Moving along to consider the 3D-case of a cylindrical tube one might expect the velocity field to be the shape of a paraboloid. In the following we will show that this is actually true. This flow is also known as Poiseuille flow. The Navier-Stokes equation in 3D-cylindrical coordinates and the continuity equation for incompressible fluids will be assumed to fully describe the problem

$$\frac{\partial \mathbf{u}}{\partial t} + (\mathbf{u}\cdot\boldsymbol{\nabla})\mathbf{u} = -\frac{1}{\rho}\boldsymbol{\nabla}p + \frac{\mu}{\rho}\nabla^2\mathbf{u}, \tag{4.2}$$

$$\boldsymbol{\nabla}\cdot\mathbf{u} = 0. \tag{4.3}$$

Here ρ is the mass density, μ the viscosity, p the pressure and $\mathbf{u}$ the velocity field. The z-component of equation (4.2) reads

$$\frac{\partial u_z}{\partial t} + u_z\frac{\partial u_z}{\partial z} + u_r\frac{\partial u_z}{\partial r} + u_\varphi\frac{1}{r}\frac{\partial u_z}{\partial \varphi} = -\frac{1}{\rho}\frac{\partial p}{\partial z} + \frac{\partial^2 u_z}{\partial z^2} + \frac{1}{r}\frac{\partial}{\partial r}\left(r\frac{\partial u_z}{\partial r}\right) + \frac{1}{r^2}\frac{\partial^2 u_z}{\partial \varphi^2}, \tag{4.4}$$

where we have used the Laplacian operator in cylindrical coordinates. The flow is driven by a pressure gradient in the z-direction, and as we are looking for the

steady state solution the velocity is

$$\mathbf{u}(r, \varphi, z) = u(r)\mathbf{e}_z. \tag{4.5}$$

Inserting this velocity field in the Navier-Stokes equation, a considerable simplification is obtained. We need only to solve for $u(r)$. Furthermore the continuity equation and the steady state assumption yields $\frac{\partial u_z}{\partial z} = 0$ and $\frac{\partial}{\partial t} = 0$, respectively. All terms on the left-hand side of equation (4.4) thus vanish. On the right-hand side the second term vanish because of the continuity equation and the last term vanish because of rotational symmetry. We finally arrive at

$$\frac{\partial p}{\partial z} = \frac{\mu}{r}\frac{\partial}{\partial r}\left(r\frac{\partial u}{\partial r}\right). \tag{4.6}$$

The above equation yields upon integrating twice

$$u(r) = \frac{1}{2\mu}\frac{\partial p}{\partial z}r^2 + A\ln(r) + B. \tag{4.7}$$

As $\ln(r) \to -\infty$ for $r \to 0$ we must require $A = 0$, and using the no-slip boundary condition $u(a) = 0$ we find

$$u(r) = \frac{1}{2\mu}\frac{\partial p}{\partial z}(r^2 - a^2). \tag{4.8}$$

This can be rewritten in terms of the mean velocity U as follows

$$U = \frac{1}{\pi a^2}\int_0^{2\pi}\left[\int_0^a u(r)rdr\right]d\varphi = -\frac{1}{2\mu}\frac{\partial p}{\partial z}\frac{a^2}{2} \tag{4.9}$$

yielding

$$\frac{1}{2\mu}\frac{\partial p}{\partial z} = -\frac{2U}{a^2}. \tag{4.10}$$

Inserting the last result in equation (4.8) gives

$$u(r) = 2U\left(1 - \frac{r^2}{a^2}\right), \tag{4.11a}$$

$$u(r) = u_{max}\left(1 - \frac{r^2}{a^2}\right), \tag{4.11b}$$

where $u_{max} = u(0)$ is the maximum velocity. The minus sign in equation (4.10) appears because the pressure gradient $\frac{\partial p}{\partial z}$ assumes a negative value when u is positive. Furthermore we notice: $u_{max} = 2U$. The Poiseuille flow profile will play an important role in the discussion of the so-called Taylor dispersion.

4.2 Velocity Profile in a Turn

In this section the velocity profile in a turn with a rectangular cross section will be calculated expanding the solutions on a complete set of basis functions. A thorough description of this method of solving differential equations is made by Asmar (2000). The geometry is sketched in Figure 4.1.

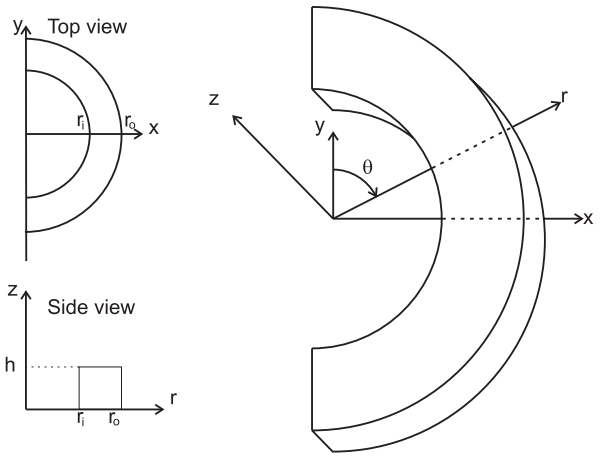

Figure 4.1: Geometry of the domain where the solution is found with system of coordinates. Be aware that the angular coordinate θ is defined from the y-axis.

Assuming the velocity field to be purely azimuthal, $\mathbf{u} = u(r,z)\mathbf{e}_\theta$, the Navier-Stokes equation yields

$$\frac{\partial}{\partial r}\left(\frac{1}{r}\frac{\partial}{\partial r}(ru)\right) + \frac{\partial^2 u}{\partial z^2} = \frac{1}{\mu r}\frac{\partial p}{\partial \theta}, \tag{4.12}$$

rearranging

$$r\frac{\partial^2 u}{\partial r^2} + \frac{\partial u}{\partial r} - \frac{u}{r} + r\frac{\partial^2 u}{\partial z^2} = \frac{1}{\mu}\frac{\partial p}{\partial \theta}. \tag{4.13}$$

The equation is made non-dimensional as follows

$$r' = \frac{r}{r_o}, \qquad z' = \frac{z}{h}, \qquad u' = \frac{u\mu}{r_o \frac{\partial p}{\partial \theta}}. \tag{4.14}$$

For notational convenience the primes (') will be omitted from this point and on. Notice we have assumed $\frac{\partial p}{\partial \theta}$ to be constant. Hence

$$r\frac{\partial^2 u}{\partial r^2} + \frac{\partial u}{\partial r} + \frac{u}{r} + \left(\frac{r_o}{h}\right)^2 r\frac{\partial^2 u}{\partial z^2} = 1 \tag{4.15}$$

In order to obtain an analytical solution to the above inhomogeneous partial differential equation we will expand the solution on a complete set of basis functions. To get a good idea of which basis functions to use for the expansion, we consider firstly the homogeneous equation only. Consider a solution of the form.

$$u(r,z) = R(r)Z(z). \tag{4.16}$$

Inserting equation (4.16) into the homogeneous form of equation (4.15) yields

$$\frac{r^2R''(r) + rR'(r) - R(r)}{r^2R(r)} = -\frac{(r_o/h)^2 Z''(z)}{Z(z)} = k_0, \tag{4.17}$$

where k_0 must be a constant because everything on the left-hand side of the first equality sign depends only on r and everything on the right-hand side depends only on z. Equation (4.17) gives two ODE's

$$r^2R''(r) + rR'(r) - (k_0r^2 + 1)R(r) = 0 \quad (4.18)$$

$$Z''(z) + (h/r_o)^2k_0Z(z) = 0 \quad (4.19)$$

Equation (4.19) must be solved with the boundary conditions $Z(0) = Z(1) = 0$. For $k_0 \leq 0$ the only solution is the trivial $Z(z) = 0$. For $k_0 > 0$, however, we find the eigenfunctions

$$Z_n(z) = \sin(n\pi z), \quad n \in \mathbf{N} \quad (4.20)$$

The general solution of equation (4.18) for $k_0 = 0$ is found to be

$$R(r) = Ar + Br^{-1}, \quad (4.21)$$

where A and B are constants. However, the boundary conditions $R(r_i/r_o) = R(1) = 0$, where $r_i/r_o \neq 1$ gives only the trivial $R(r) = 0$ solution. When $k_0 = \gamma^2 > 0$ we obtain the modified Bessel's differential equation with index 1 with the solution

$$R(r) = CI_1(\gamma r) + DK_1(\gamma r), \quad (4.22)$$

where C and D are constants. Trying to satisfy the boundary conditions we encounter the requirement

$$\frac{I_1(\gamma)}{I_1(\gamma r_i/r_0)} = \frac{K_1(\gamma)}{K_1(\gamma r_i/r_0)} \quad (4.23)$$

No values of γ can satisfy the above equation. With $k_0 = -\gamma^2 < 0$, however, we obtain Bessel's differential equation with index 1, and consequently

$$R(r) = CJ_1(\gamma r) + DY_1(\gamma r), \quad (4.24)$$

where C and D are constants. Applying again the boundary conditions, $R(1) = 0$ and $R(r_r/r_o) = 0$ yields the solutions

$$R_m(r) = Y_1(\gamma_m r) - \frac{Y_1(\gamma_m)}{J_1(\gamma_m)}J_1(\gamma_m r), \quad m \in \mathbf{N}. \quad (4.25)$$

Here γ_m are the positive zero points of the function

$$R_m(r_i/r_o) = 0, \quad (4.26)$$

Based on the two complete sets of eigenfunctions given by equations (4.20) and (4.25) we can write u as the following general superposition

$$u(r,z) = \sum_{n=1}^{\infty}\sum_{m=1}^{\infty} E_{nm}\sin(n\pi z)\left(Y_1(\gamma_m r) - \frac{Y_1(\gamma_m)}{J_1(\gamma_m)}J_1(\gamma_m r)\right), \quad (4.27)$$

where E_{nm} are expansion coefficients to be determined [1] . By construction $u(r,z)$ satisfy the boundary conditions $u = 0$ everywhere on the surface. Inserting

[1] We have here applied: If ϕ_n is a basis for $L^2(I)$ and ψ_m is a basis for $L^2(J)$, then $\phi_n\psi_m$ is a basis for $L^2([I \times J])$.

equation (4.27) in equation gives (4.15)

$$\sum_{n=1}^{\infty}\sum_{m=1}^{\infty} E_{nm}\sin(n\pi z)rR_1(\gamma_m r)\left(\gamma_m^2+\left(\frac{r_o n\pi}{h}\right)^2\right)=-1. \tag{4.28}$$

Multiplying on each side of equation (4.28) with $\sin(n\pi z)R_1(\gamma_m r)$ and integrating gives

$$\begin{aligned} E_{nm}\left(\gamma_m^2+\left(\frac{r_o n\pi}{h}\right)^2\right)\int_0^1\sin^2(n\pi z)dz\int_0^1 R_1^2(\gamma_m r)rdr \\ =-\int_0^1\sin(n\pi z)dz\int_0^1 R_1(\gamma_m r)dr, \end{aligned} \tag{4.29}$$

which upon rearranging gives the expansion coefficients

$$E_{nm}=\frac{-4G_m}{D_m(2n-1)}\left[\gamma_m^2+\left(\frac{r_o n\pi}{h}\right)^2\right]^{-1} \tag{4.30}$$

where

$$D_m=\tfrac{1}{2}\left[\tfrac{1}{2}R_0(1)-R_2(1)\right]^2-\tfrac{1}{2}\left(\tfrac{r_i}{r_o}\right)^2\left[\tfrac{1}{2}R_0(\tfrac{r_i}{r_o})-R_2(\tfrac{r_i}{r_o})\right]^2 \tag{4.31}$$

$$G_m=\tfrac{1}{\gamma_m}\left[R_0(\tfrac{r_i}{r_o})-R_0(1)\right]. \tag{4.32}$$

A MatLab program has been developed to find the velocity profile. The code is given in Appendix G. Examples of a velocity profile is shown in Figures 4.2 and 4.3.

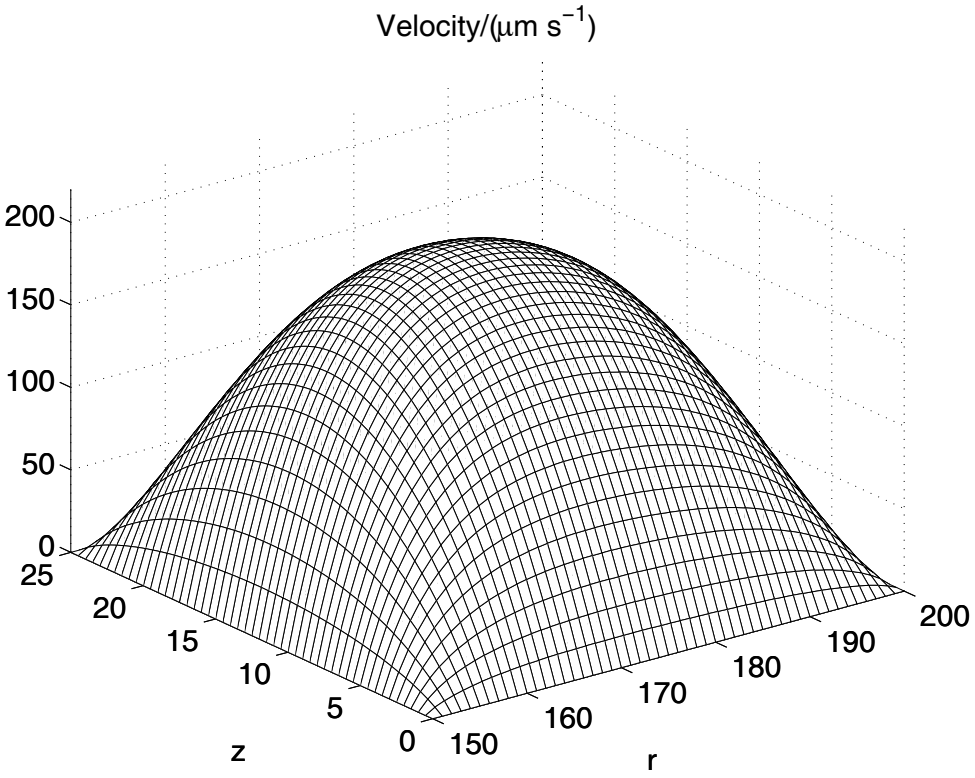

Figure 4.2: Velocity profile.

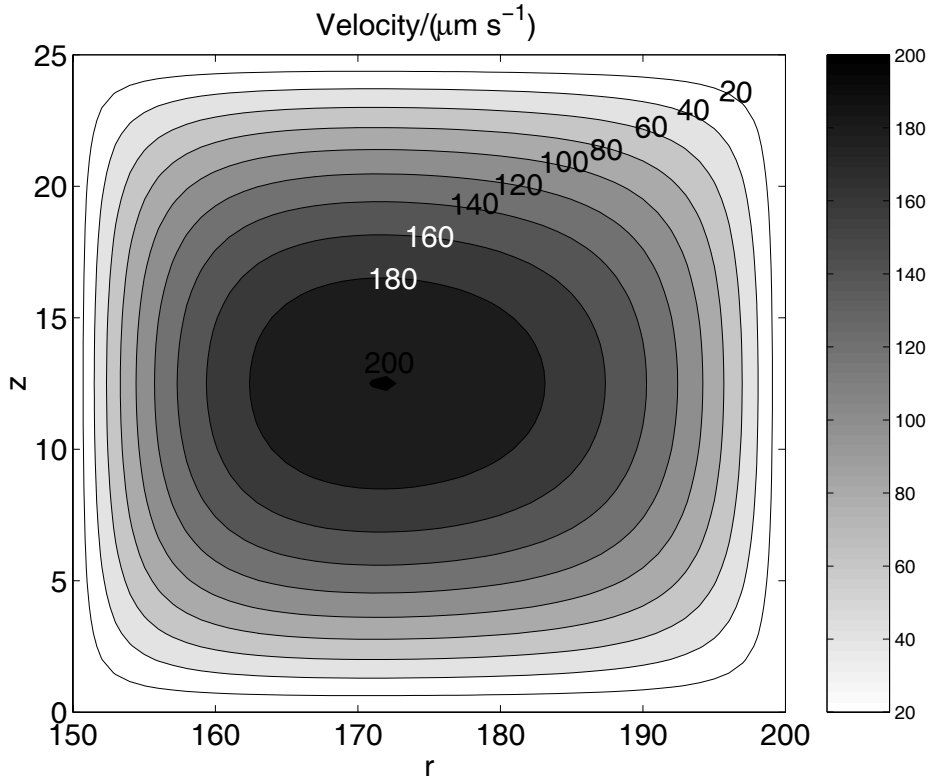

Figure 4.3: Contour of velocity profile. Notice the asymmetry. The peak of the profile is closer to the inner wall than the outer wall.

Summary: In the preceding chapter we have found the velocity profiles for a pressure driven flow in a tube. This will be applied in the theory on Taylor dispersion in the following chapter. Furthermore we have found an analytical expression for the velocity profile of a pressure driven flow in a turn with a rectangular cross section. This velocity profile is applied to the grid dependency analysis. The method for solving boundary value problems for partial differential equations, as we have described it above, will also be used in Chapter 6.

Chapter 5

Dispersion

Whenever dispersion is mentioned throughout this thesis, one should imagine the spreading of some species flowing in some liquid. The degree of the dispersion of some species is often measured in terms of the standard deviation of the species concentration profile. In this thesis we will focus on three physical effects causing dispersion:

- Diffusion: The transport of some species caused by gradients in the concentration, given by Fick's law.
- Geometry effects: The dispersion which may be caused by the geometry of the system, through which a species is transported.
- Gradients in velocity profiles: When a species is transported by convection, any gradients in the velocity profile will cause dispersion, because some part of the species is travelling faster than other parts.

5.1 Taylor Dispersion

In the following section we will consider dispersion and diffusion in a capillary tube. The velocity profile of a pressure driven flow in a cylindrical tube in such a geometry will naturally be of great importance. Next, the theory of Taylor dispersion will be dealt with, followed by a discussion of when other approximations than Taylor's can be made. Taylor dispersion in channels with a square cross section is especially interesting for microchannels in μ-TAS. Channels having sloping walls have been investigated by Daridon (2000). Geometries having other cross sections have been investigated by Dutta (2000). In this thesis we will only consider the tube shaped geometry.

5.1.1 Taylor Dispersion

The dispersion of one miscible liquid into another, due to a non-constant velocity profile combined with diffusion orthogonal to the flow direction, is termed *Taylor dispersion*. In the following theory we follow the work by Probstein (1994). To illustrate the meaning of Taylor dispersion consider the following:

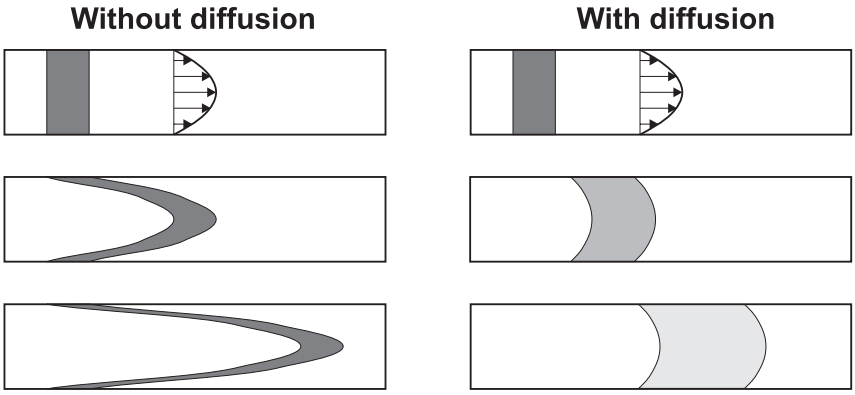

Figure 5.1: The figure shows the dispersion of a sample in a tube with and without diffusion present at the initial stage, $t = 0$, and at two later stages $t_1 > 0$ and $t_2 > t_1$. The gray scale represent the density of species.

Example: As an illustration of the following example see Figure 5.1. First assume no diffusion. Take a long circular tube containing a fluid and place within a sample. If we at time $t = 0$ begin to move the fluid a parabolic velocity profile will build up. This gives rise to a dispersion of the sample, since we have a maximum fluid velocity at the center of the tube and zero velocity at the inner wall. Now consider radial diffusion. Because of radial concentration gradients we will see the following: The faster-travelling molecules from the center of the tube will diffuse into the low-velocity region near the wall and the slower travelling sample molecules near the wall will diffuse into the high-velocity region at the center of the tube. This mixing will smear out the parabolic shape as time goes and will result in a cylindrical shaped sample for large times.

The Taylor Dispersion Equation
The axially symmetric convective diffusion equation with a constant diffusion is given below

$$\frac{\partial c}{\partial t} + u(r)\frac{\partial c}{\partial x} = D\,\nabla^2 c \tag{5.1}$$

where D is the diffusion coefficient. Transforming the equation into a moving reference frame, with space-time coordinates (x', t') moving in the x-direction at speed U, i.e.

$$\left\{ \begin{array}{c} x' = x - Ut \\ t' = t \end{array} \right\} \qquad \text{or} \qquad \left\{ \begin{array}{c} x = x' + Ut \\ t = t' \end{array} \right\} \tag{5.2}$$

we obtain

$$\frac{\partial c'}{\partial t'} + u'(r)\frac{\partial c'}{\partial x'} = D\nabla^2 c' \tag{5.3}$$

Taylor made the assumption that in this moving frame of reference, the flow is quasi-steady, meaning that $\frac{\partial}{\partial t'} \simeq 0$. Furthermore disregarding axial diffusion

(this assumption is discussed later in this section), equation (5.3) is simplified to

$$u'(r)\frac{\partial c'}{\partial x'} = \frac{D}{r}\frac{\partial}{\partial r}\left(r\frac{\partial c'}{\partial r}\right) \tag{5.4}$$

where $u'(r)$ is the velocity profile in the moving frame of reference. From the previous subsection we found the paraboloid velocity profile $u(r) = \frac{dx}{dt} = 2U\left(1-\frac{r^2}{a^2}\right)$, hence $u'(r) = \frac{dx'}{dt} = \frac{dx}{dt} - U = U\left(1-2\frac{r^2}{a^2}\right)$ giving

$$U\left(1-2\frac{r^2}{a^2}\right)\frac{\partial c'}{\partial x'} \quad = \quad \frac{D}{r}\frac{\partial}{\partial r}\left(r\frac{\partial c'}{\partial r}\right). \tag{5.5}$$

The solution is

$$c' \quad = \quad \frac{Ua^2}{4D}\left(\frac{r^2}{a^2}-\frac{1}{2}\frac{r^4}{a^4}\right)\frac{\partial c'}{\partial x'} + A\ln(r) + B, \tag{5.6}$$

where A and B are integration constants, which remain to be determined from boundary conditions. As c must be finite for $r = 0$ we must require $A = 0$. For $r = 0$ we obtain $B = c'(0) \equiv c_0$, the concentration at the axis of symmetry. c_0 is determined from the boundary condition $\frac{\partial c'}{\partial r}\mid_{r=a} = 0$ to be

$$c'_0 = \frac{Ua^2}{2D}\left(\frac{r^4}{a^4}-1\right)\frac{\partial c'}{\partial x'}. \tag{5.7}$$

Hence the concentration as function of the radius is

$$c'(r) = c'_0 + \frac{Ua^2}{4D}\left(\frac{r^2}{a^2}-\frac{1}{2}\frac{r^4}{a^4}\right)\frac{\partial c'}{\partial x'}. \tag{5.8}$$

The mean concentration is found to be

$$\bar{c'} = \frac{1}{\pi a^2}\int_0^{2\pi}\left[\int_0^a c'(r)rdr\right]d\varphi = c'_0 + \frac{1}{3}\frac{Ua^2}{4D}\frac{\partial c'}{\partial x'}, \tag{5.9}$$

so that

$$c'(r) = \bar{c} + \frac{Ua^2}{4D}\left(-\frac{1}{3}+\frac{r^2}{a^2}-\frac{1}{2}\frac{r^4}{a^4}\right)\frac{\partial c'}{\partial x'}. \tag{5.10}$$

Taylor proposed at this point that

$$\frac{\partial c'}{\partial x'} \simeq \frac{\partial \bar{c}'}{\partial x'} \tag{5.11}$$

could be assumed to be true if the following inequality was true

$$\frac{Ua^2}{4D}\left(\frac{1}{L}\right) \ll 1. \tag{5.12}$$

where L is the characteristic length over which the greatest change in c' occurs. We notice that the concentration gradient $\frac{\partial c'}{\partial x'}$ has been replaced by $\frac{\Delta c}{L}$. As Δc is small compared to $\bar{c}$ it is sufficient to consider $1/L$ in equation (5.12). This makes

good sense as small values of L necessarily gives rise to larger concentration gradients (in average) than larger L. An example of this is given for Gaussian curves in Figure (5.2).

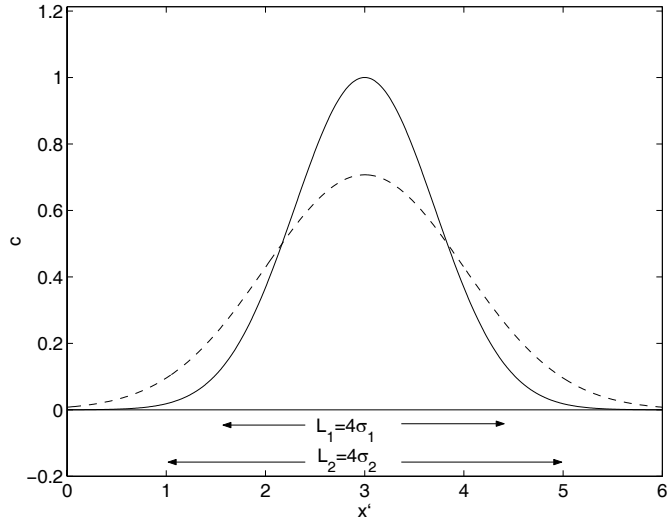

Figure 5.2: Two Gaussian curves with different characteristic length scales L are given. Notice that L_1, which is shorter than L_2, has larger concentration gradients. σ_1 and σ_2 are the standard deviations for the two Gaussians.

Using equation (5.11) we can integrate to find the mass flux

$$\bar{J}_{\text{mass}} = \frac{1}{\pi a^2}\int_0^{2\pi}\int_0^a \rho u' r dr d\varphi = \frac{U^2 a^2}{48D}\frac{\partial \bar{\rho}}{\partial x'}. \tag{5.13}$$

Hence the effective diffusion coefficient is given by

$$D_{\text{eff}} = \frac{U^2 a^2}{48D} = \frac{1}{48} Pe^2 D, \tag{5.14}$$

and with the continuity condition

$$\frac{\partial \bar{\rho}}{\partial t'} = -\frac{\partial \bar{J}_{\text{mass}}}{\partial x'}, \tag{5.15}$$

we find in the moving frame of reference

$$\frac{\partial \bar{c}'}{\partial t} = D_{\text{eff}}\frac{\partial^2 \bar{c}'}{\partial x'^2}. \tag{5.16}$$

Going back to the original frame of reference, using equations (5.2), we find for the two terms in equation (5.16), respectively,

$$\frac{\partial \bar{c}'(t',x')}{\partial t'} = \frac{\partial \bar{c}(t,x)}{\partial t'} = \frac{\partial \bar{c}}{\partial t}\frac{\partial t}{\partial t'} + \frac{\partial \bar{c}}{\partial x}\frac{\partial x}{\partial t'} = \frac{\partial \bar{c}}{\partial t} + U\frac{\partial \bar{c}'}{\partial x}, \tag{5.17}$$

$$\begin{aligned}\frac{\partial^2 \bar{c}'}{\partial x'^2} &= \frac{\partial}{\partial x'}\frac{\partial \bar{c}'(x',t')}{\partial x'} = \frac{\partial}{\partial x'}\frac{\partial \bar{c}(x,t)}{\partial x'} = \frac{\partial}{\partial x'}\left(\frac{\partial \bar{c}}{\partial x}\frac{\partial x}{\partial x'} + \frac{\partial \bar{c}}{\partial t}\frac{\partial t}{\partial x'}\right)\\ &= \frac{\partial \frac{\partial \bar{c}}{\partial x}}{\partial x}\left(\frac{\partial x}{\partial x'}\right)^2 + \frac{\partial \frac{\partial \bar{c}}{\partial x}}{\partial t}\frac{\partial t}{\partial x'} = \frac{\partial^2 \bar{c}}{\partial x^2}\end{aligned} \tag{5.18}$$

Inserting these two transformations in equation (5.16) we obtain

$$\frac{\partial \bar{c}}{\partial t} + U\frac{\partial \bar{c}}{\partial x} = D_{\text{eff}}\frac{\partial^2 \bar{c}}{\partial x^2} \tag{5.19}$$

This is known as Taylor's dispersion equation.

Regions of Validity for Different Approximations
During the derivation of the Taylor dispersion equation we made two assumptions: We disregarded the axial diffusion and we assumed the following to be true

$$\frac{Ua^2}{4D}\left(\frac{1}{L}\right) \ll 1 \tag{5.20}$$

For axial diffusion to be negligible compared to the dispersion we will require the diffusion coefficient (D) to be much less than the Taylor dispersion coefficient, i.e.

$$D \ll D_{\text{eff}} = \frac{a^2U^2}{48D} = \frac{1}{48}Pe^2D \tag{5.21}$$

Equations (5.20) and (5.21) can, respectively, be rewritten as

$$Pe \ll \frac{4L}{a} \tag{5.22}$$

$$Pe \gg \sqrt{48} \simeq 7 \tag{5.23}$$

which are the requirements for the Taylor dispersion equation to be valid, written in terms of the Peclets number and the ratio of the characteristic lengths a and L (the radial and axial lengths over which there is appreciable concentration change).

In the following other approximations will be considered. Firstly three important characteristic time scales are defined:

$$\text{Radial diffusion time:} \quad \frac{a^2}{D} \tag{5.24}$$

$$\text{Axial diffusion time:} \quad \frac{L^2}{D} \tag{5.25}$$

$$\text{Convection time:} \quad \frac{L}{U} \tag{5.26}$$

Radial diffusion is negligible if the radial diffusion time is much larger than the convection time, i.e.

$$\frac{a^2}{D} \gg \frac{L}{U} \quad \Leftrightarrow \quad \frac{Ua}{D} = Pe \gg \frac{L}{a} \tag{5.27}$$

Axial diffusion is negligible if the axial diffusion time is much larger than the convection time, i.e.

$$\frac{L^2}{D} \gg \frac{L}{U} \quad \Leftrightarrow \quad \frac{Ua}{D} = Pe \gg \frac{a}{L} \tag{5.28}$$

Normally in a thin capillary we expect: $L > a \Leftrightarrow \frac{L}{a} > 1 > \frac{a}{L}$. Hence, for both axial and radial diffusion to be negligible we only require

$$Pe \gg \frac{L}{a} \tag{5.29}$$

Neglecting diffusion means that that we have pure convection. Going to the other limit where the convection time is assumed small compared to the two characteristic diffusion times, we find similarly,

$$\frac{a^2}{D} \ll \frac{L}{U} \qquad \Leftrightarrow \qquad \frac{Ua}{D} = Pe \ll \frac{L}{a} \tag{5.30}$$

$$\frac{L^2}{D} \ll \frac{L}{U} \qquad \Leftrightarrow \qquad \frac{Ua}{D} = Pe \ll \frac{a}{L} \tag{5.31}$$

Hence, using $L > a$ the requirement to fully neglect convection is $Pe \ll \frac{a}{L}$. Since we are considering a long capillary tube the radial concentration gradients will rapidly turn to zero and we are left with nothing but axial diffusion.

Convective axial diffusion:
The case where axial diffusion is large compared to the Taylor dispersion, meaning $D \gg D_{\text{eff}}$, is referred to as convective axial diffusion. As the effective diffusion is derived on the basis of the approximation: $Pe \ll 4L/a$, we obtain in terms of the Peclet number:

$$Pe \ll 7 \qquad Pe \ll 4L/a \tag{5.32}$$

Taylor-Aris:
From the above we notice that there is a range of Peclet numbers which have not been covered, namely the range where neither $Pe \ll 7$ nor $Pe \gg 7$ is true. Say the region corresponds to $Pe \in [0.7, 70]$. In that region Aris (1956) have proved that the effective diffusion coefficient is simply the sum of the mass diffusion coefficient (D) and the Taylor dispersion coefficient ($\frac{Pe^2}{48}$), i.e.

$$D_{\text{eff}} = D(1 + \frac{Pe^2}{48}) \tag{5.33}$$

Still we also need to require: $Pe \ll 4L/a$.

The regions of validity for the different approximations explained above have been collected in figure (5.3). The signs '$\ll$' and '$\gg$' have been converted to '10 times less' and '10 times larger', respectively.

Analytical Solution of the Taylor Dispersion Equation
For certain initial conditions analytical solutions to the Taylor dispersion equation exist. E.g. if the delta function is used as an initial condition (t=0)

$$\bar{c} = \frac{n_0}{\pi a^2}\delta(x) \tag{5.34}$$

then the analytical solution is given as

$$\bar{c} = \frac{n_0}{\pi a^2}\frac{1}{2\sqrt{\pi D_{\text{eff}} t}} \exp\left(-\frac{(x-Ut)^2}{4D_{\text{eff}} t}\right) \tag{5.35}$$

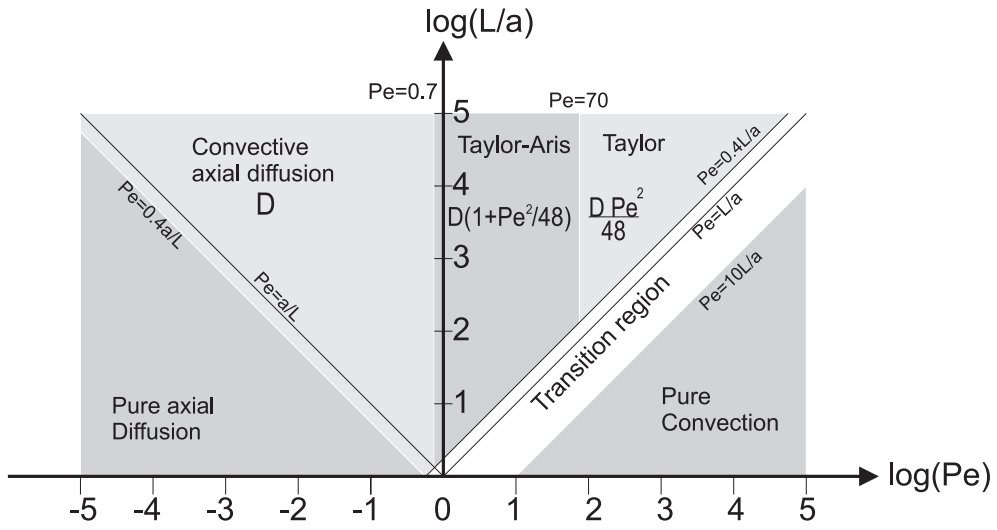

Figure 5.3: Visualization of regions where different approximations can be made regarding the problem of sample broadening in a capillary tube. (From Probstein (1994), after A.A. Sonin).

which is recognized as time increases as a gaussian curve travelling right while increasing the standard deviation. An example is given in figure (5.4). For any practical purposes the initial concentration profile would never be described by a delta function. A more realistic initial concentration profile is the gaussian shaped concentration profile. The solution for this initial problem is in fact already given above, as this problem is simply a shift in the time variable. This is demonstrated below. Say, we at time $t = -t_0$, where t_0 is a positive time have

$$\bar{c} = \frac{n_0}{\pi a^2}\delta(x), \tag{5.36}$$

then according to equations (5.34) and (5.35) this is equivalent to the initial condition

$$t = 0: \quad \bar{c} = \frac{n_0}{\pi a^2}\frac{1}{2\sqrt{\pi D_{\text{eff}} t_0}}\exp\left(-\frac{(x - Ut_0)^2}{4D_{\text{eff}} t_0}\right), \tag{5.37}$$

and the solution for $t > 0$

$$\bar{c} = \frac{n_0}{\pi a^2}\frac{1}{2\sqrt{\pi D_{\text{eff}}(t + t_0)}}\exp\left(-\frac{(x - U(t + t_0))^2}{4D_{\text{eff}}(t + t_0)}\right). \tag{5.38}$$

Taylor Dispersion for Rotational Symmetric Velocity Profiles

It may not always be the case that the velocity profile in the capillary tube is shaped as a paraboloid. E.g. in Electroosmotic driven flows the profile is more flat. For the general case we write the rotational velocity profile as

$$u(r) = Uf(r, a) \tag{5.39}$$

where $f(r, a)$ is a function of the distance from the axis of symmetry r and a is the tube radius. U is the mean velocity. In analogy to the previous derivation

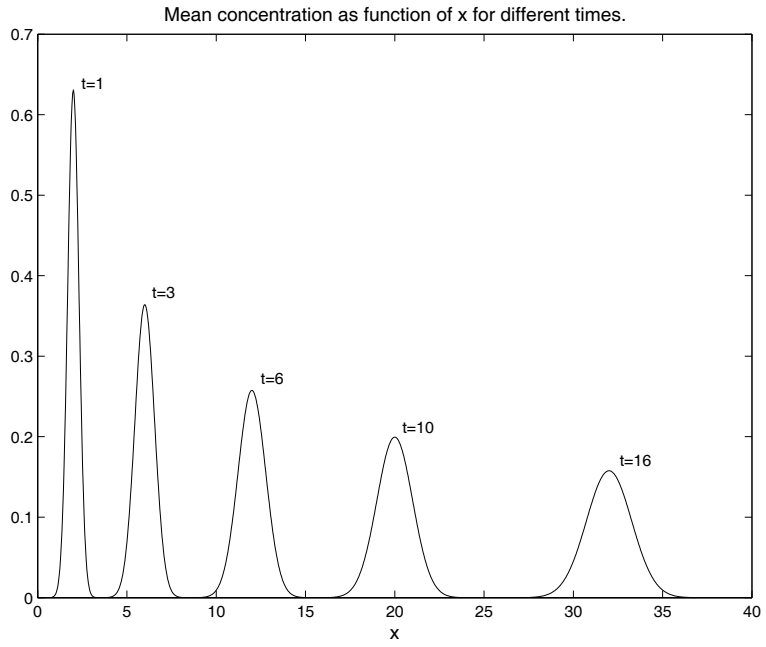

Figure 5.4: Concentration profiles for different times. $\frac{n_0}{\pi a^2} = 0.5$, $U = 2$, $D_{\text{eff}} = 0.05$.

of the effective dispersion coefficient, it will be shown that for any rotational symmetric velocity profile the effective dispersion coefficient is

$$D_{\text{eff}} = D(1 + \alpha_T Pe^2) \tag{5.40}$$

where α_T is a dimensionless constant. In case of Taylor dispersion with the paraboloid velocity profile we have found $\alpha_T = 1/48$. Going into the moving frame of reference the velocity profile becomes

$$u'(r) = \frac{dx'}{dt} = \frac{dx}{dt} - U = U(f(r,a) - 1). \tag{5.41}$$

Inserting this expression in the diffusion equation we find

$$\frac{\partial}{\partial r}\left(r\frac{\partial c}{\partial r}\right) = \frac{Ur}{D}\Big(f(r,a) - 1\Big)\frac{\partial c}{\partial x'} \tag{5.42}$$

Integrating twice and using boundary conditions similar to the ones used deriving equation (5.8) we obtain

$$c(r) = \frac{a^2 U}{4D}\frac{\partial c'}{\partial x} I(r,a) + c_0 \tag{5.43}$$

where c_0 is the concentration at the axis of symmetry and

$$I(r,a) = \frac{4}{a^2}\left[\int \frac{1}{r}\left[\int r(f(r,a) - 1)dr\right]dr\right]. \tag{5.44}$$

Expressing the concentration in terms of the mean concentration $\bar{c}$ we find similar to equation (5.10)

$$c = \bar{c} + \frac{Ua^2}{4D}\frac{\partial c'}{\partial x}\left(c_1 + I(r,a)\right) \tag{5.45}$$

where

$$c_1 = -\frac{2}{a^2}\int_0^a I(r,a) r dr \tag{5.46}$$

is equal to some real number. In the case of a parabolic velocity profile $c_1 = -1/3$. Again assuming

$$\frac{Ua^2}{4D}\frac{1}{L} \ll 1 \tag{5.47}$$

we can approximate

$$\frac{\partial c'}{\partial x'} \simeq \frac{\partial \bar{c}'}{\partial x'}, \tag{5.48}$$

and find similar to equation (5.13)

$$\bar{J} = -\frac{Ua^2}{D}\frac{\partial \bar{\rho}}{\partial x'}\left(\frac{-2}{a^4}\int_0^a (f(r,a)-1) r \left[\int \frac{1}{r}\left[\int (f(r,a)-1) r dr\right] dr\right] dr\right) \tag{5.49}$$

From the above expression the effective diffusion coefficient is found to be

$$D_{\text{eff}} = \alpha_T Pe^2 D \tag{5.50}$$

where

$$\alpha_T = \frac{-2}{a^4}\int_0^a (f(r,a)-1) r \left[\int \frac{1}{r}\left[\int (f(r,a)-1) r dr\right] dr\right] dr. \tag{5.51}$$

Remark
The integrals in squared brackets in equations (5.44), (5.49) and (5.51) should be regarded as the indefinite integrals of the functions within, with the constant of integration equal to zero.

Example I
In the following we will calculate α_T for a more general velocity profile than the paraboloid. Consider

$$u(r) = u_{max}\left[1 - \left(\frac{r}{a}\right)^n\right], \tag{5.52}$$

where n is some number, e.g. $n = 2$ for the paraboloid velocity profile. The mean velocity U of the above profile is found to be

$$U = \frac{2}{a^2}\int_0^a u(r) r dr = \frac{n}{2+n} u_{\max}. \tag{5.53}$$

Hence in terms of the mean velocity the profile, equation (5.52), is given by

$$u(r) = U\frac{2+n}{n}\left[1 - \left(\frac{r}{a}\right)^n\right], \tag{5.54}$$

which means that the $f(r,a)$ function appearing in the formula for α_T, equation (5.51), is

$$f(r,a) = \frac{2+n}{n}\left[1-\left(\frac{r}{a}\right)^n\right]. \tag{5.55}$$

Inserting the above expression into equation (5.51) yields

$$\alpha_T = \frac{1}{2(2+n)(4+n)}. \tag{5.56}$$

Notice that when $n = 2$ we find $\alpha_T = 1/48$, as expected. Furthermore we notice that for $n \to \infty$, $\alpha_T \to 0$. This is also expected. When $n \to \infty$, $u(r) \to u_{\max}$ for all r except at $r = 1$, where $u = 0$. Hence there are no gradients in the velocity, and no Taylor dispersion can be present. In Figure 5.5 a plot of the velocity profiles for different n's are given together with a plot of α_T as function of n. Notice how the velocity profile becomes more and more flat as n is increased.

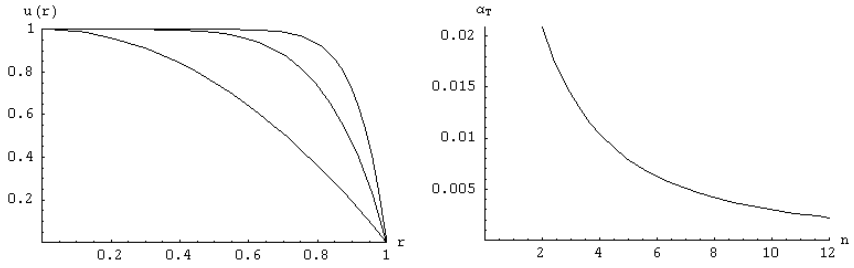

(a) (b)

Figure 5.5: Figure (a) shows the velocity profile for $n = 2$, $n = 6$ and $n = 12$. Figure (b) shows α_T as a function of n.

Example II

For non-Newtonian suspensions an empirical relation for flow in a cylindrical geometry have been suggested by Chang et. al (2000)

$$\tau = k\left(\dot{\gamma}\right)^n, \tag{5.57}$$

where k is a viscosity constant for non-Newtonian fluids with the unit Pa s^n, $\dot{\gamma}$ is the shear rate, which in this case corresponds to $\frac{\partial u}{\partial r}$, and τ is the shear stress. The above empirical relation yields the velocity profile

$$u(r) = u_{max}\left[1-\left(\frac{r}{a}\right)^{\frac{n+1}{n}}\right]. \tag{5.58}$$

For $n = 1$ the paraboloid velocity profile is found again. Rewriting the above profile into a form containing the mean velocity U instead of u_{max} we obtain $f(r,a)$ needed to calculate α_T from equation (5.51). We find

$$\alpha_T = \frac{n^2}{2+16n+30n^2}. \tag{5.59}$$

When $n = 1$ we obtain as expected $\alpha_T = 1/48 \simeq 0.02083$. According to Chang et al. (2000) Walburn and Schneck have found $n = 0.785$ for human blood. This value of n yields

$$\alpha_T \simeq 0.01865, \tag{5.60}$$

which is less than $\alpha_T = 0.02083$ for ordinary Newtonian fluids. The velocity profile in blood might hence yield less dispersion of some injected chemical substance, than if a paraboloid velocity profile was assumed. Be aware that the above calculations are based on the assumptions that blood is a continuum. This might not be true in all cases because of the chemical composition of blood, which includes the large red blood cells. The shape of these molecules may depend on various parameters. Furthermore we have assumed that no chemical reactions will affect the flow.

5.2 Geometry Effects

By geometry effects we think of the dispersion of a species caused by the geometry of the system, through which the species is transported. As an example of this effect we will firstly consider the *race-track* effect.

5.2.1 The Race Track Effect

When a channel is bent some angle (e.g. a U-turn corresponds to an angle of π radians) the so-called racetrack effect is introduced to the flow (see figure (5.6))

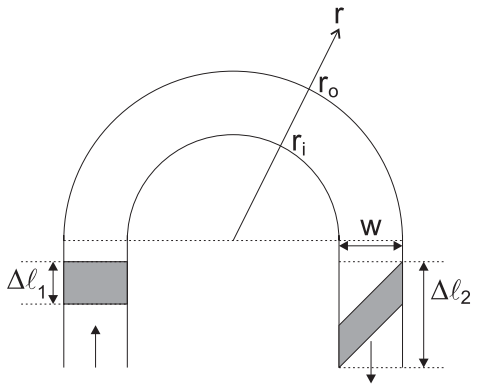

Figure 5.6: Channel with a U-turn.

The racetrack effect can be explained as follows: A molecule flowing just next to the inner wall around a turn travel a shorter distance than a molecule travelling next to the outer wall. Assuming that the molecules travel with the same speed the inner molecule will finish the turn faster than the other molecule. This leads to a dispersion due to the geometry of the channel. There is, naturally, also a dispersion due to the diffusion caused by concentration gradients in the sample. We will consider the combined effect of these dispersions at a later stage.

Consider the 2D-case shown in Figure 5.6. We will neglect diffusion and assume a constant velocity profile over the entire width of the channel. The

velocity is also assumed constant in any cross-section of the turn. If a rectangular shaped sample is sent into a circular turn the shape of the sample will be transformed into a parallelogram at the downstream side of the turn. This can be seen from simple geometry. Consider a turn with an angle of θ in radians. Denoting the length of the sample, $\Delta\ell_1$, before the turn $\Delta\ell_2$ after the turn, we find that the sample has been dispersed

$$\Delta\ell_2 - \Delta\ell_1 = \theta w. \tag{5.61}$$

$\Delta\ell_1$, $\Delta\ell_2$, and w are defined in Figure 5.6. We shall in the following show that for electrokinetically driven fluids the dispersion under certain assumptions is approximately doubled to $2\theta w$.

5.2.2 Electrokinetically Driven Fluids.

It is important to notice that the case described above is valid only when the speed can be assumed to be constant over the entire width. This requirement is e.g. not fulfilled in the case of electrokinetically driven fluids. Assume the Helmholtz-Smoluchowski relations between the electrical field and the fluid velocity, $\mathbf{u} = -\alpha\nabla\psi = \alpha\mathbf{E}$, to be valid, where α is the mobility, which can be either an electroosmotic mobility or an electrophoretic mobility[1]. The magnitude of the electric field must be smaller at the outer wall compared to the inner wall. This can be realized by a simple consideration. The potential drop U over the turn for the inner and outer "lane" is the same, but the outer "lane" is longer ($d_{\text{outer}} > d_{\text{inner}}$) . Since $U = E\,d$, the electric field must be smallest at the outer wall and largest at the inner wall. The effect of having a difference in the electric field will be examined in the following. For the inner and outer paths of the turn we can write

$$L_i = \theta r_i \quad \text{and} \quad v_i = \alpha E_i = \frac{\alpha U}{\theta r_i} \tag{5.62}$$

$$L_o = \theta r_o \quad \text{and} \quad v_o = \alpha E_o = \frac{\alpha U}{\theta r_o} \tag{5.63}$$

From the above equations we find the travelling time for a molecule to flowing along the inner and outer paths, respectively.

$$t_i = \frac{L_i}{v_i} = \frac{(\theta r_i)^2}{\alpha U} \tag{5.64}$$

$$t_o = \frac{L_o}{v_o} = \frac{(\theta r_o)^2}{\alpha U} \tag{5.65}$$

The time difference is hence

$$\Delta t = t_o - t_i = \frac{\theta^2}{\alpha U}(r_o^2 - r_i^2) = \frac{\theta^2}{\alpha U}(r_o + r_i)(r_o - r_i) = \frac{\theta^2}{\alpha U} 2 r_c w_t \tag{5.66}$$

Because of continuity the average fluid velocity in the straight parts of the channel must equal the average velocity in the turns. Since $\mathbf{u} = \alpha\mathbf{E}$, this means that the average electric field ($\mathbf{E}_{av}$) in the turn must equal the average electric

[1] In some articles μ is used for the mobility instead of α. We will, however, reserve the symbol μ to the dynamic viscosity.

field in the straight parts, but the electric field in the straight part is constantly $\mathbf{E}$. Hence $\mathbf{E}_{av} = \mathbf{E}$. The magnitude of electric field in the turn is given by

$$E(r) = \frac{U}{\theta r}, \quad r_i < r < r_o, \quad w = r_o - r_i \tag{5.67}$$

averaging yields

$$E_{av} = \frac{1}{w}\int_{r_i}^{r_o} \frac{U}{\theta r} dr = \frac{U}{w\theta} \ln\left(\frac{r_o}{r_i}\right) = \frac{U}{w\theta} \ln\left(1 + \frac{1}{\frac{r_c}{w} - \frac{1}{2}}\right) \tag{5.68}$$

$$\simeq \frac{U}{w\theta}\frac{w}{r_c} \tag{5.69}$$

where we have used the first term in the series expansion of $\ln(1+x)$ and neglected the $\frac{1}{2}$-term assuming $\frac{r_c}{w} \gg \frac{1}{2}$. In experiments conducted by Culbertson et. al. (1998) $2.5 < \frac{r_c}{w} < 10$. Taking only the first term in the series expansion then yields

$$E_{av} \simeq \frac{U}{w\theta}\frac{1}{\frac{r_c}{w}} = \frac{U}{\theta r_c} = E_c \tag{5.70}$$

where E_c is the magnitude of the electric field at the center curve in the turn. The relative error between E_c and E_{av} is given by

$$\frac{|E_{av} - E_c|}{E_{av}} = 1 - \left[\frac{r_c}{w} \ln\left(1 + \frac{1}{\frac{r_c}{w} - \frac{1}{2}}\right)\right]^{-1} \tag{5.71}$$

A plot of the relative error is given in figure (5.7). The error for $\frac{r_c}{w} = 2.5$ is approximately 1.4% and for higher values the error is even more negligible.

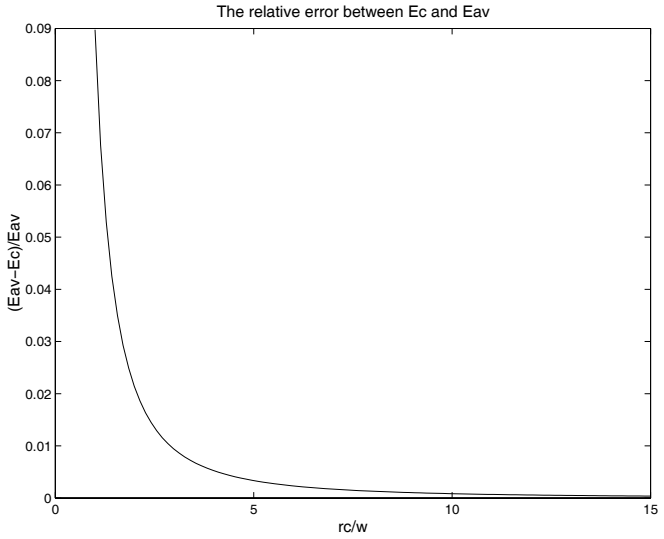

Figure 5.7: Relative error between E_c and E_{av}.

Now, using $U = E_c\theta r_c \simeq E_{av}\theta r_c$, rewrite equation (5.66) into

$$\Delta t = \frac{2\theta w_t}{\alpha E_{av}} = \frac{2\theta w}{v_{av}} \tag{5.72}$$

where v_{av} is the average speed of the fluid. The increase of the sample width in the direction of the flow is then increased

$$\Delta l = v_{av}\Delta t = 2\theta w \tag{5.73}$$

Comparing this to the result with just a constant velocity profile over the entire width of the channel, we notice that the broadening of the band has doubled.
Example: The increase of the bandwidth is for $\theta = \pi$ and a channel width in the turn of $w_t = 55$ μm found to be: $\Delta l = 346$ μm.
With $\zeta = 0.1$ V we obtain for water at 25^o C a mobility of: $\alpha = 8.0 \times 10^{-8}$ $\frac{\mathrm{m}^2}{\mathrm{Vs}}$.
$E = 30$ kV, then gives a time difference of: $\Delta t = 0.14$ s.

A way to mend this problem could be to use different zeta-potentials at the inner and outer wall, so t_o and t_i are equal. From the Helmholtz-Smoluchowski equation we know: $\alpha = -\frac{\epsilon\zeta}{\mu}$, where ζ is the zeta-potential, which depend on various things, among others material parameters of the wall. The condition for the two time parameters to be equal is found

$$t_o = \frac{\theta r_o}{v_o} = \frac{\theta r_o}{\alpha_o \frac{U}{\theta r_o}}, \tag{5.74}$$

$$t_i = \frac{\theta r_i}{v_i} = \frac{\theta r_i}{\alpha_i \frac{U}{\theta r_i}}, \tag{5.75}$$

equating the above times gives

$$\frac{\alpha_i}{\alpha_o} = \left(\frac{r_i}{r_o}\right)^2. \tag{5.76}$$

Hence the ratio of the α-parameters should equal the ratio of the radii of curvature squared. In practice a straight channel is often connected to the two ends of a turn. The electroosmotic mobility α of these straight parts should give rise to a discharge equal to the discharge in the turn, or similarly the mean velocity in the straight parts should equal the mean velocity in the turn. This gives a relation between α, α_o, α_i, r_i and r_o, which is found in the following. The mean velocity in the straight part is simply: αE_s, where E_s is the magnitude of the electric field in the straight parts. The mean velocity in the turn is the mean of the velocities at the outer wall and the inner wall of the turn, since the velocity in the turn must be a linear function of the radius, i.e.

$$\bar{v}_t = \frac{U}{2\theta}\left(\frac{\alpha_i}{r_i} + \frac{\alpha_o}{r_o}\right) = \alpha E_s. \tag{5.77}$$

E_s can be found from the fact that the mean electric field in any cross-section of the channel must be equal, hence using equation (5.67), we find

$$\bar{E} = \frac{1}{r_o - r_i}\int_{r_i}^{r_o} E(r)dr = \frac{1}{r_o - r_i}\int_{r_i}^{r_o} \frac{U}{\theta r}dr = \frac{U}{\theta}\frac{\ln(r_o/r_i)}{r_o - r_i} = E_s. \tag{5.78}$$

Combining equations (5.76),(5.77) and (5.78) gives

$$\alpha_i = 2\alpha\frac{\ln(r_o/r_i)}{r_o^2 - r_i^2}r_i^2 \tag{5.79}$$

$$\alpha_o = 2\alpha\frac{\ln(r_o/r_i)}{r_o^2 - r_i^2}r_o^2. \tag{5.80}$$

The above expressions are enough to handle the plane 2D-case. In three dimensions, however, the electroosmotic mobility of the top and bottom patch of the turn should also be changed. In fact, they must be equal and dependent on the radius in the turn. From $v(r)$ and $E(r)$ (equation (5.67)) the top and bottom mobilities is found to be

$$\alpha(r) = \frac{v(r)}{E(r)} = 2\alpha \frac{\ln(r_o/r_i)}{r_o^2 - r_i^2} r^2, \quad \text{where} \quad r_i < r < r_o. \tag{5.81}$$

In an article by Chen and Zhu (1999), examples are given that it is actually possible to control the electroosmotic mobility with external radial electric fields. The electroosmotic mobility can also be changed by laser modification of the channels, Johnson (2001). Other means of minimizing turn induced dispersion have been suggested by Griffiths (2001), where a tapering of the turns are studied.

In the above we have completely neglected the effect diffusion has on the dispersion. This we will remedy with the considerations below. Firstly, two time scales are important

- t_D, the transverse diffusion equilibrium time. $t_D = \frac{w^2}{2D}$, where D is the mass diffusion coefficient.
- t_t, sample transit time around a turn. It is defined as the maximum time a molecule can spend in the turn, i.e. $t_t = \frac{\theta r_o}{v_o} = \frac{\theta r_o^2}{v_c r_c} \simeq \frac{\theta r_o^2}{v_{av} r_c}$.

The ratio between these parameters, t_D/t_t, is hence a measure of how much diffusion takes place during the time it takes for a molecule to travel through the turn. In the previous calculations we have therefore actually assumed that $t_D/t_t \to \infty$ or similarly $D = 0$. According to Culbertson et. al. (1998,[5]) this assumption is, however, usually not met on microchips, and the article gives a suggestion of the dispersion caused by the turn $\Delta\ell$ when taking diffusion into account[2]

$$\Delta l = 2\theta w[1 - \exp(-t_D/t_t)]. \tag{5.82}$$

A plot of $\Delta\ell$ as function of t_D/t_t is given in figure (5.8). The equation (5.82) and figure (5.82) shows that for t_D/t_t going to infinity, as expected we return to $\Delta l = 2\theta w$. For t_D/t_t going to zero $\Delta\ell$ goes to zero. It should be noted that $\Delta\ell$ going to zero, does not mean there is no dispersion. There is still the diffusion in the flow direction to be considered.

[2] The expression is found from computational simulations based on Fick's law.

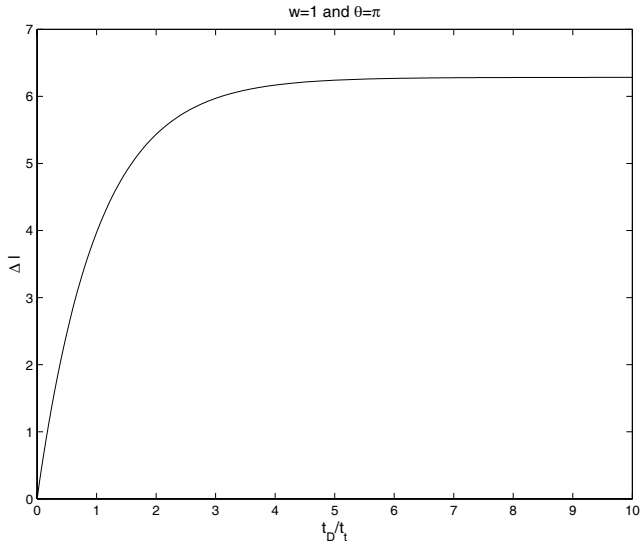

Figure 5.8: $\Delta\ell$ as function of t_D/t_t.

Example: The self diffusion coefficient for water at 25^{o}C is: $D_{mass} = 2.26 \times 10^{-9}$ m^{2}s^{-1}. Say the width of channel in the turn is: $w = 69$ μm, then the transverse diffusion equilibrium time is: $t_D = 1.05$ s. With radius of curvature: $r_c = 500\mu$ m, $\theta = \pi$ and $v_{av} = \alpha E_{av} = 8 \times 10^{-8}$ m^{2}V^{-1}s$^{-1} \times 30$ kVm^{-1}, we find $t_t = 0.32$ s. Hence: $\frac{t_D}{t_t} = 3.3$. I this case according to figure (5.8) we see that the diffusion is less important when determining the geometrical dispersion, since for $\frac{t_D}{t_t} = 3.3$ the Δl has almost reached its constant value.

Summary: In general three different effects contributing to dispersion in microchannels are studied, namely diffusion, geometry effects, and gradients in the flow velocity profiles.

The theory of Taylor dispersion has been presented. The theory is extended with a more general formula for the Taylor dispersion coefficient valid for rotationally symmetric velocity profiles. Two examples applying the formula are also given. Next the so-called race-track effect is studied. The additional dispersion worsening effects arising when flows are electrokinetically driven are accounted for. We have shown that altering the electroosmotic mobilities specified at the walls of a turn the sample distortion can be decreased. Formulae for the optimal change are also given. Finally possibilities for optimizing the geometry of turns are studied.

Chapter 6

Dispersion Control by Electric Fields

The mixing of one species into another may be undesired. In this chapter we will propose a method of separating two species of opposite charge applying an electric field.

When a specific electric field is applied in some geometry, charged species will be redistributed accordingly. The redistribution process is described by the Nernst-Planck equation. The speed of the charge redistribution is determined by the diffusion coefficient, while the charge density is determined by the electric potential. This will be shown in detail in the following chapter. The electric field created when separating the ions must also be accounted for. This can be done using the Poisson equation.

Imagine the separation of species is taking place in a microchannel. Translating the electric potential in any desired direction along the channel would then move the species along with the potential. Using this method to transport charged species in a microchannel the dispersion of the species is fully controlled. See Figure 6.1. The translation speed should be adjusted according to the diffusion so that the species is close to the steady state distribution in the potential at all times. Thus the diffusion coefficient is the limiting factor for the speed at which the species can be transported.

6.1 Practical Considerations

Some practical considerations should be made regarding the construction of microchannels for the purpose of dispersion control by electric fields. The electrodes generating the electric field should be placed close enough for the desired electric field to be resolved acceptably. In the article by Ajdari (1999) electrode arrays were placed along a channel with a spacing of approximately 60μm. Brown (2000) has made electrode arrays with 50μm intervals. According to Søren Jensen it is, however, possible to place 2μm wide electrodes along a channel with a spacing of 5μm or even as low as 2μm[1].

[1] Private communication with Søren Jensen, Ph. D. student at Mikroelektronik Centret - MIC, Technical University of Denmark.

The theory is quite similar to the Debye layer theory. In the first section we will consider a 1D channel. Later we will consider the cylindrical tube 3D case, which because of the rotational symmetry of the problem can be solved as a 2D boundary value problem.

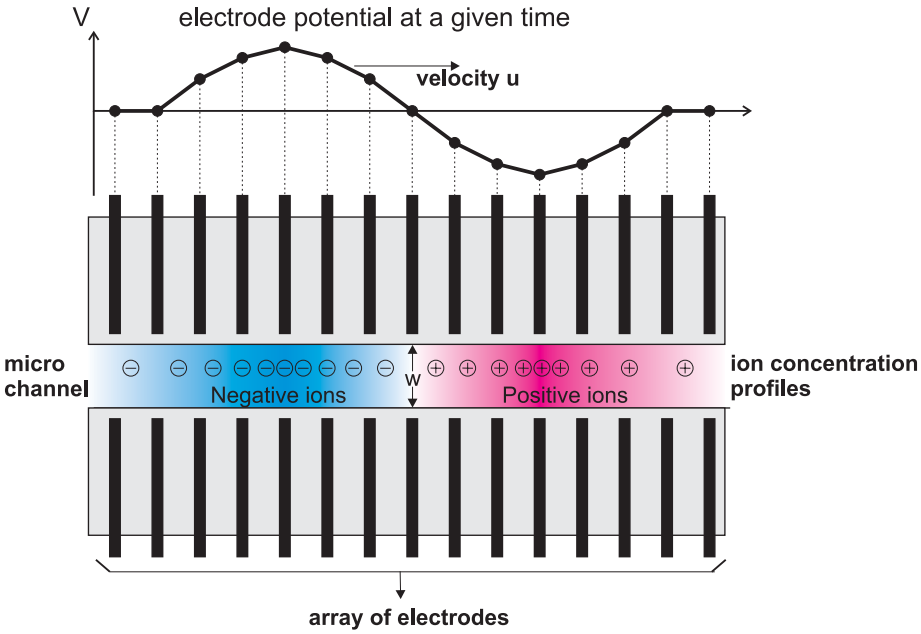

Figure 6.1: Sketch of the separation idea. A number of electrodes are imagined placed along a channel. Varying the voltages in time it is possible to transport the ions along the channel.

6.2 Dispersion Control in a 1D channel

For simplicity consider the 1D case on the x-axis in the interval $-L < x < L$. In this interval we place an amount of positive and negative ions with the concentrations $c_+(x)$ and $c_-(x)$. We also place a parabolic applied potential: $\phi_a = \phi_0 x^2$. This gives rise to a separation of the positive and negative ions, which then again gives rise to an intrinsic potential (ϕ_{in}). The distribution of the positive and negative ions is determined from the total potential: $\phi_{\text{tot}} = \phi_a + \phi_{in}$ together with the Nernst-Planck equation (2.26)

$$-\nu_i z_i F c_i \nabla \phi_{\text{tot}} - D_i \nabla c_i = 0, \tag{6.1}$$

where the convective term is neglected because we will consider the steady state only. Upon integration the concentration of the negative and positive ions are found to be

$$c_\pm(x) = c_0^\pm \exp\left(-\frac{z_\pm F \phi_{\text{tot}}(x)}{RT}\right), \tag{6.2}$$

where the constants $c_0^{\pm}$ are to be determined from the initial amounts of positive ions, n_+, and negative ions, n_-, i.e.

$$n_{\pm} = A \int_{-L}^{L} c_{\pm}(x) dx. \tag{6.3}$$

where A is a unit area. Because of Poisson's equation we must require the dimension of the concentration to be mol/m^3 even though we are working in 1D, hence the unit area A. Using Poisson's equation the intrinsic potential can be found

$$\frac{d^2\phi_{in}}{dx^2} = -\frac{\rho_e}{\epsilon} \tag{6.4}$$

where

$$\rho_e = (z_+ c_+ + z_- c_-)F. \tag{6.5}$$

Equations (6.2), (6.4) and (6.5) form a differential equation for ϕ_{in}

$$\frac{d^2\phi_{in}}{dx^2} = \\ -\frac{F}{\epsilon}\left[z_+ c_+^0 \exp\left(\frac{-z_+F}{RT}(\phi_0 x^2 + \phi_{in})\right) + z_- c_-^0 \exp\left(\frac{-z_-F}{RT}(\phi_0 x^2 + \phi_{in})\right)\right]. \tag{6.6}$$

When the applied potential is symmetric about $x = 0$ we can solve equation (6.6) numerically by iterative methods using the following conditions

$$\left.\begin{array}{l} \frac{d\phi_{in}}{dx} = 0 \\ \phi_{in} = C_0 \end{array}\right\} \quad \text{at} \quad x = 0. \tag{6.7}$$

where C_0 is some arbitrary reference potential.

Example: 1D numerical solution
In the following we will consider solutions of equation (6.6). Firstly we have assumed $z = z_+ = -z_-$ and made the problem dimensionless, i.e.

$$\frac{d^2\phi'_{in}}{dx'^2} = -\frac{1}{2\lambda'_+}\exp\left[-(\phi'_a + \phi'_{in})\right] + \frac{1}{2\lambda'_-}\exp\left[+(\phi'_a + \phi'_{in})\right], \tag{6.8}$$

where the differential equation has been made non-dimensional in the following manner

$$\phi' = \frac{zF\phi}{RT}, \qquad x' = \frac{x}{L}, \tag{6.9}$$

$$\lambda'_{\pm} = \frac{1}{L}\left(\frac{\epsilon RT}{2F^2 z^2 c_{\pm}^0}\right)^{\frac{1}{2}}, \qquad \frac{d^2}{dx'^2} = L^2\frac{d^2}{dx^2}. \tag{6.10}$$

The two factors λ'_+ and λ'_- is determined from the initial amounts, equation (6.2). The non-dimensional amounts of ions are given as

$$n'_{\pm} = n_{\pm}\frac{2F^2 z^2 L}{A\epsilon RT} = \frac{1}{{\lambda'_{\pm}}^2}\int_{-1}^{1}\exp(\mp\phi'_{\text{tot}}(x'))dx' \tag{6.11}$$

The non-dimensional amounts of ions are chosen to be $n'_{\pm} = 1$. An example of results from such a simulation is given in figure 6.2 with the potential, $\phi'_a = 6x'^2$, and $L = 500\mu$m. Notice we have obtained the desired separation of positive and negative ions. The positive ions are mainly concentrated around the middle $x' = 0$, and the negative ions are mainly concentrated at the ends $x = \pm 1$. Going back to real physical dimensions $\phi' = 6$ corresponds to

$$\phi = \frac{RT}{zF}\phi' = \frac{8.31451\ \mathrm{JK^{-1}mol^{-1}} \cdot 298\ \mathrm{K}}{9.6485 \times 10^4\ \mathrm{Cmol^{-1}}} \cdot 6 = 0.15V. \tag{6.12}$$

The ion concentration corresponds to

$$\frac{n_+}{V} = \frac{n_+}{AL} = \frac{\epsilon RT}{F^2 z^2 L^2} = 3.8 \times 10^{-10}\ \mathrm{mol\,m^{-3}}. \tag{6.13}$$

We will move on to investigate to consider a fully three dimensional problem in the next section.

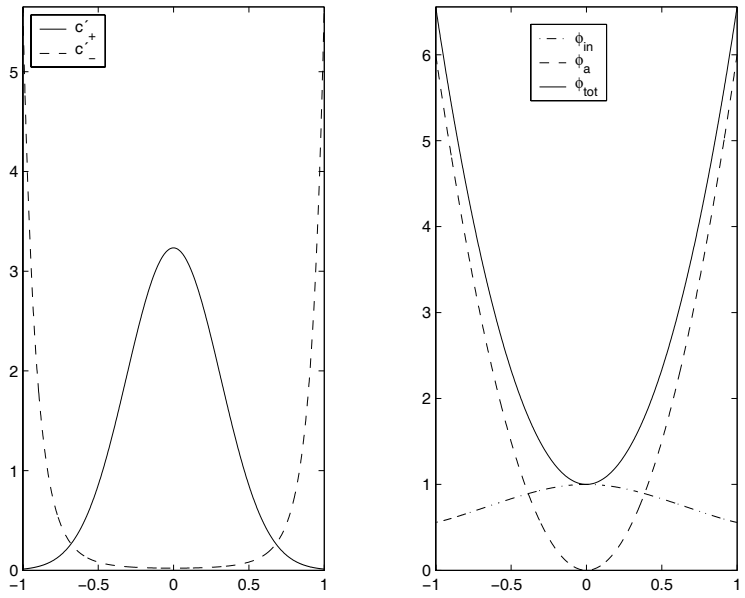

Figure 6.2: Left figure: Distribution of positive and negative ions given as dimensionless concentration. Right figure: Dimensionless applied, intrinsic and total potential. The applied potential is for this example given as: $\phi'_a = 6x'^2$, and $L = 500\,\mu$m.

6.3 Dispersion Control in a 3D Tube

We now consider a tube of length L and radius a. Within this tube we place a dilute solution of positive and negative ions. Suppressing an electric potential along the outer edge of the tube we expect to separate the positive and negative ions.

Applying the Nernst-Planck equation for the positive and negative ions we

find for the steady state situation

$$\frac{-z_{\pm}F}{RT}c_{\pm}\nabla\phi_{\text{tot}} = \nabla c_{\pm}, \tag{6.14}$$

since there is no net flux of species and no convection. $z_{\pm}$ is the valence of the positive and negative ions ($c_{\pm}$), respectively, and

$$\phi_{\text{tot}} = \phi_a + \phi_{in}, \tag{6.15}$$

where ϕ_a is an applied electric potential, and ϕ_{in} is the intrinsic potential given by the distribution of the ions. The equation connecting the intrinsic potential and the distribution of the ions are given by Poisson's equation

$$\nabla^2\phi_{in} = \frac{-\rho_e}{\epsilon}, \tag{6.16}$$

where

$$\rho_e = F(z_+c_+ + z_-c_-). \tag{6.17}$$

The electrons generating the applied potential are assumed to exist outside the tube. Hence the Poisson equation for the applied potential simplifies to the Laplace equation

$$\nabla^2\phi_a = 0. \tag{6.18}$$

The equation for the total potential is hence

$$\nabla^2\phi_{in} + \nabla^2\phi_a = \nabla^2\phi_{\text{tot}} = \frac{-\rho_e}{\epsilon}. \tag{6.19}$$

In order to find the concentrations $c_{\pm}$ we return to the Nernst-Planck equation. Splitting the equation into a radial and an axial component we obtain

$$\frac{-z_iF}{RT}c_i\frac{\partial\phi_{\text{tot}}}{\partial r} = \frac{\partial c_i}{\partial r}, \tag{6.20}$$

$$\frac{-z_iF}{RT}c_i\frac{\partial\phi_{\text{tot}}}{\partial z} = \frac{\partial c_i}{\partial z}. \tag{6.21}$$

Integrating the above we find

$$c_i(r,z) = A_i(z)\exp\left(\frac{-z_iF}{RT}\phi_{\text{tot}}(r,z)\right) \tag{6.22}$$

$$c_i(r,z) = B_i(r)\exp\left(\frac{-z_iF}{RT}\phi_{\text{tot}}(r,z)\right), \tag{6.23}$$

where $A_i(z)$ are functions, which can at most depend on z and $B_i(r)$ are functions, which can at most depend on r. Hence $A_i(z)$ and $B_i(r)$ must equal the same constant, which we will denote c_i^0, where the '0' indicates that $c_i = c_i^0$ when $\phi_{tot} = 0$. Hence the distribution of the ions is given by

$$c_i(r,z) = c_i^0\exp\left(\frac{-z_iF}{RT}\phi_{\text{tot}}(r,z)\right). \tag{6.24}$$

As we are considering a closed system, the total amounts of ions must be fixed initially given values, $n_\pm$, equal to the volume integral of the concentrations

$$n_\pm = \int_0^{2\pi}\left[\int_0^a\left[\int_0^L c_\pm(r,z)rdz\right]dr\right]d\theta = 2\pi\int_0^a\left[\int_0^L c_\pm(r,z)rdz\right]dr. \quad (6.25)$$

Equations (6.24) and (6.25) gives and expression for $c_\pm^0$. We can hence write the following partial differential equation for the total electric potential

$$\begin{aligned}&\frac{\partial^2\phi_{tot}}{\partial r^2}+\frac{1}{r}\frac{\partial\phi_{tot}}{\partial r}+\frac{\partial\phi_{tot}}{\partial z^2}\\&=\frac{-F}{2\pi\epsilon}\left[\frac{z_+n_+\exp\left(\frac{-z_+F}{RT}\phi_{tot}\right)}{\int_0^a\int_0^L\exp\left(\frac{-z_+F}{RT}\phi_{tot}\right)rdzdr}+\frac{z_-n_-\exp\left(\frac{z_-F}{RT}\phi_{tot}\right)}{\int_0^a\int_0^L\exp\left(\frac{z_-F}{RT}\phi_{tot}\right)rdzdr}\right],\end{aligned} \quad (6.26)$$

which must be solved with the appropriate boundary conditions. Making the equation non-dimensional we obtain

$$r'^2\frac{\partial^2\phi'_{tot}}{\partial r'^2}+r'\frac{\partial\phi'_{tot}}{\partial r'}+r'^2\frac{a^2}{L^2}\frac{\partial\phi'_{tot}}{\partial z'^2}=r'^2f(\phi'_{tot}), \quad (6.27)$$

where

$$f(\phi'_{tot})=\frac{1}{2}\left[-\frac{n'_+\exp\left(-\phi'_{tot}\right)}{\int_0^1\int_0^1\exp\left(-\phi'_{tot}\right)r'dz'dr'}+\frac{n'_-\exp\left(\phi'_{tot}\right)}{\int_0^1\int_0^1\exp\left(\phi'_{tot}\right)r'dz'dr'}\right]. \quad (6.28)$$

The non-dimensional variables are defined as follows

$$r'=\frac{r}{a} \qquad z'=\frac{z}{L} \quad (6.29)$$

$$\phi'_{tot}=\frac{zF}{RT}\phi_{tot} \qquad c'=\frac{2a^2z^2F^2}{\epsilon RT}c, \quad (6.30)$$

where c' is the non-dimensional concentration.

In the case we are going to consider the total potential will be fixed along the edges of the tube in the following manner

$$\phi'_{tot}=\begin{cases}A & \text{for} \quad z'=0, \quad 0\le r'\le 1\\ A\cos(2\pi z') & \text{for} \quad r'=1, \quad 0\le z'\le 1\\ A & \text{for} \quad z'=1, \quad 0\le r'\le 1\end{cases} \quad (6.31)$$

For notational convenience the primes on the z and r variables are omitted from this point and on. With the Dirichlet boundary condition above we have a boundary value problem. A suggestion on how to solve the problem is given in the following. We will proceed by separating variables and expanding the solution on a complete basis set. First we separate the problem into two boundary value problems, see Figure 6.3, One problem with homogeneous boundary conditions and an inhomogeneous PDE and another problem with inhomogeneous boundary conditions and a homogeneous PDE. Given the two solutions ϕ_1 and ϕ_2, respectively, we can find the total potential

$$\phi'_{\text{tot}}=\phi_1+\phi_2. \quad (6.32)$$

With the total electrical potential at hand the non-dimensional concentration distribution can be found

$$c_{\pm} = c_{\pm}^{0} \exp\left(\mp \phi'_{tot}\right). \tag{6.33}$$

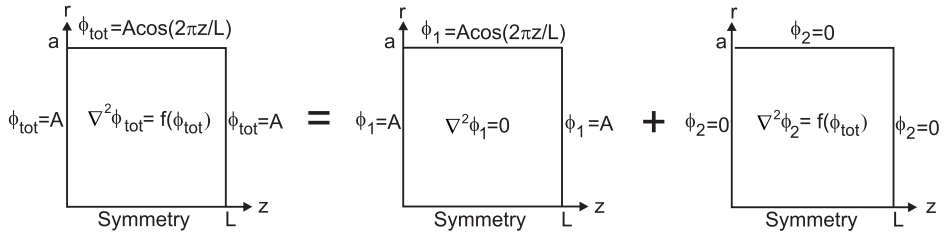

Figure 6.3: Splitting of the boundary value problem into two cases, which are easier solved. Finding ϕ_1 and ϕ_2 the solution is given as: $\phi'_{tot} = \phi_1 + \phi_2$.

We begin by considering the homogeneous PDE. Assuming the solution can be separated, means

$$\phi'_{tot}(r, z) = R(r)Z(z). \tag{6.34}$$

Inserting this into the homogeneous form of the PDE given by equation (6.27) and rearranging yields

$$\frac{r^2R''(r) + rR'(r)}{r^2R(r)} = \frac{-(a/L)^2Z''(z)}{Z(z)} = k \tag{6.35}$$

where k must be some constant independent on r and z, since the fraction on the left-hand side of the first equal sign above is dependent only on r and the fraction on the right-hand side of the first equal sign is dependent only on z. Thus we obtain two ODE's for the radial and axial direction respectively.

$$r^2R''(r) + R'(r) - kr^2R(r) = 0 \tag{6.36}$$

$$Z''(z) + k(L/a)^2Z(z) = 0 \tag{6.37}$$

In order to solve the homogeneous PDE with the inhomogeneous boundary conditions we split the problem into three sub boundary value problems. See figure 6.4. We hence obtain ϕ_1 as the sum of ϕ_{1a}, ϕ_{1b} and ϕ_{1c}.

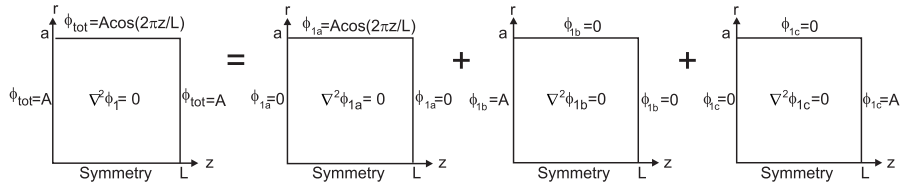

Figure 6.4: Splitting of the boundary value problem into three cases, which are easier solved. Finding ϕ_{1a}, ϕ_{1b} and ϕ_{1c} we obtain: $\phi_1 = \phi_{1a} + \phi_{1b} + \phi_{1c}$.

Firstly consider the BVP with homogeneous BC's at the ends of the tube. Searching for solutions in the axial direction we find that k must be positive to avoid the trivial solution Z(z)=0. Imposing the boundary conditions Z(0)=Z(1)=0, yields the eigenfunctions

$$Z_m(z) = \sin(m\pi z), \quad m \in \mathbf{N} \tag{6.38}$$

With k positive the solution to the ODE for the radial direction, equation (6.36), is given by a linear combination of the modified Bessel functions of zeroth order

$$R_m(r) = CI_0(\gamma_m r) + DK_0(\gamma_m r), \tag{6.39}$$

where C and D are constants to be determined, and $\gamma_m = \frac{am\pi}{L}$. Since $K_0 \to \infty$ for $r \to 0$ we must require $D = 0$. This also ensures that the symmetry condition, $R'(0) = 0$, is fulfilled. At this point we hence assume

$$\phi_{1a}(r, z) = \sum_{m=1}^{\infty} C_m I_0(\gamma_m r) \sin(m\pi z), \tag{6.40}$$

where C_m are constants to be determined from the last boundary condition,

$$\phi_{1a}(1, z) = A\cos(2\pi z) = \sum_{m=1}^{\infty} C_m I_0(\gamma_m) \sin(m\pi z). \tag{6.41}$$

The constants $C_m I_0(\gamma_m)$ can be interpreted as the Fourier sine coefficients of the function $A\cos(2\pi z)$ on the interval $z \in [0, 1]$. Multiplying on both sides of the last equal sign and integrating over all $z \in [0, 1]$ yields

$$A \int_0^1 \{\sin[\pi z(m-2)] + \sin[\pi z(m+2)]\}\, dz = C_m I_0(\gamma_m) \tag{6.42}$$

Integrating we obtain

$$C_k = \frac{2A}{\pi I_0(\gamma_{2k-1})} \left(\frac{1}{2k-3} + \frac{1}{2k+1} \right), \quad k \in \mathbf{N}, \tag{6.43}$$

where we have substituted $m = 2k - 1$, because only uneven m gives non-zero coefficients. Be aware of the case $m = 2$ which must be examined separately by inserting before integrating analytically. The coefficient for $m = 2$, however, also yields zero. Thus we have found

$$\phi_{1a}(r, z) = \sum_{k=1}^{\infty} \frac{2AI_0(\frac{a(2k-1)\pi}{L} r)}{\pi I_0(\frac{a(2k-1)\pi}{L})} \left(\frac{1}{2k-3} + \frac{1}{2k-1} \right) \sin((2k+1)\pi z) \tag{6.44}$$

We could have made the solution more general with a more general boundary condition, say $\phi_{1a}(1, z) = A\cos(n_0\pi z)$, where $n_0 \in \mathbf{N}$ or even $n_0 \in \mathbf{R}$. We will however only consider the special case $n_0 = 2$, which already contains most of the physical aspects of interest. See Appendix B for the coefficients for an arbitrary n_0.

We move on to find ϕ_{1b}, which is the case with homogeneous boundary conditions at the end where $z = 1$ and along the edge where r=1. Searching for

solutions in the radial direction we find that only $k < 0$ gives solutions different from the trivial solution, R(r)=0. Defining $k = -\gamma^2$ the solution is given as a linear combination of the Bessel functions of zeroth order

$$R(r) = CJ_0(\gamma r) + DY_0(\gamma r), \tag{6.45}$$

where C and D are constants to be determined. Immediately we realize that we must require $D = 0$ because $Y_0(r) \to -\infty$ for $r \to 0$. This also ensures that the symmetry condition, R'(0)=0, is fulfilled. The boundary condition $R(1) = 0$ gives

$$J_0(\gamma) = 0 \quad \Rightarrow \quad \gamma = \gamma_n \tag{6.46}$$

where γ_n is the n'th zero point of J_0. In the axial direction we need to solve

$$Z''(z) + (\gamma_n L/a)^2 Z(z) = 0. \tag{6.47}$$

Defining $\lambda_n = \frac{\gamma_n L}{a}$ the solution is given as

$$Z_n(z) = Ae^{-\lambda_n z} + Be^{\lambda_n z}. \tag{6.48}$$

Imposing the boundary condition Z(1)=0 gives the solution

$$\phi_{1b}(r, z) = \sum_{n=1}^{\infty} B_n(e^{\lambda_n z} - e^{\lambda_n(2-z)})J_0(\gamma_n r), \tag{6.49}$$

where B_n are constants to be determined from the boundary condition at $z = 0$,

$$\phi_{1b}(r, 0) = A = \sum_{n=1}^{\infty} B_n(1 - e^{2\lambda_n})J_0(\gamma_n r), \tag{6.50}$$

where $B_n(1 - e^{2\lambda_n})$ can be interpreted as the expansion coefficients of J_0 for $\phi_{1b}(r, 0) = A$. Multiplying on both sides of the second equal sign by $J_0(\gamma_m r)r$ and integrating over all $r \in [0, 1]$ yields

$$B_n = \frac{2A}{\gamma_n J_1(\gamma_n)(1 - e^{2\lambda_n})}. \tag{6.51}$$

Thus we can write the solution

$$\begin{aligned} \phi_{1b}(r, z) &= \sum_{n=1}^{\infty} \frac{2A}{\gamma_n} \frac{J_0(\gamma_n r)}{J_1(\gamma_n)} \frac{e^{\lambda_n z} - e^{\lambda_n(2-z)}}{1 - e^{2\lambda_n}} \\ &= \sum_{n=1}^{\infty} \frac{2A}{\gamma_n} \frac{J_0(\gamma_n r)}{J_1(\gamma_n)} \frac{e^{\lambda_n(z-2)} - e^{-\lambda_n z}}{e^{-2\lambda_n} - 1}. \end{aligned} \tag{6.52}$$

The last fraction involving the exponentials have been paraphrased in order to avoid that any of the terms tends towards infinity for $n \to \infty$. This is quite important when implementing the series in a computer program, since the number of terms possible to calculate otherwise would be very limited. The solution ϕ_{1c} is similar to the above derivations found to be

$$\phi_{1c}(r, z) = \sum_{n=1}^{\infty} \frac{2A}{\gamma_n} \frac{J_0(\gamma_n r)}{J_1(\gamma_n)} \frac{e^{\lambda_n(z-1)} - e^{-\lambda_n(z+1)}}{1 - e^{-2\lambda_n}}. \tag{6.53}$$

Finally we expand the solution for the inhomogeneous boundary value problem with homogeneous boundaries on a complete basis set

$$\phi_2(r,z) = \sum_{n=1}^{\infty}\sum_{m=1}^{\infty} E_{mn}\sin(m\pi z)J_0(\gamma_n r), \tag{6.54}$$

where E_{mn} are constants to be determined. Notice that the boundary conditions are satisfied regardless of E_{mn}. Inserting into the inhomogeneous PDE we obtain

$$\sum_{n=1}^{\infty}\sum_{m=1}^{\infty} E_{mn}\sin(m\pi z)r^2\left(\gamma_n^2 + \left(\frac{am\pi}{L}\right)^2\right)J_0(\gamma_n r) = r^2 f(\phi'_{tot}), \tag{6.55}$$

where $f(\phi'_{tot})$ is given by equation (6.28). Notice we have not inserted equation (6.55) into $f(\phi'_{tot})$. Later we are going to deal with this problem, as ϕ'_{tot} will be sought iteratively. Assume $f(\phi'_{tot})$ to be known in the following. Firstly we notice that r^2 can divided out from the above equation (6.55). Then multiplying both sides by $sin(n'\pi z)J_0(\gamma_{m'})r$ and integrating over all $r, z \in [0,1]$ yields

$$E_{mn} = -\frac{4\int_0^1\int_0^1 f(\phi'_{tot}(r,z))\sin(m\pi z)J_0(\gamma_n r)rdrdz}{\left(\gamma_n^2 + \left(\frac{am\pi}{L}\right)^2\right)J_1^2(\gamma_n)}, \tag{6.56}$$

which inserted in equation (6.54), gives the solution to the inhomogeneous equation, ϕ_2.

6.4 Numerical Solution

The expressions derived in the previous section have been implemented in a MatLab code to obtain solutions. A pseudo code is shown in figure 6.5.

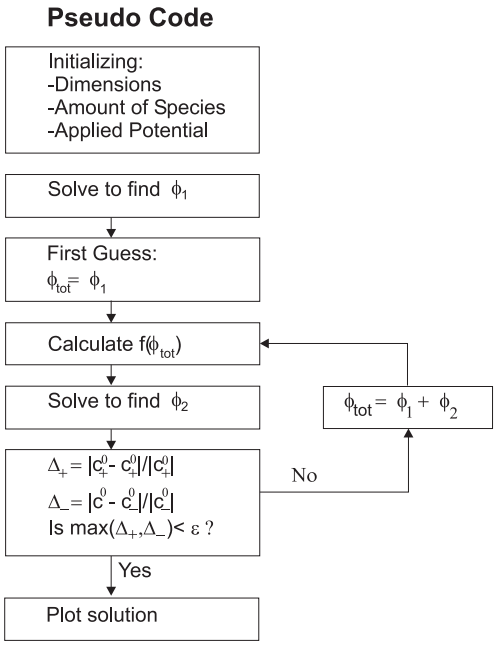

Figure 6.5: Flow chart sketching the pseudo code.

The entire MatLab code for the above flow chart is given in Appendix C. With the solution procedure described above no guarantees are given regarding convergence, and unfortunately, the iteration procedure only converged for very low concentrations.

Other ways of solving this boundary value problem might be attempted. For example a finite difference discretization combined with some iteration procedure for the non-linear term. Another possibility is to use existing CFD software. Using CFD software the entire time dependent solution ought to be obtainable. Attempts to use Coventor for this purpose was made. However, the Coventor software had some very unfortunate limitations. In order to generate a geometry where the electrodes are electrically isolated from the channel containing the ions, internal walls are needed. See Figure 6.6. The electrodes need to be isolated from the species, because the species otherwise is absorbed by the electrodes.

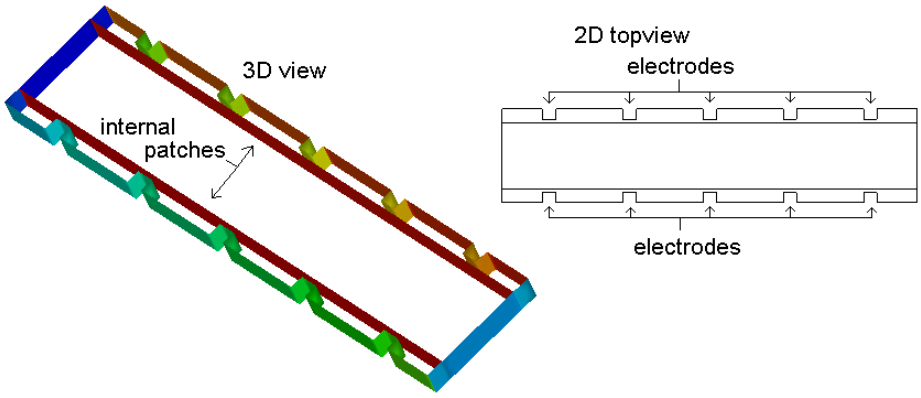

Figure 6.6: Flow chart sketching the pseudo code.

It is possible to specify the condition `Wall` to the internal patches. However, after extensive correspondence with the Coventor Support group in Amsterdam, I have realized that the `Wall` condition only behaves as a wall in respect to fluids driven by convection. When fluids move by diffusion the internal walls are simply nonexisting, meaning that fluids can diffuse through internal patches with the condition `Wall` specified. Species cannot, however, diffuse through Non-internal patches given the `Wall` condition. For this reason it is not possible to isolate the electrodes from the species.

In the following solution examples from the MatLab program are given. Each example begins with a box listing the important parameters for the simulation: L is the length of the tube, a is the radius of the tube, c is the concentration, T is the temperature, A is the voltage specified at the ends of the tube, and ϵ_c is the convergence criteria on c_+^0 and c_-^0.

Example 1:
In Figure 6.7 the distribution of positive and negative ions is given. The parameters used are given in the box below

$L = 100\mu\text{m}$, $a = 10\mu\text{m}$, $c = 10^{-12}\text{mol m}^{-3}$, $T = 298\text{K}$, $A = 0.1\text{V}$, $\epsilon_c = 2e-4$

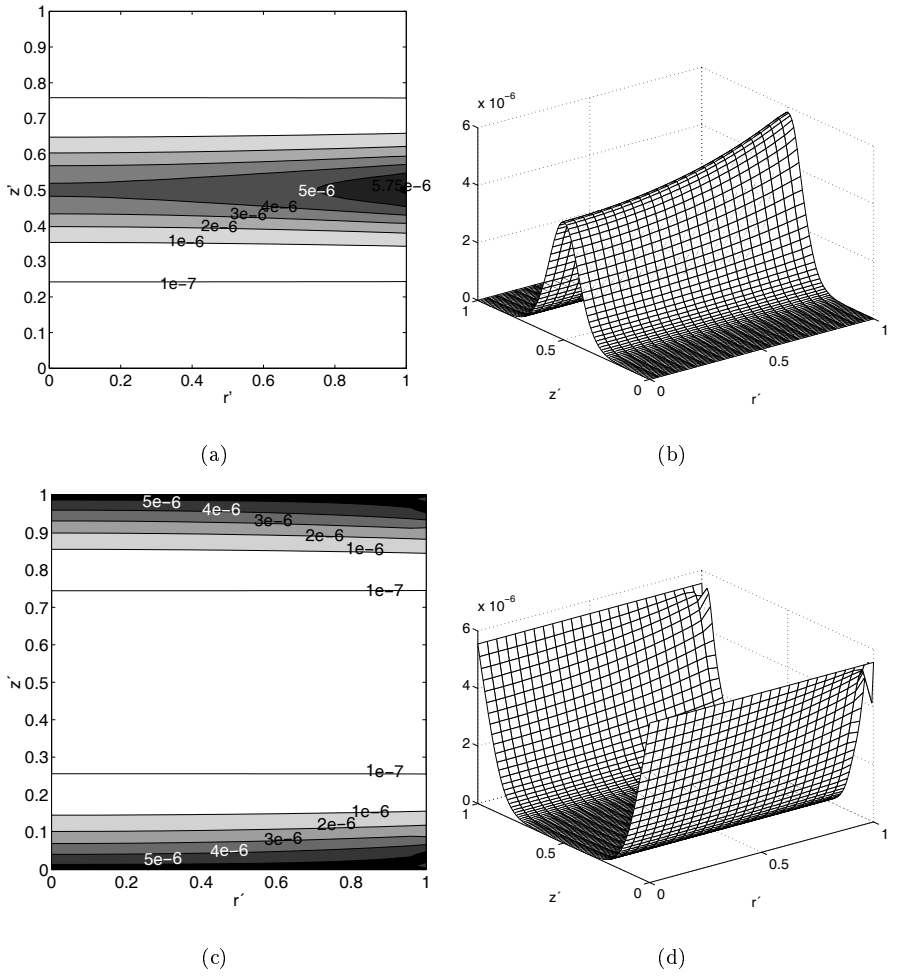

Figure 6.7: Distribution of positive and negative ions. Panels (a) and (b) show how the positive ions have been driven into the middle of the tube. Panels (c) and (d) show how the negative ions have been driven out to the ends of the tube.

Example 2:
In Figure 6.7 the distribution of positive and negative ions is given. The parameters used are given in the box below

$L = 100\mu\text{m}$, $a = 5\mu\text{m}$, $c = 10^{-12}\text{mol m}^{-3}$, $T = 298\text{K}$, $A = 0.1\text{V}$, $\epsilon_c = 2e-4$

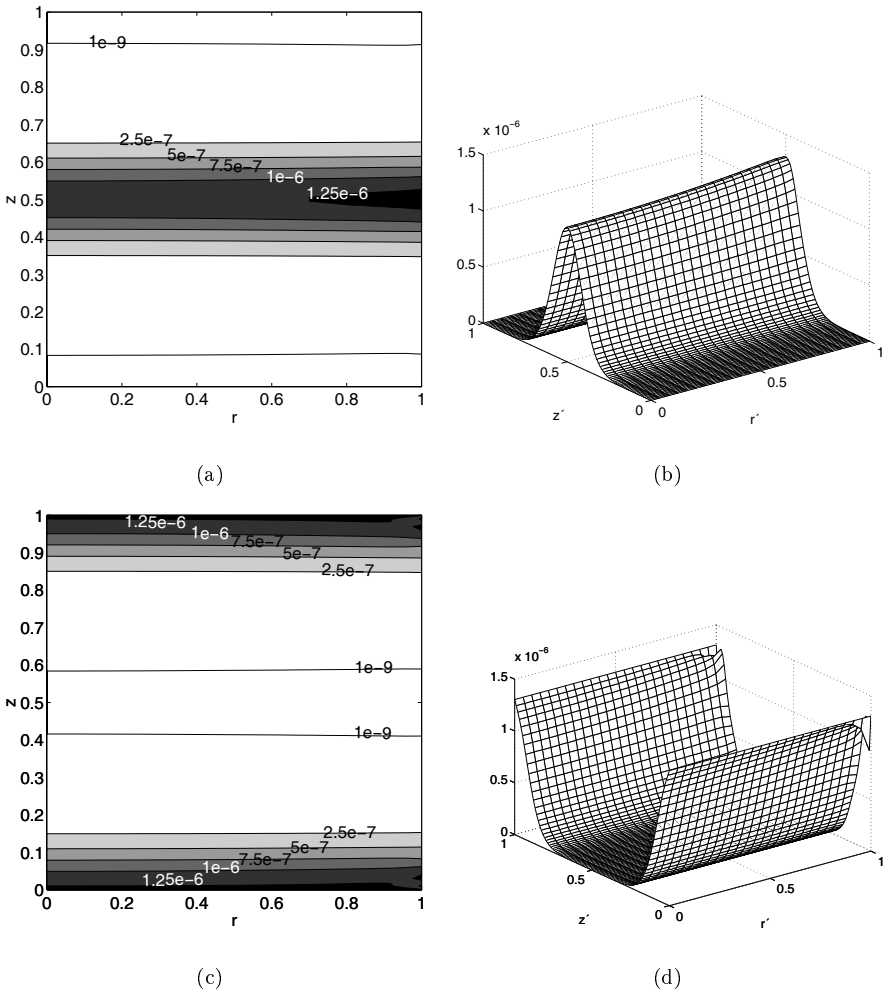

Figure 6.8: Distribution of positive and negative ions. Panels (a) and (b) show how the positive ions have been driven into the middle of the tube. Panels (c) and (d) show how the negative ions have been driven out to the ends of the tube.

Chapter 7

CFD Applied to Dispersion Problems

In the following chapter different simulations concerning the dispersion of a sample travelling in a microchannel will be presented. In Table 7.1 a table is given with diffusion coefficients for different solutions. We will use the self diffusion coefficient for water as a starting point for the simulations presented in this chapter.

Chemical	Diffusion Coefficient/$(m^2\ s^{-1})$
Water(in water)	2.26×10^{-9}
Ethanol	1.24×10^{-9}
K^+	9.60×10^{-10}
H^+	9.31×10^{-9}
Na^+	1.33×10^{-9}
OH^-	5.30×10^{-9}
Cl^-	2.03×10^{-9}
Glycine	1.06×10^{-9}
Dextrose	6.73×10^{-10}
Succrose	5.22×10^{-10}

Table 7.1: Selected diffusion coefficients for different dilute solutions in water at the temperature: 298 K.

For the simulations presented we will apply the finite volume method. A thorough description of this method is given by Versteeg and Malalasekera (1994). We will consider two different geometries. Firstly, two straight channels connected by a 180° turn will be studied. Secondly, we will consider a special spiral geometry, which, in fact, is constructed by turns and straight channels.

However, several problems arise regarding the measuring of dispersion even before we can study the results. This will be the subject of the first section.

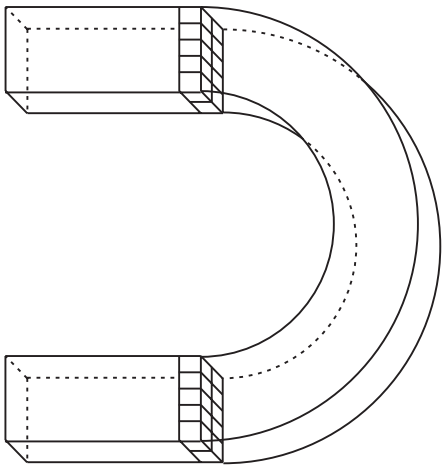

Figure 7.1: Sketch of the grid and the geometry used in the numerical simulation of flow taking a 180° turn.

7.1 Measuring the Dispersion

In Chapter 5 we mention that often dispersion is measured in terms of the standard deviation of the species concentration profile. In this context the standard deviation σ is found as follows: (1) Find the mean concentration in each cross section of the channel, and plot it as function of the length coordinate of the channel. (2) Calculate the standard deviation of the obtained curve. If the concentration profile is a Gaussian, 4σ corresponds to 95.5% of the sample. When comparing simulation results with respect to dispersion we simply compare the σ values.

It is not in Coventor possible directly to obtain a measure of σ as function of time. However, it is possible to obtain a value, as function of time, of some quantity in a region specified by the user. Say, we specify two box shaped regions with a width of one cell, one just before the turn inlet and one just after the turn outlet. A sketch of these regions are shown in Figure 7.1. We can thus get the amount of species in the cell layer just before the turn as function of time, and on the basis of this obtain a time based standard deviation σ_{in}. Similarly obtaining a time based standard deviation for the turn outlet, we can obtain another time based standard deviation σ_{out}. The difference, $\sigma_{\text{out}} - \sigma_{\text{in}}$, then corresponds to the dispersion caused by the turn including diffusion.

The time based standard deviation obtainable as described above, is different to the standard deviation obtained at a specific time, because the first part of a sample entering a measuring region will have experienced less diffusion than the last part of the sample going through the measuring region.

The above described way of measuring dispersion does not require anything on the distribution of the sample. If we on the other hand assume that the sample is distributed as a Gaussian at all times we have another possibility: Reading off the peak concentration at each time step we can calculate the standard deviation, and thus get is as a function of time. This procedure will be applied in one of the following sections.

7.2 Parametric Studies

In this section we will investigate when good convergence is obtained. Parameters such as grid cell size, solution tolerance and magnitude of time steps will be estimated for the simulations following in the next sections.

7.2.1 Pressure Driven Flow in a Turn

We consider a 180° turn with a rectangular cross section. The inner radius is: $r_i = 150$ μm and the width is: $w = 50$ μm. Three different depths are investigated: $h = 25$ μm, $h = 50$ μm, and $h = 75$ μm. The flow is pressure driven with a pressure drop of $\Delta P = 1 \times 10^{-6}$ MPa.

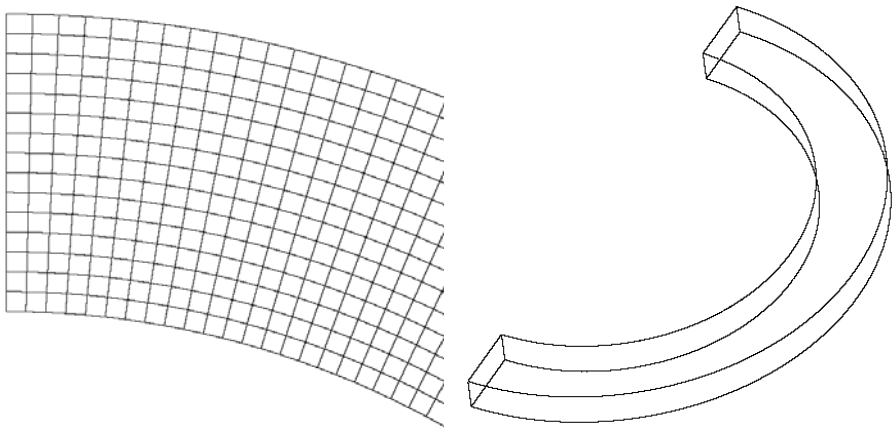

(a) (b)

Figure 7.2: Sketch of the grid and the geometry used in the numerical simulation of flow taking a 180° turn.

The simulation results are shown in Appendix F. In Chapter 4 an analytical expression has been derived for the velocity profile in a turn with a rectangular cross-section. A MatLab program to calculate the profile has been developed to obtain values to compare with the simulations. The code is shown in Appendix G. From the program we have found the flow rate and the maximum velocity, which are given in Table 7.2. In the MatLab code the size of the matrices containing the velocities were increased to obtain convergence of the flowrate and the maximum velocity. From the charts given in Appendix F, we notice that convergence was obtained for 50×50 matrices. The calculations with 100×100 matrices did not change the result within the accuracy given in Table 7.2. The number of terms needed in the basis function expansions for the velocity was also increased until convergence. A contour plot of the velocity for the 25 μm deep turn is shown in figure 7.3. The contour plot is obtained with the MatLab code in Appendix G.

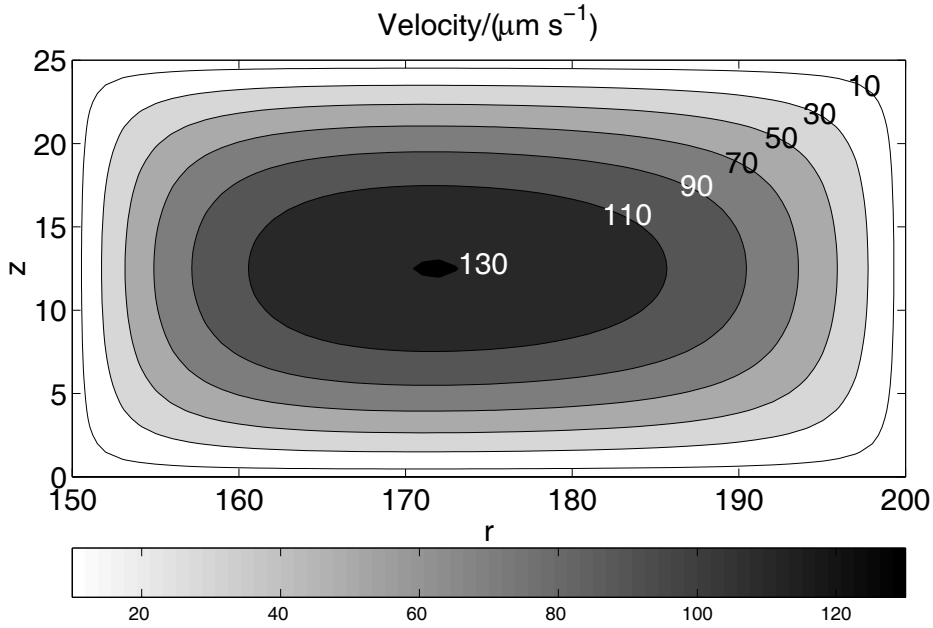

Figure 7.3: Contour plot of the velocity profile in the cross section of a 180° turn. The pressure drop from turn inlet to turn outlet is 1×10^{-6} MPa. The contour plot is obtained with the MatLab code in Appendix G.

Depth/μm	$\frac{\text{Flowrate(MatLab)}}{\mu\text{m}^3\ \text{s}^{-1}}$	$\frac{\text{Flowrate(Coventor)}}{\mu\text{m}^3\ \text{s}^{-1}}$	Deviation
25	0.81×10^5	0.83×10^5	2.31%
50	3.99×10^5	4.03×10^5	0.90%
75	8.32×10^5	8.38×10^5	0.73%

Table 7.2: Results obtained using the MatLab code given in Appendix G and selected simulation results. For the simulation results the cell size is 2.5μm.

The cells at the inner radius are closest to being cubic. We define the *cell size* as being the edge length of the cubic cell. The cells have been made cubic as there are no directions more important than others when a species is introduced. The concentration gradient of the species should be equally well resolved in all directions in order to avoid a dominant numerical diffusion[1] in one of the directions.

Consider the simulation results given in Appendix F. For each cell size the solution tolerance has been increased until convergence in the flow rate deviation was obtained. Convergence is approximately obtained in the interval from 10^{-6} to 10^{-8} for the solution tolerance. In some of the cases shown in Appendix F the flow rate deviation increases as the tolerance is decreased. See Table 7.3.

[1] Discretizations of terms in differential equations may yield terms similar to diffusion terms.

Res File	Sol. Tol.	FlowRate	Max Vel.	FlowRate deviation
turn5015res1	10^{-4}	4.003×10^5	3.309×10^2	0.33%
turn5015res2	10^{-6}	4.052×10^5	3.354×10^2	1.55%
turn5015res3	10^{-8}	4.053×10^5	3.355×10^2	1.58%

Table 7.3: Example of the simulation results shown in Appendix F. Sol. Tol. is an abbreviation for solution tolerance. We notice that decreasing the the solution tolerance actually increase the FlowRate deviation, which might not be expected. The important thing is, however, that the FlowRate deviation converge as the solution tolerance is decreased.

Table 7.3 should not be misinterpreted in the way that a numerically large tolerance gives better results. Convergence must be found for the flow rate deviation for each cell size, before statements about the accuracy of a given cell size can be given.

The results shown in Appendix F gives the clear picture that decreasing the cell size also decreases the deviation between the theoretical expected value and the simulated, which is the important feature to notice in Appendix F.

From the results in Appendix F we also observe that keeping the cell size constant and increasing the depth of the channel, the flow rate deviation decreases. This can be interpreted in the following way: to obtain a small flow rate deviation it is important how many cells there are in each cross section of the turn, the physical dimensions of the turn are less important[2], because more cells give a better resolution of the velocity profiles.

The above grid dependency analysis will be used in the process of constructing the systems investigated in the following sections. We have obtained an idea of how fine grids should be, to obtain acceptable accuracies. We will accept a flow rate deviation in the range from 1% to 3%. It is with the current computer performances difficult to obtain more accurate solutions when making time dependent simulations. Steady state solutions were typically obtained within 1-2 hours. The time dependent simulation results, however, were typically obtained after 6 to 18 hours of simulation time.

7.2.2 Diffusion in a Straight Channel

In this subsection we will investigate the grid dependency with respect to diffusion. How fine a mesh is needed before we can trust the results? To this end we will consider a box shaped channel with the width $w = 50\mu$m, depth $d = 25\mu$m, and length $l = 500\mu$m. The box is open in both ends so the sample is able to diffuse out of the volume. Within this box we place a sample with a Gaussian density distribution in the length direction and equal in concentration in all cross sections. We can calculate analytically the time it takes for the peak concentration to drop to half its initial value. Comparing this value to simulated values we obtain a measure of how well the diffusion is simulated. The mean concentration for each cross section is given as

$$c(x,t) = \frac{S}{2\sqrt{(\pi D(t_0+t))}} \exp\left(\frac{-x^2}{4D(t+t_0)}\right), \tag{7.1}$$

[2]Of course, the dimensions cannot be increased to the extent that we enter the turbulent flow regime.

where x is the space coordinate in the length direction, D is the diffusion coefficient, and t is time. t_0 is the time it would take for the delta function, $c_\delta(x) = S\delta(x)$, to diffuse into the shape of $c(x,0)$. S determine how much species there is in total. When the initial standard deviation σ of the Gaussian is known t_0 is found as follows

$$t_0 = \frac{\sigma^2}{2D}. \tag{7.2}$$

The peak value as function of time is given by

$$c_{peak} = \frac{S}{2\sqrt{\pi D(t_0 + t)}}. \tag{7.3}$$

The time $t_{1/2}$ it takes for the peak concentration to fall to half its initial value is found to be

$$t_{1/2} = 3t_0 = \frac{3\sigma_0^2}{2D} = \frac{3\sigma_C^2}{4D}, \tag{7.4}$$

where σ_0 is the standard deviation of the sample at the initial stage. The σ_C is a Coventor parameter specifying the initial shape of the sample, which quite oddly is defined different from the usual standard deviation. The results of a series of simulations are shown in Table 7.4. From Table 7.4 we see as expected that decreasing the cell size, solution tolerance or time step also decreases the deviation between the theoretically expected $t_{1/2}$

$$t_{1/2} = \frac{3\sigma_C^2}{4D} = \frac{3(50\mu\text{m})^2}{4 \cdot 2.26 \times 10^3 \mu\text{m}^2\,\text{s}^{-1}} = 0.830\,\text{s}, \tag{7.5}$$

and the $t_{1/2}$ found from the simulations. All deviations are below 1% indicating that diffusion is quite well simulated even for relatively coarse grids, large time steps and high solution tolerances.

Cell size/μm	Sol. Tol.	Time step/s	$t_{1/2}/s$ estim.	$t_{1/2}$ deviation
10	10^{-4}	0.1	0.823	0.84%
10	10^{-4}	0.01	0.828	0.22%
10	10^{-7}	0.1	0.831	0.11%
5	10^{-4}	0.1	0.832	0.28%
5	10^{-4}	0.01	0.830	0.07%
5	10^{-4}	0.001	0.829	0.10%
5	10^{-7}	0.1	0.832	0.24%
5	10^{-7}	0.01	0.829	0.10%

Table 7.4: Grid dependency analysis for diffusion in a box. Only diffusion make the sample disperse. The diffusion coefficient for water in water has been chosen: $D = 2.26 \times 10^3\,\mu\text{m}^2\,\text{s}^{-1}$.

Two extra simulations were made to investigate the effect of driving the flow with electroosmosis, i.e. a flat velocity profile, no gradients. The results are shown in Table 7.5.

Cell size/μm	Sol. Tol.	Time step/s	$t_{1/2}/s$ estim.	$t_{1/2}$ deviation
5	10^{-4}	0.01	0.830	0.07%
5	10^{-4}	0.0025	0.830	0.07%

Table 7.5: Grid dependency analysis for diffusion in a box. The species diffusing is driven by electroosmosis, meaning a constant velocity profile. As we have no velocity gradients only diffusion should make the sample disperse. The diffusion coefficient for water in water has been applied: $D = 2.26 \times 10^3\ \mu\mathrm{m}^2\ \mathrm{s}^{-1}$.

Hence, comparing to the grid dependency analysis of the velocity profile in a turn, it is the resolution of the velocity profile determines the cell size required for acceptable convergence rather than diffusion. We have here only compared with the velocity profile made by a pressure driven flow. E.g. velocity profiles for flows driven with electroosmosis in a turn could also be considered.

In the following simulations grid cell sizes and solution tolerances will be chosen with the analysis above in mind.

7.3 Dispersion in a Turn, Part 1

In this section we will examine simulation results using the time based standard deviation found from the turn-inlet/turn-outlet discharge of species as functions of time. We will consider three different cases for flow in two straight channels connected by a 180^o turn. See Figure 7.4.

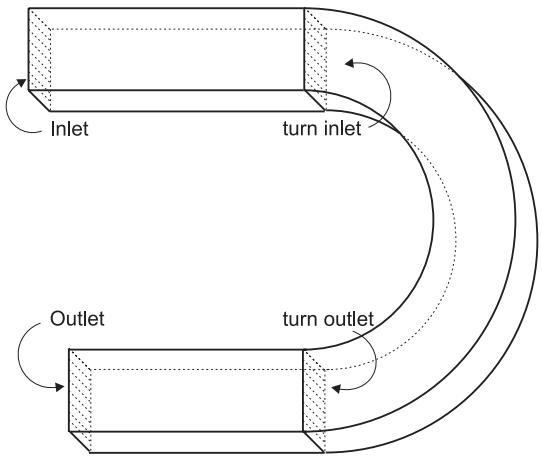

Figure 7.4: Sketch of two straight channels connected by a 180^o turn.

- First, the simple case with the same electroosmotic mobility at all walls. At inlet and outlet no pressure is specified, meaning that no pressure difference exist anywhere in the system. At the inlet and outlet the voltages U_{in} and U_{out} are specified, yielding an electric field in the system driving the fluid. The electric field is found by solving the Laplace equation in the whole geometry.

- Secondly, we consider a case where the turn is short circuited. Practically we imagine it possible to place electrodes so that no potential gradients are present in the turn. E.g. four electrodes with voltages: $U_1 > U_2 = U_3 > U_4$. Place U_1 at the inlet of the whole system, place U_2 at the turn inlet, U_3 at the turn outlet, and U_4 at the outlet of the whole system. This setup is, however, not possible to create using Coventor, because this would require internal patches with a voltages applied. It is not possible to obtain a transport of species through a patch with a specified boundary condition, such as a voltage[3].

  Instead we will choose the electroosmotic mobility of the walls in the turn to be zero. This gives effectively the same velocity boundary conditions as short circuiting the turn would have done, since the velocity at the boundaries is the product of the electric field and the electroosmotic mobility.

- In the third case we will consider the system with modified electroosmotic mobilities at the walls of the turn. The mobilities have been changed according to equations (5.79) and (5.80) for the 2D case.

Consider electroosmotic driven flow in two straight channels connected by a turn. Earlier on we have discussed the problems arising when a sample enters such a turn. The sample will be dispersed because of the geometric effect. Furthermore the sample will be dispersed because of the higher velocity at the inner wall compared to the outer wall. Say, we short circuit the turn. Then the last effect is eliminated. However, unfortunately another source of dispersion arises: Gradients in the velocity profile. The flow in the turn is now pressure driven with no-slip boundary conditions. Not only do we obtain gradients in the velocity profile in the turn, there will also be velocity profile gradients in the straight channels.

At first we will consider the 2D case of this problem. See Figure 7.5. The 2D case contains all of the interesting physical aspects of the problem. This is followed by simulations to support the reason for trusting the simulation results from Coventor. Secondly 3D simulations are made to obtain physically realistic results.

[3] It is possible to have a species transport through an internal patch if no boundary condition is specified.

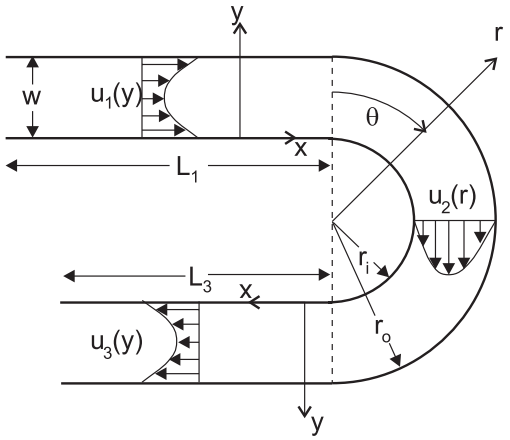

Figure 7.5: Sketch of the two straight channels connected by a 180° turn. The 2D flow profiles are sketched to illustrate that short circuiting the turn affects the profiles in the electroosmotic flow in the straight channels.

There will be a certain transition zone when going from a straight channel to the turn and vice versa. Far from this zone the velocity profiles can be assumed to be dependent only on r in the turn and y in the straight parts. Assuming the flow to be inertia free the extension of these zones will be zero. The Reynolds number is approximately

$$Re = \frac{Uw}{\nu} = \frac{100 \times 10^{-6}\mathrm{m/s} \quad 50 \times 10^{-6}\mathrm{m}}{1 \times 10^{-6}\mathrm{m}^2/\mathrm{s}} = 5 \times 10^{-3}, \tag{7.6}$$

where U is a characteristic velocity, w the width of the channel, which is a characteristic length scale and ν is the kinematic viscosity. This very small Reynolds number indicates that we can indeed assume the flow to be inertia free. The Navier-Stokes equation in cylindrical coordinates yield the profiles

$$u_1(y) = C_1(y^2 - wy) + u_1^*, \tag{7.7}$$

$$u_2(r) = C_2\frac{r}{2}\left[\ln(r) - \frac{1}{2}\right] + \frac{1}{2}Ar + \frac{B}{r}, \tag{7.8}$$

$$u_3(y) = C_3(y^2 - wy) + u_3^*, \tag{7.9}$$

where u_1^* is the electroosmotic given velocity at the wall in the first straight channel and u_3^* is the corresponding velocity in the last channel. A and B remains to be determined from the no-slip boundary conditions. C_1, C_2 and C_3 are given by

$$C_1 = \frac{1}{2\mu}\frac{\partial p}{\partial x}, \quad C_2 = \frac{1}{\mu}\frac{\partial p}{\partial \theta}, \quad C_3 = \frac{1}{2\mu}\frac{\partial p}{\partial x}. \tag{7.10}$$

Since the pressure is varying linearly along the length of the straight channels and varying linearly with the angle in the turn we write

$$C_1 = \frac{p_1 - p_0}{2\mu L1}, \quad C_2 = \frac{p_3 - p_1}{\mu\pi}, \quad C_3 = \frac{p_0 - p_3}{2\mu L3}. \tag{7.11}$$

Requiring the discharges in the straight channels to equal the discharge in the turn gives relations eliminating p_1 and p_3 from the equations. p_0 is a boundary condition to be chosen at the ends of the system. The pressure gradients in the system is independent of p_0, likewise is the velocity profiles. The absolute pressures, however, do depend on p_0.

The procedure described above to find C_1, C_2, and C_3 and so the velocity profiles can be made analytically. It is, however, quite a task to perform the algebra by hand. Therefore the profiles have been found using Mathematica. In Figure 7.6 a plot of the velocity profiles are shown for the case:

$$u_1^* = u_3^* = 200\mu\mathrm{m\,s}^{-1},\ L_1 = 300\mu\mathrm{m},\ L_3 = 700.$$
$$\mu = 10^{-3}\,\mathrm{kg\,m}^{-1}\,\mathrm{s}^{-1},\ r_i = 150\mu\mathrm{m},\ r_o = 200\mu\mathrm{m},\ w = 50\mu\mathrm{m}.$$

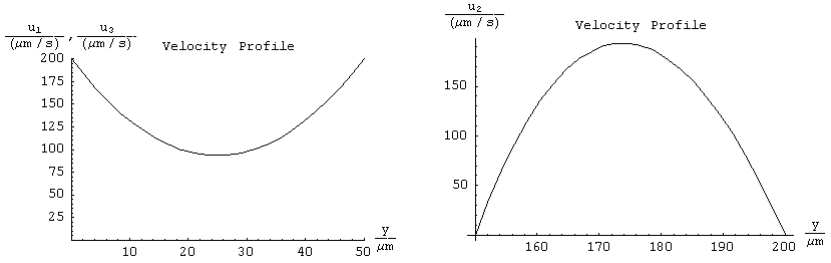

(a) (b)

Figure 7.6: The velocity profiles for the system shown in Figure 7.5. The profiles u_1 and u_3 are equal because the boundary velocities u_1^* and u_3^* are equal.

In Figure 7.7 the analytical expressions for the profiles are given. Would it be possible to improve the velocity profiles? Consider the case where there is equal electroosmotic mobilities in the straight channels before and after the turn. This is the case in many real experiments, when all walls are composed of the same material. If the velocity profile in the straight channels are constant the discharge is: $Q = Uw$, where U is the constant velocity and w is the width of the channel. Let us denote the pressure difference across the turn needed to produce the same discharge, ΔP. Cunningly we place this pressure difference across the whole system, so that the pressure at the inlet is ΔP higher than at the outlet. The effect must be that no pressure drop can exist in the straight channels. The entire pressure drop must exist across the turn, yielding constant velocity profiles in the straight channels and a parabola-like velocity profile in the turn. A 3D simulation showing such a profile is presented in Figure 7.8.

```
u1new = Simplify[u1[y] /. C1 → (p1 - p0)/(2 μ L1) /. p1s]

ulb -
  (6 (w - y) y (- (ri^2 - ro^2) (3 L3 (ri^2 - ro^2) (ulb - u3b) - 2 π ulb w^2) + 12 L3 ri^2
        ro^2 (ulb - u3b) Log[ri]^2 - 24 L3 ri^2 ro^2 (ulb - u3b) Log[ri] Log[ro] +
      12 L3 ri^2 ro^2 (ulb - u3b) Log[ro]^2)) /
   (w^2 (- (ri^2 - ro^2) (3 L1 ri^2 + 3 L3 ri^2 - 3 L1 ro^2 - 3 L3 ro^2 - 2 π w^2) +
      12 (L1 + L3) ri^2 ro^2 Log[ri]^2 - 24 (L1 + L3) ri^2 ro^2 Log[ri] Log[ro] +
      12 (L1 + L3) ri^2 ro^2 Log[ro]^2))

u2new = Simplify[Simplify[u2[r] /. consts] /. C2 → (p3 - p1)/(μ Pi) /. p1s /. p3s]

(12 (L1 ulb + L3 u3b) w
    (r^2 (ri^2 - ro^2) Log[r] + ri^2 (-r^2 + ro^2) Log[ri] + (r^2 - ri^2) ro^2 Log[ro])) /
  (r ((ri^2 - ro^2) (3 L1 ri^2 + 3 L3 ri^2 - 3 L1 ro^2 - 3 L3 ro^2 - 2 π w^2) -
      12 (L1 + L3) ri^2 ro^2 Log[ri]^2 + 24 (L1 + L3) ri^2 ro^2 Log[ri] Log[ro] -
      12 (L1 + L3) ri^2 ro^2 Log[ro]^2))

deltaP = Flatten[Simplify[Solve[Q2 == ulb w, p3]]]

{p3 → (8 π (ri^2 - ro^2) ulb w μ) / ((ri^2 - ro^2)^2 -
      4 ri^2 ro^2 Log[ri]^2 + 8 ri^2 ro^2 Log[ri] Log[ro] - 4 ri^2 ro^2 Log[ro]^2)}
```

Figure 7.7: Results extracted from Mathematica. *u1new* corresponds to the u_1 and u_3 velocity profiles. *u2new* corresponds to the u_2 velocity profile. *deltaP* corresponds to equation (7.12).

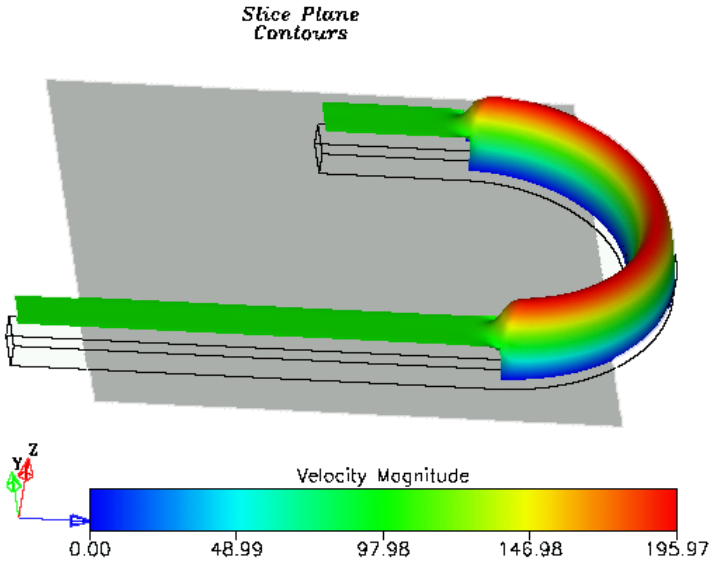

Figure 7.8: The velocity profile for a slice plane placed at the z-value equal to half the depth of the channel. A pressure drop from inlet to outlet has removed the velocity gradients in the straight channels.

Using Mathematica an analytical expression for ΔP for the 2D case is found, after some simplifications, to be

$$\Delta P = \frac{8\pi w\mu(r_i^2 - r_o^2)u_1^*}{r_i^2 - r_o^2 - 4r_i^2 r_o^2 \left[\ln\left(\frac{r_i}{r_o}\right)\right]^2}, \tag{7.12}$$

after some simplification of the expression given in Figure 7.7. The above formula is used in the following 2D simulations. In many microfluidic systems the microchannels are meanders with several 180° turns. Consider a meander having n short circuited turns. The pressure drop needed across the entire meander ΔP_{tot} to avoid velocity gradients in the straight channels of the meander must then simply be

$$\Delta P_{\text{tot}} = n\,\Delta P. \tag{7.13}$$

Removing the velocity profile gradients in the straight channels only diffusion contributes to the dispersion of a sample. Thus yielding less dispersion compared to the case without a pressure drop over the whole system. Now, the question is: Will the effect of removing the velocity gradients in the straight channels reduce the overall dispersion compared to the common case electroosmotic flow in the turn? Simulations are needed to answer this question.

7.3.1 Simulations

For the following simulations we will use the physical properties of water as they are given by Coventor.

Density(kg/μm^3)	9.9982×10^{-16}
TCE(1/K)	1.8000×10^{-4}
ThermalCond(pW/μmK)	$5.9840 \times 10^{+5}$
SpecificHeat(pJ/kgK)	$4.1800 \times 10^{+15}$
ElectricCond(pS/μm)	$1.0000 \times 10^{+2}$
Dielectric	$8.0200 \times 10^{+1}$
Viscosity(kg/μm/s)	1.0020×10^{-9}

Table 7.6: Physical properties for water used by Coventor.

The physical parameters given below are used for the simulation series presented in Figure 7.9.

$L_1 = 300\mu$m	$L_2 = 50\mu$m
$r_i = 150\mu$m	$r_o = 200\mu$m
$\Delta U = 10V$	$EO_{\text{mobility}} = 30000\ \mu\text{m}^2\ \text{V}^{-1}\ \text{s}^{-1}$

Table 7.7: Physical parameters of the channel used in the simulations.

The most important features of Figure 7.9 have been summarized in Table 7.8. In the Table we have given the T_D values for the outlet, only, where

$$T_D = 4\sigma. \tag{7.14}$$

The T_D values for the inlet are practically equal for simulations having the same diffusion coefficient. This was expected because only diffusion contributes to the dispersion in the straight channels. This is also the case for the short circuited turn, because we have applied a pressure drop across the whole system cancelling out the velocity gradients in the straight channels. From the T_D values measured at the outlet we can determine the effect of short circuiting turns in microchannels. From the table below we conclude that short circuiting the turns will increase the dispersion caused by the turn. Moreover, we conclude that optimizing the electroosmotic mobility in the turn according to equations (5.79) and (5.80) will decrease the dispersion.

D$/(\mu\mathrm{m}^2\,\mathrm{s}^{-1})$	T_D/s (short circuit)	T_D/s (EO in turn)	T_D/s (optimized EO)
226	1.754	0.949	0.445
2260	1.371	1.310	1.252

Table 7.8: Results from a 2D simulation. The T_D values are measured at the outlet. The T_D values measured at the inlet were practically equal for simulations having the same diffusion coefficient. From the above we conclude that short circuiting a turn increases the dispersion. Furthermore we notice that optimizing the electroosmotic mobilities according to equations (5.79) and (5.80) will decrease the dispersion.

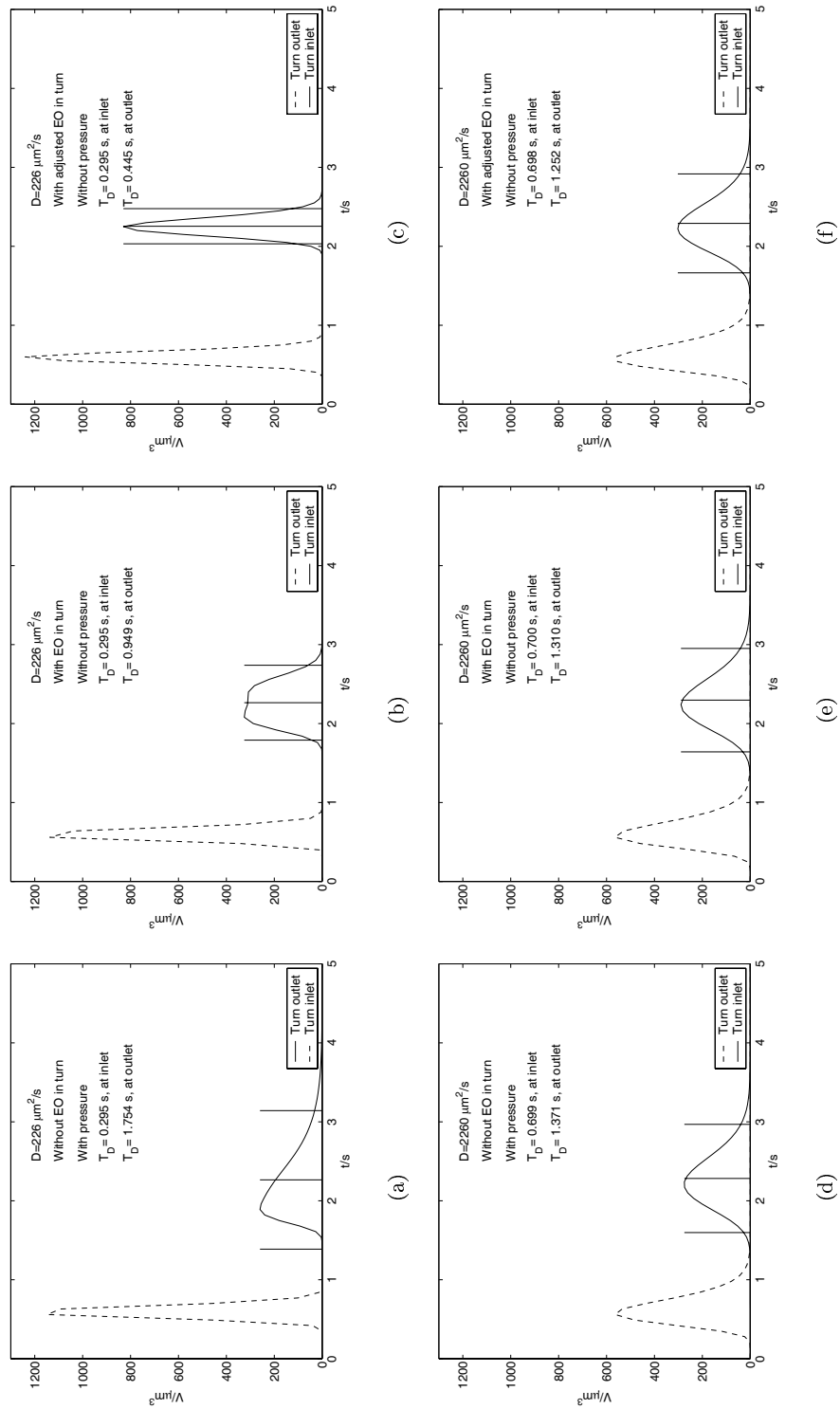

Figure 7.9: Figures (a) and (d) are examples of the short circuited turn made with an applied pressure to remove velocity gradients in the straights. Figures (b) and (e) are made with all walls, also the turn, having the same electroosmotic mobility. Figures (c) and (f) are made with optimised electroosmotic mobilities in the turn according to equations (5.79) and (5.80).

7.3.2 3D Simulations

We have concluded that short circuiting turns increase the dispersion for 2D geometries. In Figure 7.10 four simulations are presented for a 3D case. A pressure drop over the whole system has been added in order to remove velocity gradients in the straight channels for the short circuited cases. A plot of the geometry can be seen in Figure 7.4. The velocity profile on the figure corresponds to the short circuited turn. The results are summarized in Table 7.9. We notice that without diffusion the short circuited turn clearly yield much more dispersion. For the case with $D = 2260\,\mu\mathrm{m}^2\,\mathrm{s}^{-1}$ there is practically no difference in the dispersion. We thus conclude that short circuiting the turns in microchannels does not yield less dispersion for both 2D and 3D cases.

$\mathrm{D}/(\mu\mathrm{m}^2\,\mathrm{s}^{-1})$	T_D/s (short circuit)	T_D/s (EO in turn)
0	6.753	3.545
2260	6.915	6.962

Table 7.9: Results from 3D simulations. The T_D values are measured at the outlet. The T_D values measured at the inlet were practically equal for simulations having the same diffusion coefficient. From the above we conclude that short circuiting a turn increases the dispersion.

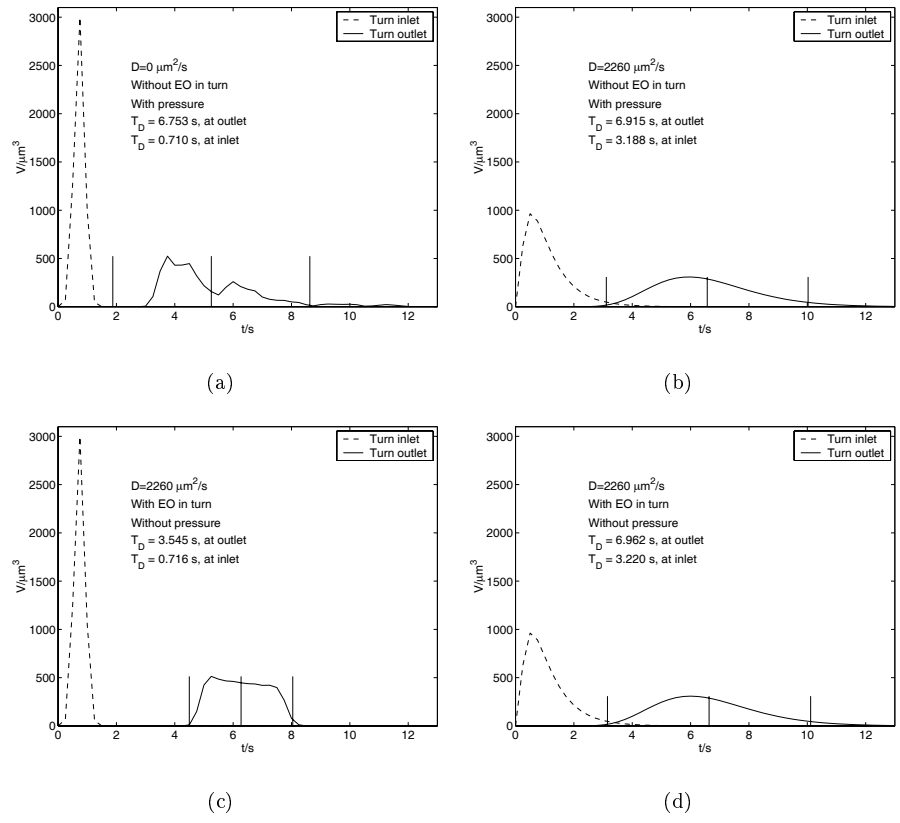

Figure 7.10: Simulation results for a 3D simulation of a sample travelling through a turn connecting two straight channels.

7.4 Dispersion in a Turn, Part 2

In this section we will examine simulation results with respect to dispersion reading off the peak concentrations as functions of time. The results will be compared to the article by Culbertson et al. (1998).

Our goal will be to find the effective dispersion coefficient as a function of time for a species going through a 2D turn. In the following we will assume that the species is distributed as a Gaussian. This assumption can be quite questionable when diffusion is not the dominant contribution to the dispersion. When the peak concentration as function of time and the total amount of species is known, we can obtain a measure of the diffusion coefficient. This is shown in the following. Recall the translating and dispersing Gaussian

$$c(x,t) = \frac{C}{2\sqrt{\pi D_{\text{eff}}(t)(t_0+t)}} \exp\left(-\frac{(x-Ut)^2}{4D_{\text{eff}}(t)\ t}\right). \tag{7.15}$$

Notice we have written $D_{\text{eff}}(t)$ to emphasize that the effective diffusion coefficient is a function of time, and C is defined as

$$C = \int_{-\infty}^{\infty} c(x,t)dx. \tag{7.16}$$

The peak concentration as a function of time is given by

$$c_{\text{peak}}(t) = \frac{C}{2\sqrt{\pi D_{\text{eff}}(t)(\frac{\sigma^2}{2D}+t)}}, \tag{7.17}$$

where we have inserted the t_0 value given by equation (7.2). Rewriting this expression gives

$$\frac{C^2}{4\pi c_{\text{peak}}^2(t)} = D_{\text{eff}}(t)\left(\frac{\sigma^2}{2D}+t\right). \tag{7.18}$$

Plotting $\frac{C^2}{4\pi c_{\text{peak}}^2}$ versus $\left(\frac{\sigma^2}{2D}+t\right)$ the slope of the curve yields $D_{\text{eff}}(t)$. In the following figures, where $D_{\text{eff}}(t)$ is determined, we have for notational convenience defined

$$Cc = \frac{C^2}{4\pi c_{\text{peak}}^2}, \tag{7.19}$$

$$Ct = \frac{\sigma^2}{2D} + t. \tag{7.20}$$

Cc is comparable to a length scale squared and Ct is a time scale shifted t_0 compared to t.

7.4.1 Simulations

In the following we will present 2D simulations where the effective dispersion coefficient have been determined. The results are presented in the following figures.

- Figure 7.12 is a simulation with the short circuited turn.
- Figures 7.14 and 7.15 are simulations with equal electroosmotic mobilities specified on all walls for two different diffusion coefficients.
- Figures 7.16 and 7.17 are simulations where the electroosmotic mobilities in the walls have been optimized to reduce dispersion.

All the figures have an (a) and a (b) part. The (a) subfigures show the points obtained from the simulations. The peak value and the corresponding time have been determined from the simulations. There is in the current release of Coventor no easy way to obtain these points. The values have been obtained in the following manner.

It is possible to use a feature called *IsoVolume*. A lower and upper bound of the parameter to be investigated must be specified. We are considering the *species mass fraction*, which ranges between 0 and 1. Specifying a lower bound of, say, 0.3 and an upper bound of 0.7, only the volumes having *species mass fraction* between 0.3 and 0.7 will be visible and colored according to the value. The peak value can then be found choosing the upper bound to be 1 and gradually increasing the lower bound until only the peak value is visible. An example is in given for the initial concentration profile in Figure 7.11. The peak value and the corresponding time have then been typed into a MatLab program for linear regression and plotting. After some correspondence with the Coventor Support, I have realized that there is no easier way to perform this quite tedious procedure. According to the Coventor Support, improvements on this point are planned for the next release of their software.

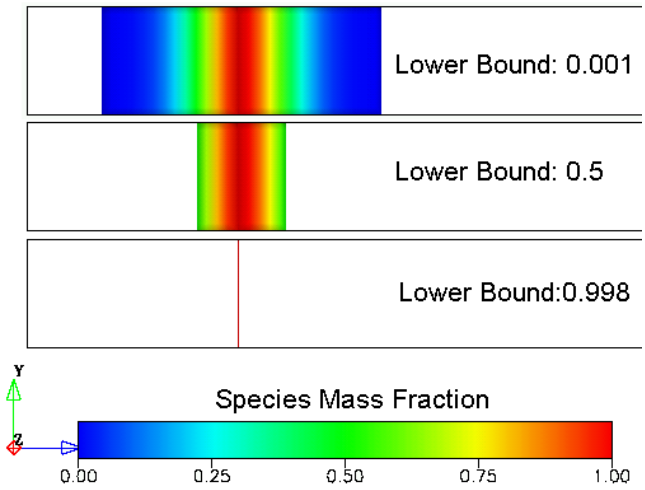

Figure 7.11: Visualization of the procedure to find the peak concentration in Coventor's simulation Visualizer. The lower bound is raised until only the peak is visible.

In all the figures linear regression has been made according to equation (7.18). The effective dispersion coefficients are also given in the plots. The first coefficient corresponds to the left most line, the next coefficient corresponds to the next line and so on.

Before we begin a discussion of the simulations, the method for predicting the dispersion introduced by a turn is briefly recaptured. Refer to equation (5.82).

The Culbertson Method
The dispersion introduced by the turn was given by

$$\Delta l = 2\theta w \left(1 - \exp(-t_D/t_t)\right). \tag{7.21}$$

This length is assumed to correspond to 4σ, which is 95% of a Gaussian when placed around the mean value. Hence the variance is given by

$$\sigma^2 = \frac{\Delta l}{16}. \tag{7.22}$$

The effective dispersion coefficient is then given by

$$D_{\text{eff}} = \frac{\sigma^2}{2t} + D, \tag{7.23}$$

where t is the time it takes for the sample to travel through the turn. This is valid only when there is electroosmotic flow in the turn.

Discussion
Consider in Figure 7.12, a simulation of the short circuited turn with pressure applied to avoid velocity gradients in the straight channels. The left most line corresponds to the effective dispersion coefficient in the straight channel. Since the velocity profile is without gradients in this region, we expect only diffusion to contribute to the dispersion. Indeed this is observed as the effective dispersion coefficient is found to be $D_{\text{eff}} = 2266\ \mu\text{m}^2\,\text{s}^{-1}$, which compared to the diffusion coefficient $D = 2260\ \mu\text{m}^2\,\text{s}^{-1}$, is within the accuracy expected of the simulation. The effective dispersion coefficient in the turn corresponding to the other linear fit is found to be $D_{\text{eff}} = 2968\ \mu\text{m}^2\,\text{s}^{-1}$. The value is expected to be larger than the diffusion coefficient, because there are contributions to the dispersion from the race-track effect and the gradients in the parabola like velocity profile.

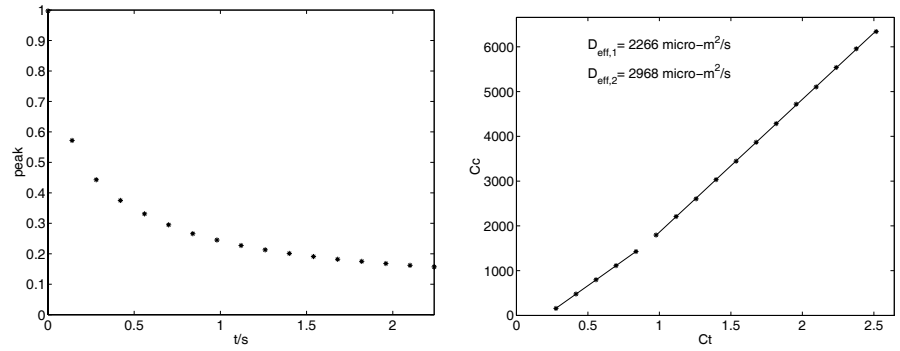

(a) (b)

Figure 7.12: Simulation with a parabolic velocity profile in the turn. A pressure drop has been added to remove velocity gradients in the straight channels. The diffusion coefficient for the simulation is: $D = 2260\ \mu\text{m}^2\,\text{s}^{-1}$.

In Figure 7.14 four linear fits have been made. The linear fits corresponds to the first straight channel, the turn, the second straight channel, and finally the last part of the second straight channel. The first coefficient is seen to be almost identical to the diffusion coefficient as expected. The third coefficient is larger than the diffusion coefficient even though the only contribution to the dispersion in the second straight channel is diffusion. This could be explained by the distortion of the sample, as it has travelled through the turn. The distortion of the sample gives rise to concentration gradients in the direction orthogonal to the direction of the flow. Hence diffusion in both the flow direction and the orthogonal direction of the flow contribute to the dispersion of the sample. The fourth line is a linear regression to the last four points corresponding to peak values further downstream the second channel. The effective dispersion coefficient is observed to equal the diffusion coefficient again. This is interpreted as follows: After some time the sample is smeared out, and there is no longer any distortion of the sample, i.e. it is again distributed as a Gaussian in the flow direction, and only diffusion in the flow direction contributes to the dispersion. Figures 7.13 show the sample at different times, and indeed we notice the distortion of the sample just after the turn and the smearing out afterwards. A certain transition zone, where we go from the larger dispersion in the turn to a smaller in the straight channels, should hence be taken into account. This transition zone before the Gaussian distribution is obtained again has not been taken into account in the article by Culbertson et al.

When the diffusion time scale t_D is much larger than the transit time[4], t_t, the diffusion will dominate the dispersion, and this transition zone will be negligible, thus under these conditions the method by Culbertson et al. can be applied successfully.

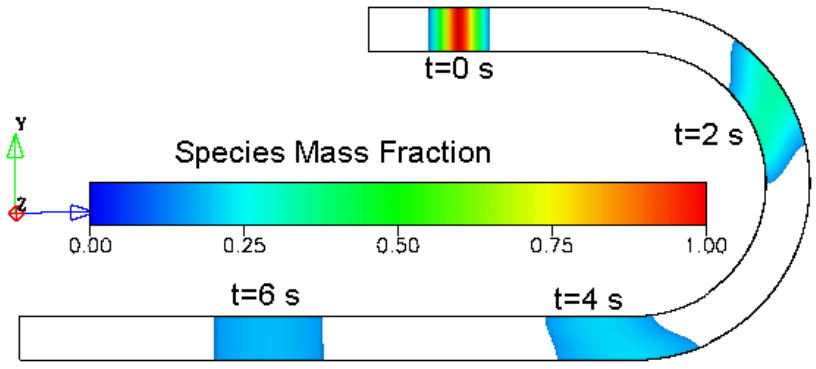

Figure 7.13: The sample at the times: $t = 0$, $t = 2$, $t = 4$, $t = 6$. The lower bound was set to 0.15 and the upper bound was 1, meaning that only concentrations in that range are visualized.

[4]The transit time is defined as the time it takes for the sample to travel through the turn.

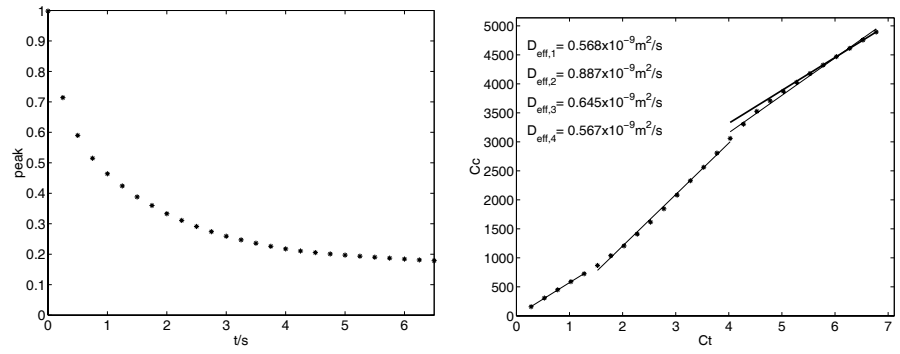

(a) (b)

Figure 7.14: Simulation with all walls having the same electroosmotic mobility. The diffusion coefficient for the simulation is: $D = 565\ \mu\mathrm{m}^2\ \mathrm{s}^{-1}$.

The settings for the simulation shown in Figure 7.15 are identical to the settings for the simulation shown in Figure 7.14 except for the diffusion coefficient, which is four times larger, or equal to the self diffusion in water. We notice that the effective dispersion coefficient is only slightly larger in the turn, meaning that diffusion is the dominating contribution to the dispersion in the turn. In Table 7.10 the results from Figures 7.14 and 7.15 are given and compared to the method proposed by Culbertson et al. The deviations are within the expected error of the simulations. See Table 7.10.

Comparing $D_{\mathrm{eff}} = 2968\ \mu\mathrm{m}^2\ \mathrm{s}^{-1}$ from Figure 7.12 to the corresponding effective dispersion coefficient from Figure 7.15, $D_{\mathrm{eff}} = 2370\ \mu\mathrm{m}^2\ \mathrm{s}^{-1}$, we again conclude that short circuiting the turn worsen the dispersion of samples.

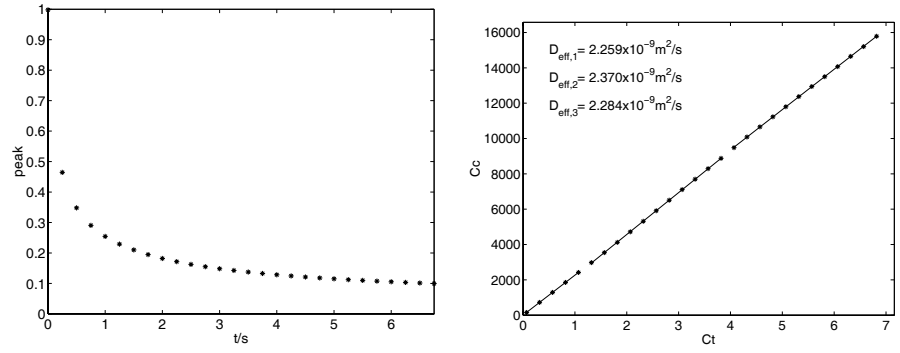

(a) (b)

Figure 7.15: Simulation with all walls having the same electroosmotic mobility. The diffusion coefficient for the simulation is: $D = 2260\ \mu\mathrm{m}^2\ \mathrm{s}^{-1}$.

	Row no.	$\frac{D_{\text{eff}}}{\mu\text{m}^2\ \text{s}^{-1}}$,predicted	$\frac{D_{\text{eff}}}{\mu\text{m}^2\ \text{s}^{-1}}$,simulated	deviation
Figure 7.14	1	565	561	0.7%
	2	887	940	5.9%
	3	565	577	2.1%
Figure 7.15	1	2260	2259	0.04%
	2	2370	2294	3.2%
	3	2260	2284	1.1%

Table 7.10: Effective dispersion coefficients from from Figures 7.14 and 7.15. The first rows (no. 1) correspond to D_{eff} for the first straight channel, the second rows (no. 2) correspond to D_{eff} for the turn, and the third rows (no. 3) correspond to D_{eff} in the straight channel after the turn.

The simulations shown in Figures 7.16 and 7.17 are made with modified electroosmotic mobilities at the walls in the turn for two different diffusion coefficients. For both figures we notice that the effective diffusion coefficient in the turn is close to being equal to the diffusion coefficient. This indicates that the modification of the electroosmotic mobilities of the walls in the turn is in fact optimal. We thus realize that to obtain even less dispersion, we need to be able to control diffusion. This remains the most difficult task, which so far has not been solved. To this end we will remind the reader about the previous chapter, where we proposed a method to control dispersion of a charged species using electric fields. Further studies into these matters could prove to be very fruitful.

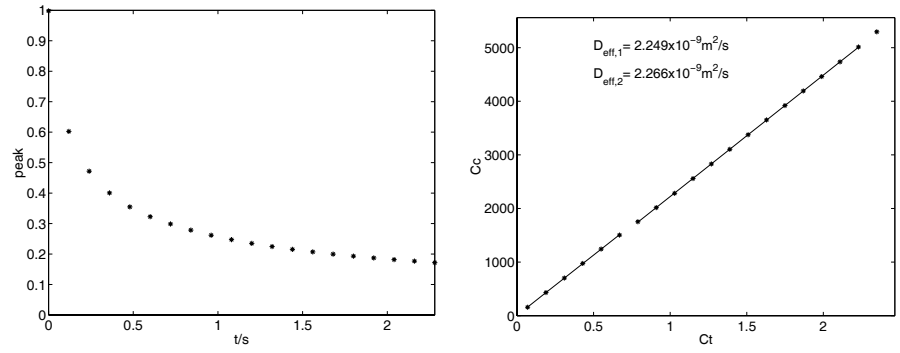

(a) (b)

Figure 7.16: Simulation with the walls of the straight channel having the same electroosmotic mobility and modified electroosmotic mobilities on the walls in the turn. The diffusion coefficient for the simulation is: $D = 2260\ \mu\text{m}^2\ \text{s}^{-1}$.

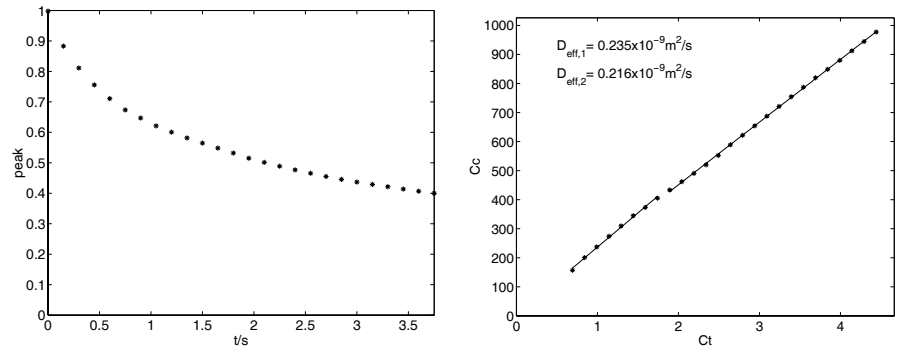

(a) (b)

Figure 7.17: Simulation with the walls of the straight channel having the same electroosmotic mobility and modified electroosmotic mobilities of the walls in the turn The diffusion coefficient for the simulation is: $D = 226\ \mu\mathrm{m}^2\,\mathrm{s}^{-1}$.

7.5 Spirals

In many microfluidic systems there is a need for rather long channels, because certain chemical reactions should have time to occur before leaving the channel. Of course, it is not clever to make just one long straight channel, if we wish the channel to stay within some small microfluidic device. Hence we need to bend the channel several times. This has through the years been done in different ways. Often meanders have been made, i.e. series of straight channels connected by turns. For such straight channels to lie close enough turns with rather small radii of curvature are needed. Turns with small radii of curvature have, as we have seen previously in this thesis undesired effects regarding dispersion. Another possible way of bending the channels is to consider spirals. This has been done by Culbertson (2000). One advantage of spirals is that the radii of curvature will be small only in the center of the spirals. In this section we will consider spiral shaped microchannels. See Figure 7.18. The spiral below has the extra advantage that both inlet and outlet are placed at the edge of the spiral. This is useful when a two dimensional point of view is to be maintained. For example if the inlet of a spiral was placed in outer edge of the spiral and the outlet was placed at the center, we would have to go into the third dimension to get out the transported liquid. The spiral below is, in fact just as the meanders, created by straight channels and turns. Hence we expect the theory by Culbertson et al., previously applied, to be useful in predicting the dispersion. The compactness of channels is important to obtain long channels in small areas. The spiral considered here is indeed very compact:

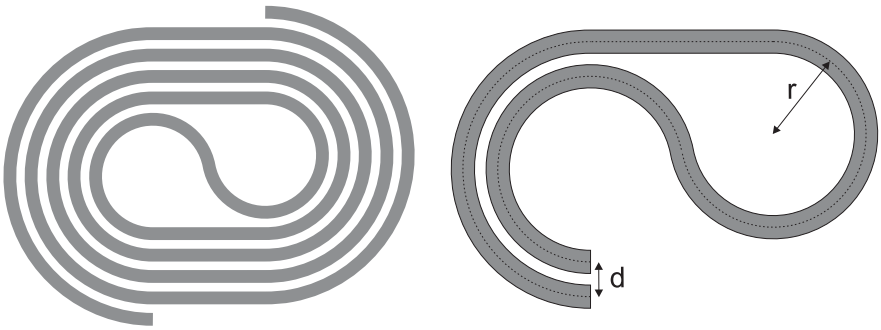

Figure 7.18: Sketch of a spiral.

With the smallest radius of curvature r and the distance between the centerlines of the channels d given, the spiral shown in Figure 7.18 is the most compact way of making a spiral, if both inlet and outlet is wanted at the edge of the spiral, opposite to the case where one end of the spiral is at the edge and the other end at the center of the spiral. This can be realized by the following consideration: In order for the channel to spiral both into the center and out again, there must be room for two circles of radius r at the center of the spiral. Now, since the channel is folded as compactly as possible outside the two circles, determined by d, the spiral is packed in the most compact way possible.

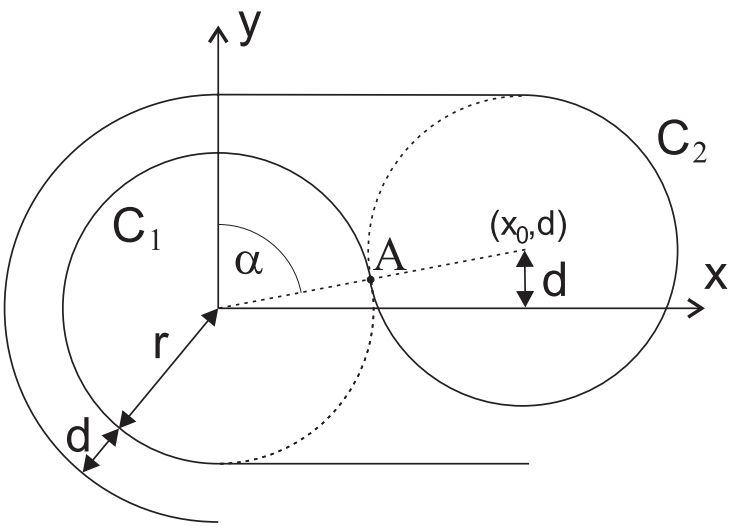

Figure 7.19: Sketch of a spiral.

Before we can make any simulations a grid must be constructed. This is done using the software I-DEAS, which has very extensive tools for generating geometries and grids. The possibilities for generating grids in Coventor is at this point very limited. Even when generating the grids for the straight channels connected by a turn the possibilities in Coventor are less than acceptable. In order to construct the spiral the angle α must be determined. From Figure 7.19 we find

$$\mathrm{C}_1: \qquad x^2 + y^2 = r^2, \tag{7.24}$$

$$\mathrm{C}_2: \quad (x - x_0)^2 + (y - d)^2 = r^2, \tag{7.25}$$

The two circles must intersect at the point

$$A = \left(\frac{x_0}{2}, \frac{d}{2}\right). \tag{7.26}$$

Inserting the point A into the equation for C_1 yields

$$x_0^2 = 4r^2 - d^2. \tag{7.27}$$

Thus α can be found from the cosine relation

$$\cos(\alpha) = \frac{d}{\sqrt{x_0^2 + d^2}} = \frac{d}{2r}. \tag{7.28}$$

Using I-DEAS the inner most part of the considered spiral is constructed. We have chosen $r = 200\ \mu$m and $d = 75\ \mu$m, yielding, $\alpha = 79.19^{\mathrm{o}}$. Simulations are presented in the following.

7.5.1 Simulations

The spiral is composed of five parts as shown in Figure 7.20. For each part an effective dispersion coefficient have been found. Two simulations have been

made with equal electroosmotic mobilities on all walls, and one simulation have been made with the optimized electroosmotic mobilities at the walls.

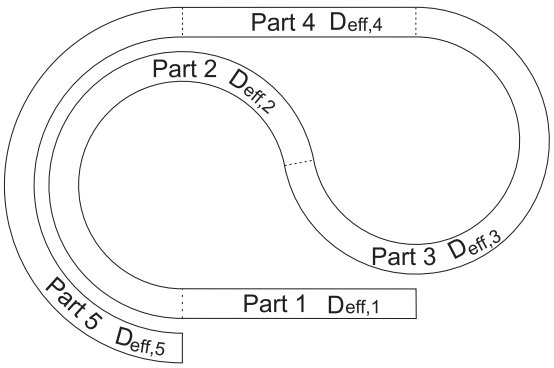

Figure 7.20: The channel geometry is composed of five parts. The first and the fourth parts are straight channels. The second and the third parts are turns bending an angle of, $180^{\circ} + 79.19^{\circ}$, and the radius of curvature at the centerline is $r = 200\,\mu$m. The fifth part is a turn bending 180°, and the radius of curvature at the centerline is $r + d = 275\,\mu$m.

Discussion: It should be mentioned that the simulation time for the following 2D simulations was approximately 20 hours, and the required hard disk space for each simulation was about 12 GByte. The reason for such extreme hard disk requirements is that for each time step all the physical data is saved, even the data which does not change in time. Hence a lot of redundant data is stored. Thus it is with the present available software and computer performance not practically possible to make 3D simulations of spirals[5].

In Tables 7.11 and 7.12 the most important results from the simulation data shown in Figure 7.21 and 7.22 are given, respectively. The predicted values of $D_{\text{eff},2}$, $D_{\text{eff},3}$, and $D_{\text{eff},5}$ have been determined by Culberton's method. The predicted values of $D_{\text{eff},1}$ and $D_{\text{eff},4}$ are simply the diffusion coefficient.

Much the same arguments as for the case with a turn can be given to explain the deviations from the predicted values. The reason that the simulated effective dispersion coefficients are in general higher than the predicted in the turns could be explained by the distortion of the samples, yielding diffusion in the direction orthogonal to the flow. Diffusion orthogonal to the flow is not accounted in the predicted values.

The reason why $D_{\text{eff},2}$ in Part2 is larger than $D_{\text{eff},3}$ in Part3 could be explained as follows: The outer wall of Part2 goes into being the inner wall of Part3 and vice versa. Thus some of the distortion created in Part2 will be corrected in Part3. This effect is especially pronounced in the simulation shown in Figure 7.22. Where the effective dispersion coefficient in Part3 is considerably lower than the predicted value. The reason for this effect to be more pronounced in the second simulation is that the flow rate is larger here compared to the first simulation seen in Figure 7.21. The larger velocity means that diffusion orthogonal to the flow direction has less time to occur, thus the distortion caused by the

[5] At a Coventor seminar in April 2002 I have been informed by Joost van Kuijk from the Coventor department in Amsterdam, that in the next release of the Coventor software, improvements have been made so the hard disk requirements are less extreme

turn will be less smeared out, and thus more of the distortion can be corrected again in Part3. This is shown in Figure 7.23.

	No.	$\frac{D_{\text{eff}}}{\mu\text{m}^2\ \text{s}^{-1}}$,predicted	$\frac{D_{\text{eff}}}{\mu\text{m}^2\ \text{s}^{-1}}$,simulated	deviation
Figure 7.21	$D_{\text{eff},1}$	454	454	0.0%
	$D_{\text{eff},2}$	663	743	10.8%
	$D_{\text{eff},3}$	663	718	7.7%
	$D_{\text{eff},4}$	454	512	11.3%
	$D_{\text{eff},5}$	567	603	6.0%

Table 7.11: Effective dispersion coefficients from Figure 7.21.

	No.	$\frac{D_{\text{eff}}}{\mu\text{m}^2\ \text{s}^{-1}}$,predicted	$\frac{D_{\text{eff}}}{\mu\text{m}^2\ \text{s}^{-1}}$,simulated	deviation
Figure 7.22	$D_{\text{eff},1}$	454	457	0.7%
	$D_{\text{eff},2}$	1246	1451	14.1%
	$D_{\text{eff},3}$	1246	1085	14.9%
	$D_{\text{eff},4}$	454	853	46.8%
	$D_{\text{eff},5}$	911	941	3.2%

Table 7.12: Effective dispersion coefficients from Figure 7.22.

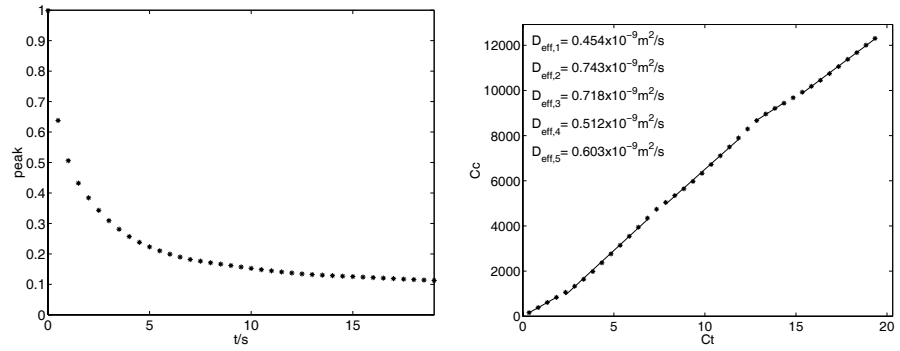

(a) (b)

Figure 7.21: Simulation results from a sample travelling through a spiral.

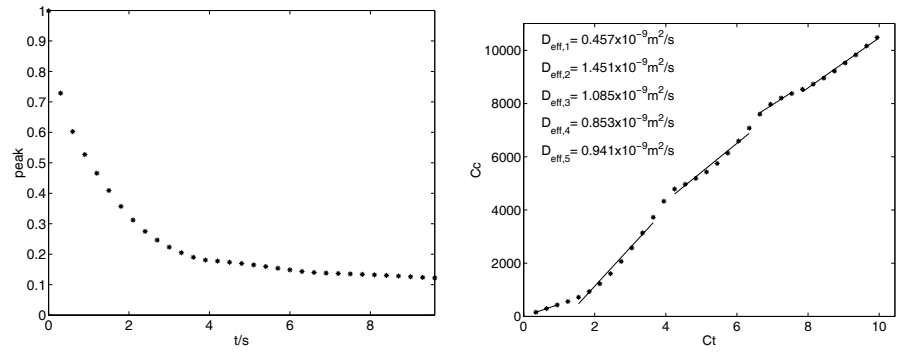

(a) (b)

Figure 7.22: Simulation results from a sample travelling through a spiral.

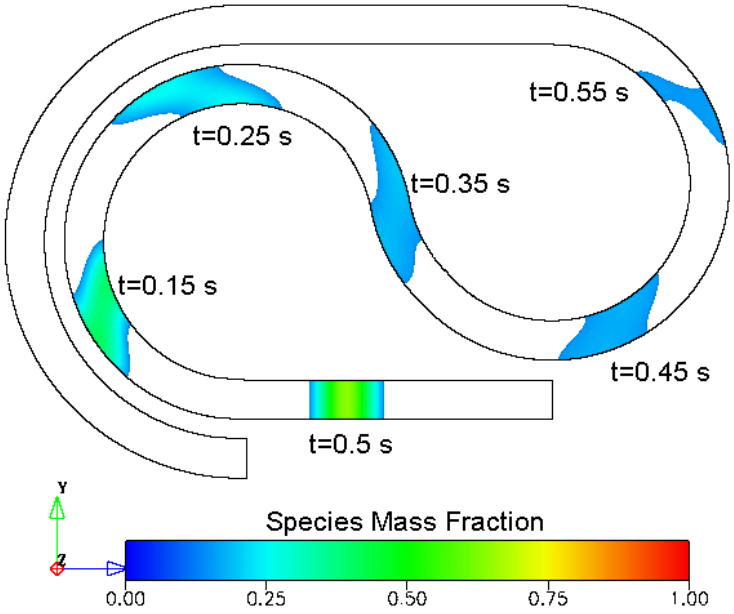

Figure 7.23: 2D Simulation of a sample travelling through a spiral. Notice that the distortion of the sample caused by the first turn is corrected to some degree in the following turn.

In Figure 7.24 a simulation is shown where the electroosmotic mobilities in the turns have been changed according to equations (5.79) and (5.80). The effective dispersion coefficient found from Figure 7.24 to be: $452\mu\text{m}^2\text{s}^{-1}$, which is practically equal to the diffusion coefficient: $D = 454\mu\text{m}^2\text{s}^{-1}$, as we would expect since the only contribution to the dispersion is diffusion. In Figure 7.25 the plug is shown at different times. The lower bound has been set to 0.05, meaning that only volumes with species mass fractions larger than 0.05 are visible. Notice that everywhere the ends of the samples are orthogonal to the channel indicating that there indeed can be no diffusion in the direction orthogonal to the flow.

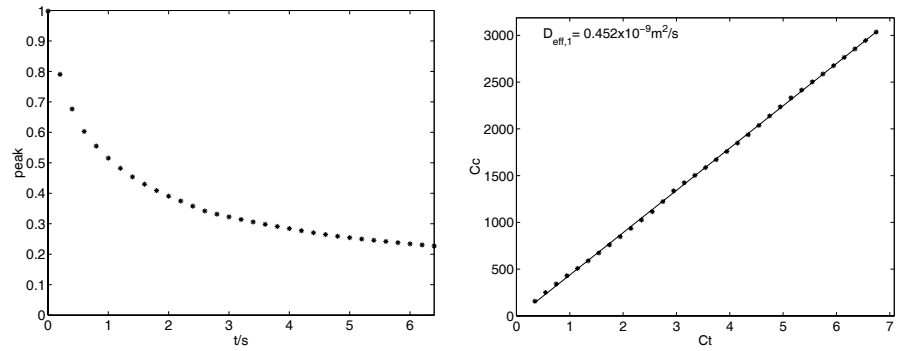

(a) (b)

Figure 7.24: Simulation results from a sample travelling through a spiral.

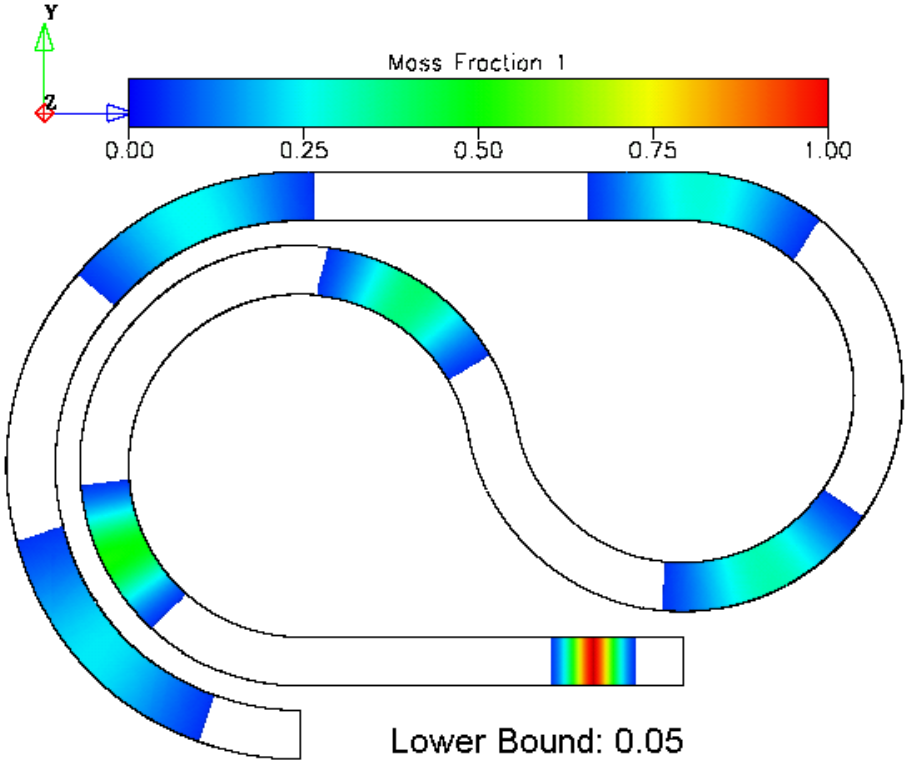

Figure 7.25: The plug as function of time.

Summary A parametric study has been made to obtain experience regarding the solution dependence on parameters such as cell size, time steps, and solution tolerance.

Next a thorough investigation of flows in a system consisting of two straight channels connected by a turn has been made. In usual electroosmotic flows the electrical field in the turn enlarge the race track effect because the electric field is stronger at the inner wall compared to the outer wall. This lead us to an idea of short circuiting the turn. Short circuiting the turn, the flow becomes pressure driven in the turn, giving gradients in the velocity profiles in both the turn and the straight channels. A method to remove the velocity gradients in the straight channel has been derived and applied to the simulations. We cannot, however, avoid the velocity gradients in the turn, and unfortunately, simulations have shown that this pressure driven flow profile causes more dispersion than the usual electroosmotic flow. Hence we will have to discard the idea of short circuiting the turn.

However, simulations have shown that changing the electroosmotic mobilities at the walls in the turn, we can reduce the turn induced dispersion down to diffusion in the flow direction.

Moreover, we have applied the method of predicting turn induced dispersion developed by Culbertson et al. (1998). We have found that the method gives reasonably good results as long as diffusion orthogonal to the flow direction can be neglected.

Finally, simulations have been made on a spiral shaped microchannel. We observed that for faster flowing species the distortion caused by the first of the inner most turn was corrected to some degree by the following turn, because the inner wall of the first turn is connected to the outer wall of the second turn and vice versa. A single simulation was made where the electroosmotic mobilities of the bending walls of the spiral were optimized. As expected we found that only diffusion in the flow direction contributed to the dispersion.

Chapter 8

Conclusion

This thesis can be viewed upon as an introductory overview of problems encountered regarding dispersion in microchannels. On top of being an overview, several novel ideas are presented and studied both theoretically and through computer aided simulations.

Basic theory on electrokinetically and pressure driven flows are presented - we need to understand the flow phenomena before we can expect to understand the more complicated situation with a species driven by the flow.

It has been realized that for flows in microchannels dispersion is mainly composed of three different effects, namely: diffusion, gradients in the velocity profile, and geometry induced dispersion.

A study of the Taylor dispersion has been made, resulting in a more general formula for Taylor's effective dispersion coefficient. The formula has been applied to an example with blood flow in a tube shaped geometry.

For flows driven by electroosmosis, formulae for minimizing turn induced dispersion have been derived. Simulations have shown the correctness of the formulae. Simulations also showed that the method proposed by Culbertson (1998) for predicting the turn induced dispersion are correct as long as diffusion orthogonal to the flow direction can be neglected. Before the physically interesting simulations were created, a parameter study was made. That is, we have investigated solution dependencies on grid, solution tolerance, and time step magnitude.

Furthermore a method for controlling the dispersion of a charged species in a microchannel applying electric fields is proposed and studied. The microchannel should be so narrow that the Debye screening length is comparable to the width of the channel. Placing an array of electrodes along a microchannel it is possible to control the electric field inside the channel. The idea of driving a sample through a microchannel under full control of dispersion is very compelling. Further studies into this idea could prove to be very fruitful.

Bibliography

[1] Armand Ajdari
Pumping Liquids using Asymmetric electrode Arrays, Physical Review 1999.

[2] Nakhlé Asmar
Partial Differential Equations and Boundary Value Problems, Prentice Hall 2000.

[3] A.B.D. Brown, C. G. Smith, A. R. Rennie
Pumping of Water with AC Electric Fields Applied to Asymmetric Pairs of Microelectrodes, Physical Review 2000.

[4] Wesley Chang, David Trebotich, Luke P. Lee, Dorian Liepmann
Blood Flow In Simple Microchannels, 1st Annual International IEEE-EMBS Special Topic Conference on Microtechnologies in Medicine & Biology October 12-14, 2000, Lyon, France.

[5] Christoffer T. Culbertson, Stephen C. Jacobsen, Michael Ramsey
Dispersion Sources for Compact Geometries on Microchips, Analytical Chemistry 1998.

[6] Christoffer T. Culbertson, Stephen C. Jacobsen, Michael Ramsey
Microchip Devices for High-Efficiency Separations., Analytical Chemistry 1998.

[7] Antoine Daridon, Peter Gravesen, Holger Dirac, Jens Peter Krog, Elisabeth Verpoorte, Nico F. de Rooij
Dispersion Studies of Pressure-Driven Flow in Deep-Reactive-Ion-Etched Microfluidic Channels, Micro Total Analysis Systems 2000.

[8] Dutta Debashis and Leighton, David T. Jr.
Dispersion Reduction in Pressure-Driven Flow Through Microetched Channels, Analytical Chemistry 2000.

[9] S. K. Griffiths and R. H. Nilson
Modeling Electrokinetic Transport for the Design and Optimization of Microchannel Systems, Micro Total Analysis Systems 2001.

[10] Timothy J. Johnson, David Ross, Michael Gaitan, Laurie E. Locascio
Laser Modification on Performed Polymer microchannels: Aplication To Reduce Band Broadening around Turns Subject to Electrokinetic Flow, Analytical Chemistry 2001.

[11] Timothy J. Johnson, David Ross, Michael Gaitan, Laurie E. Locascio
Laser Modification of Channels to Reduce Band Broadening or to Increase Mixing, Micro Total Analysis Systems 2001.

[12] Probstein, Ronald F.
Physiochemical Hydrodynamics, An Introduction, Second Edition, John Wiley & Sons, Inc. 1994.

[13] R. Qiao and N. R. Aluru
Dispersion Control in Nano-Channel Systems by Localized Zeta-Potential Variation, Micro Total Analysis Systems 2001.

[14] Versteeg, H. K. and Malalasekera, W.
An Introduction to Computational Fluid Dynamics, The finite Volue method., Longman 1995.

Appendix A

MatLab Code

A.1 ODE-solver

```
%ODE-solver
 clear all
 close all
 global lambda

lambdavec=[  10    2    1  0.4  0.2  0.1 0.01];
  zerovec=[1e-8 1e-8 1e-8 1e-6 1e-3 1e-2  0.9];
 zeta=2.79;

guess=0; delta=1e-8; error=1; maxerror=1e-4; zeta=2.79; p=0;

for k=1:length(lambdavec)
    lambda=lambdavec(k);
    zero=zerovec(k);
guess=0; delta=1e-8; error=1; maxerror=1e-4; zeta=2.79; p=0;

while error>maxerror
 p=p+1;
 for i=1:2
 [r,psi] = ode45(@vdp1,[zero 1],[guess+(i-1)*delta; 0]); rightbc(i)=psi(length(psi(:,1)),1);
 end
 slope=(rightbc(2)-rightbc(1))/delta;
 guess=guess-(rightbc(1)-zeta)/slope;
 error=abs(rightbc(2)-zeta)/zeta;
end %while
disp(p); disp(psi(1,1));

figure(1) plot(r,psi(:,1)) hold on
end %for

plot([0 1],[zeta zeta],'--')  hold on
 title('Dimensionless potential');
 axis([0 1 0 3]); xlabel('r''); ylabel('\psi'');
```

A.2 System ODE Setup

```
function dydt = vdp1(r,psi)
 global lambda
 dydt = [psi(2); sinh(psi(1))/lambda^2-psi(2)/r];
```

Appendix B

Fourier Coefficients

In the following we find the coefficients for the boundary condition $\phi_{1a}(r=1,z) = A\cos(n_0\pi z)$, i.e.

$$A\cos(n_0\pi z) = \sum_{m=1}^{\infty} C_m I_0(\gamma_m)\sin(m\pi z), \tag{B.1}$$

which after multiplying by $\sin(n\pi z), n \in \mathbf{N}$ and integrating over all $z \in [0,1]$, yields

$$C_m = \frac{2A}{I_0(\gamma_m)}\int_0^1 \cos(n_0\pi z)\sin(m\pi z)dz \tag{B.2}$$

For $m = n_0$ we find $C_m = 0$. For $m \neq n_0$ we find

$$C_m = \frac{A}{I_0(\gamma_m)}\left[\frac{-1}{\pi(m-n_0)}\cos(\pi z(m-n_0) - \frac{1}{\pi(m+n_0)}\cos(\pi z(m+n_0))\right] \tag{B.3}$$

When n_0 is even only the uneven m's yield non-zero coefficients, which are found to be

$$c_k = \frac{2A}{\pi I_0(\gamma_{2k-1})}\left(\frac{1}{2k-1-n_0} + \frac{1}{2k-1+n_0}\right), \tag{B.4}$$

where we have substituted $m = 2k-1, k \in \mathbf{N}$ in order to disregard the even m's. When n_0 is uneven only the even m's yield non-zero coefficients, which are found to be

$$c_k = \frac{2A}{\pi I_0(\gamma_{2k})}\left(\frac{1}{2k-n_0} + \frac{1}{2k+n_0}\right) \tag{B.5}$$

where we have substituted $m = 2k, k \in \mathbf{N}$ in order to disregard the uneven m's.

Appendix C

MatLab Code for Ions in a Tube

Solving for Electric Potentials in a Tube

```
% Ions in a tube

clear all
%close all

%---INITIALIZING---
L=100e-6; a=1/sqrt(L); a=20e-6; Nr=25; Nz=75; N=1; Nmax=30;
Mmax=30; Gmax=110; rvec=linspace(0,1,Nr); rmat=repmat(rvec,Nz,1);
zvec=linspace(0,1,Nz); zmat=repmat(zvec,Nr,1)'; in=1; A=2;
M=6.75e-15; %amount of ions, non-dimensional
epsilon=3e-3;
con=1; %convergence counter
%relax=1;
figurenumber=3;

phiinconv=zeros(Nz,Nr,100); phiinhom=zeros(Nz,Nr);
phitemp=zeros(Nz,Nr); phia=zeros(Nz,Nr); phitot=zeros(Nz,Nr);
phi2=zeros(Nz,Nr); phi3=zeros(Nz,Nr); phi4=zeros(Nz,Nr);
Emn=zeros(Nmax,Mmax); c0p(1)=1; c0m(1)=1;

disp('---Finding gamman.............................')
gamman=zeros(Gmax,1); gamman(1)=fzero(@besion,-0.1); nn=1; incr=1;
while nn<2
    nn=nn+1;
    gamman(nn)=fzero(@besion,gamman(nn-1)+incr);
    ch=length(find(floor(10^6*gamman(nn))==floor(10^6*gamman)));
    if ch>1
        nn=nn-1;
        incr=incr+0.1;
    end
end while nn<Gmax
    incr=gamman(nn)-gamman(nn-1);
    nn=nn+1;
    gamman(nn)=fzero(@besion,[gamman(nn-1)+0.9*incr gamman(nn-1)+1.1*incr]);
end tic

disp('---Finding homogene solution...................')
lambdan=L*gamman/a; for n=1:Gmax
%temp2=4*A/(pi*(2*n-1))*besseli(0,a*(2*n-1)*pi*rmat/L)/besseli(0,a*(2*n-1)*pi/L).*sin((2*n-1)*pi*zmat);
%phi2=phi2+temp2;
temp2=2*A*(1/(2*n-3)+1/(2*n+1))/pi*besseli(0,a*(2*n-1)*pi*rmat/L)/...
besseli(0,a*(2*n-1)*pi/L).*sin((2*n-1)*pi*zmat); phi2=phi2+temp2;
temp3=2*A/gamman(n)*besselj(0,gamman(n)*rmat)/besselj(1,gamman(n)).*...
(exp(lambdan(n)*(zmat-2))-exp(-lambdan(n)*zmat))/(exp(-2*lambdan(n))-1);
phi3=phi3+temp3;
temp4=2*A/gamman(n)*besselj(0,gamman(n)*rmat)/besselj(1,gamman(n)).*...
(exp(lambdan(n)*(zmat-1))-exp(-lambdan(n)*(zmat+1)))/(1-exp(-2*lambdan(n)));
```

```
phi4=phi4+temp4; end phihomogen=phi2+phi3+phi4;

phihomogen(1,:)=A; phihomogen(Nz,:)=A;

%---Find phia---
%phia=in*A/N*cos(2*pi*zmat/L);
phitot=phihomogen; diff=1; maxdiff=1; meandiff=1; c0mdiff=1;
c0pdiff=1; disp('---Starting while loop.....................')
while diff(con)>epsilon c0mold=c0m(con); c0pold=c0p(con);

%---Find f---
integrandm=exp(phitot).*rmat;
f2m=(sum(integrandm)-(integrandm(1,:)+integrandm(Nz,:))/2)/(Nz-1);
c0m(con+1)=M*((sum(f2m)-(f2m(1)+f2m(Nr))/2)/(Nr-1))^(-1);

integrandp=exp(-phitot).*rmat;
f2p=(sum(integrandp)-(integrandp(1,:)+integrandp(Nz,:))/2)/(Nz-1);
c0p(con+1)=M*((sum(f2p)-(f2p(1)+f2p(Nr))/2)/(Nr-1))^(-1);

f=(c0m(con+1)*exp(phitot)-c0p(con+1)*exp(-phitot))/2;

disp(sprintf('           c0m = %2.6f',c0m(con)))
disp(sprintf('           c0p = %2.6f',c0p(con)))

disp('---Finding Emn.............................')
%time1=toc;
for m=1:Mmax for n=1:Nmax sinmat=sin(m*pi*zmat);
besmat=besselj(0,gamman(n)*rmat);
integrand=f.*sinmat.*besmat.*rmat;
f2=(sum(integrand)-(integrand(1,:)+integrand(Nz,:))/2)/(Nz-1);
integral=(sum(f2)-(f2(1)+f2(Nr))/2)/(Nr-1);
Emn(n,m)=-4*(gamman(n)^2+(a*m*pi/L)^2)^(-1)/besselj(1,gamman(n))^2*integral;
end %Mmax
end %Nmax
%disp(sprintf('Calculation time=%2.4f',toc-time1))
%test3=Emn;

disp('---Finding inhomogene solution.................') for i=1:Nr
r=rvec(i); for n=1:Nmax for m=1:Mmax
temp=Emn(n,m)*sin(m*pi*zvec)*besselj(0,gamman(n)*r);
phiinhom(:,i)=phiinhom(:,i)+temp';
end %Mmax
end %Nmax
end %Nr

phidiff=abs(phitot-(phiinhom+phihomogen));
phitot=phiinhom+phihomogen;

phiinconv(:,:,con)=phitot; con=con+1;
c0mdiff(con)=abs((c0m(con)-c0mold)/c0m(con));
c0pdiff(con)=abs((c0p(con)-c0pold)/c0p(con));
diff(con)=max(c0mdiff(con),c0pdiff(con));
meandiff(con)=mean(mean(phidiff)); maxdiff(con)=max(max(phidiff));

elti=toc; mins=floor(elti/60); secs=round(elti-60*mins);
disp(sprintf('   Time elapsed=%d minutes and %d seconds.',mins,secs))
disp(sprintf(' Max difference= %2.6f (absolute)',maxdiff(con)))
disp(sprintf('Mean difference= %2.6f (absolute)',meandiff(con)))
disp(sprintf(' Max diff. c0m = %2.6f (relative)',c0mdiff(con)))
disp(sprintf(' Max diff. c0p = %2.6f (relative)',c0pdiff(con)))
end %inner while

disp(toc)

cp=c0p(con)*exp(-phitot); cm=c0m(con)*exp(+phitot);

integrandm=cm.*rmat;
f2m=(sum(integrandm)-(integrandm(1,:)+integrandm(Nz,:))/2)/(Nz-1);
Mm=((sum(f2m)-(f2m(1)+f2m(Nr))/2)/(Nr-1));

integrandp=cp.*rmat;
f2p=(sum(integrandp)-(integrandp(1,:)+integrandp(Nz,:))/2)/(Nz-1);
Mp=((sum(f2p)-(f2p(1)+f2p(Nr))/2)/(Nr-1));
```

```
disp(sprintf('Amounts of positive ions=%2.4f and negative ions=%2.4f',Mm,Mp))
disp(sprintf('lambda+/a=%2.4f and lambda-/a=%2.4f',1/sqrt(c0p(con)),1/sqrt(c0m(con))))

%convergece plot
figure(2)
semilogy(1:length(c0mdiff),c0mdiff,1:length(c0pdiff),c0pdiff)
legend('c0mdiff','c0pdiff')

%---Plotting---
figure(figurenumber) subplot(2,3,1), mesh(rvec,zvec,phihomogen)
title('\phi_{hom}') xlabel('r') ylabel('z') subplot(2,3,4),
mesh(rvec,zvec,phiinhom) title('\phi_{inhom}') xlabel('r')
ylabel('z') subplot(2,3,2), mesh(rvec,zvec,phitot)
title('\phi_{tot}') xlabel('r') ylabel('z') subplot(2,3,5),
mesh(rvec,zvec,phitot-phihomogen) title('\phi_{in}') xlabel('r')
ylabel('z') subplot(2,3,3), mesh(rvec,zvec,cp) title('c_{+}')
xlabel('r') ylabel('z') subplot(2,3,6), mesh(rvec,zvec,cm)
title('c_{-}') xlabel('r')
ylabel('z')
```

Appendix D

Coventor Support Q&A

In the following appendix questions mailed to Coventor Support during the project are presented followed by the given answers. The correspondence has taken place between Anders Brask and Flemming Rytter Hansen at MIC and Criss Welham and Joost van Kuijk at the Coventor support.

Q:

```
I am trying to examine how diffusion of a specie can be suppressed
by electric fields. For this purpose I have made a geometry as
shown in the attached mbif-file. To begin with I am only
considering the 2D-case. Hence the top and bottom patches have
been left unnamed. The patches named "w", "inlet" and "outlet"
have been set to Walls. Patches "w1" and "w5" have been set to
Voltage=-4, "w2" and "w4" are set to Voltage=-1 and "w3" are set
to Voltage=0. This generates an approximate parabolic profile of
the electric potential, which hopefully could suppress the
diffusion.
   Notice that there are two patches within the geometry, internal patches,
which have also been set to Walls. The rectangle bounded by the
"inlet=Wall", "outlet=Wall" and the to internal patches (=Wall)
now form a 2D channel. Placing a specie within this channel ONLY,
we would not expect the specie to be able to leave the channel (is
this true ?). What I notice is that the specie is diffusing
through the internal patch/Wall.
   The electrodes: "w1", "w2", "w3", "w4" and "w5" have been placed as shown
in the mbif in order to avoid contact with the specie. Diffusion
through the internal pathes/Walls is also noticed when the voltage
is zero on all electrodes.
   Solving these problems also soloves the problem described in the case:
CW_012102_01.
```

A:

```
Thanks for the description. Could you tell me what's is supposed
to physically stop the species from diffusing from the central
"electrode" part through the internal wall into the two channels
on either side?  Is it a special membrane that stops the diffusion
of the species? As the settings are, the boundary condition "wall"
does not stop diffusion, as I mentioned in my other email.

Flemming Rytter Hansen:

It is less important what prevents the species from diffusing into
the two side-channels. All I need is that no diffusion is possible
into these side-channels. I have tried making the side-channels of
some solid dielectric and the main channel of water. This would
prevent diffusion into the side-channels. However, with this setup
```

it is not possible specify any voltages on the patches of the side-channels. In fact, it is not possible specify anything on the patches of the side-channels when they are fixed. My main problem is that I want an electric field in the main channel, and at the same time I want to have a species which cannot come in contact with any of the electrodes generating this electric field. I want my simulations to be time dependent, hence the need of the electrodes to sustain the electric field. Is it possible to do this with Coventor? I have attached the mbif-file we are discussing.

Coventor Support:

At this time the model you describe will not work correctly as the wall boundary condition does not stop species diffusing. To simulate this problem we would need to implement another "membrane" boundary condition that would stop diffusion between two fluids. This, then, would stop species diffusing through the internal wall and contacting onto the electrodes w1, w2 etc.

Could you indicate to me how important this problem is for you? It is something that you were just "trying out" or is it part of an important project? The reason is that our product management team will need to priortise such an enhancement request and it will help to have some background information as to why it is important.

Flemming Rytter Hansen:

I would certainly like to have the possibility of placing a wall (membrane) through which nothing can diffuse inside a geometry. However, I have a deadline in about 3 months, and I wouldn't expect you to produce the new code within this limited period of time. I am pursuing other ways to obtain my goal.

Q:

I am using Coventor for CFD purposes applying NetFlow. When using species, is it possible to specify a charge connected with the species? E.g. how would I specify a plug of equally charged positive and negative ions. Furthermore, assume that the positive and negative ions are separated to some degree, generating an electric field. Does coventor take this into account?

Here is some more information on the Netflow settings. I gave you slightly inaccurate information in my last email. Here is the corrected version on the "dilute" and "non-dilute" options in Netflow. The non-dilute option in Netflow refers to the change in electrical conductivity caused by the presence of mobile, charged ions (this is the only type of non-dilute electrokinetics problem that we have good data for). It does not take into account the density change, or the potential generated by the charged ions themselves. The main reason for this is not the implementation of the physics into the solver but the verification with experimental data which we have not been able to find. If you believe you have experiments that can show such effects in a quantified way we would be willing to take a look at this. I hope this answers your support request JVK_310102_02 sufficiently and I will close this request. best regards,

A:

At the moment the Netflow module uses the option to set the model to "dilute" and "non_dilute". The dilute option is default and

means that there is no influence from the species on both the fluid density of the carrier and the electric field from the charge of the species. If you set the option to "non-dilute" the first limitation is lifted which means that the species do not influence the fluid density. We were working on lifting the second limitation as well but i will have to inquire on what the status is on this. I will get back to you on that, Best regards,

Q:

I am working with the MicroFluidics Solvers, NetFlow. I am trying to insert an electric field in a rather simple geometry using the VolumeBCs (Analysis->SolverSetup->VolumeBCs). I am using the InputFile LoadValue, where I choose an mbif-file from the following directory: C:\Design_Files\diffusion\Solutions\Results3. The Results3 directory contains results from a simulation giving an electric field in the correct geometry and position in the system of co-ordinates. The results from the simulation with the InputFile-electric-field are placed in the directory: C:\Design_Files\diffusion\Solutions\Results4. The problem now is that there is no electric field in the mbif results from the Results4 directory. What am I doing wrong?

A:

The procedure is correct as you have described it (use the Inputfile option, and specify the location of an MBIF that contains the electric field). There are three things to watch out for:

First, make sure that the file containing the E-field isn't in the current solution directory, or it will be erased. Second, this procedure only works with the FEMTool. Third, make sure there are no Voltage or Current surface boundary conditions.

If this doesn't solve the problem, please let me know, and I will investigate further.

Added comment: I was using the FVMTool, not the FEMTool

Q:

Is it possible to obtain more than eight boundary condition sets (Analysis->SolverSetup->SurfaceBCs, 1st column)?

A:

Unfortunately not. There's no workaround, except to try and group as many patches together as possible, to reduce the number of BCs. We are working on this for the next release.

Q:

Using Parametric Generators, why is it not possible to choose Length1 and Length2 to be zero when creating a U-turn?

A:

This is an oversight and I will submit a request for the generator to be altered to allow this in the next release.

Q:

Is it possible to have magnetic fields when using "MicroFluidics Solvers, NetFlow"?

A:

No, though it may be implemented at some point. Would you wish to supply the magnetic field strength or solve for the magnetic field?

Q:

Say we are considering a 2D simulation of an electroosmotic flow. Is it then possible to specify e.g. a varying EO_Mobility along a specific patch? Example: a linearly varying EO_Mobility from one end of the patch to the other.

A:

No, you cannot set this specific BC, yet. You would need to approximate the linear change by using a number of patches to create a stepped profile. Do you wish to simulate isoelectric focusing (IEF), in which a pH gradient is set up across the channel, and that might give rise to a linearly varying EO mobility?

Q:

When using Parametric Generators, is it then possible to specify exactly where the model should be placed in the xyz-system of coordinates? This is e.g. important when using the "Merge Mbifs...-tool".

A:

Not at the time of mesh generation. After the mesh is generated you can translate and rotate the mesh by going to the "tools->transform" menu in the mesh generators tab.

Q:

In the analyzer reference guide I found the following in the section 4.2.2.: The software internally chooses an angle to determine how many patches should be created for the perimeter. The mesh shown in Figure R4-2 results in a single patch for the perimeter of the rim, while a simpler mesh, shown in Figure R4-3, results in eight individual patches for the perimeter (in addition to one patch for the sensor top and one for the bottom) because of the larger angle change.

Is it possible to change the angle referred to above?

A:

The angle is hard coded. I will find out if it is possible to access it. Is it critical for you to be able to change it, or is it a general question?

Q:

Is it possible to split patches? Consider e.g. a cube. Is it then possible to split the top patch of the cube into two patches, which then can be assigned different properties?

A:

Yes. The way to do this is to change the material type of the appropriate elements or partition the cube into two parts. If the mesh is created in Ideas just select the elements from which you wish to form a patch and change the material type *name* so that it is different from the surrounding elements. (You could have two materials; glass1 and glass2 with identical properties). If you are not using Ideas, use the split part function in the solid modelling tab to partition the cube into two parts. Please also turn the clip function on and specify a clip mask in the layout editor. In this case you will create 3 sat files and will only need to use the one with the "-split" subscript. Open the layout and create a mask called (for example) "split". Use the split mask to define how the cube will be paritioned. For example you can split the cube into two parts. Meshing both parts together will result in separate top patches (and bottom patches)

Q:

We have been trying to make EOF simulations with a very simple case - a straight 3D channel. When trying to simulate with the FVMTool in NetFlow we, however, obtain zero velocities everywhere. We get no error messages. We have checked all settings several times, and they seem to be in order. If we use the FEMTool in NetFlow we obtain the correct results. We have previously received an email from Joost van Kuijk with an mbif-file and an mps-file. He used the FVMTool in his simulations. When running Joost's files on our computer we obtain seemingly correct results.

A:

There is a numerical problem in the FVMTool. Briefly, for some models the potential equation can solve so fast that there are non-valid boundary conditions for the momentum equation so that it is not solved.

This problem has been fixed and will be included in the next official patch release, due out next year. In the meantime I can send you the required replacement FluentWrapper.exe. Please could you let me know the OS you are using, so that I can send the appropraite file. The new file must be put into /coventorWare2001.3/bin. The as installed FluentWrapper.exe that is present should be re-named so that it is not over-written.

Q:

We have used NetFlow with FVMtool and Manhatten Bricks. In general the FVMtool works ok. We have also tried to use Free meshing which also works though it is very slow and inaccurate. Is this typically or is this type of mesh generally not suitable for FVMtool. We assume that FVMtool is an abrevation for Finite Volume Method?

So the problems/questions are the following:
---
1. Why does FEMtool not work?

2. Can we use Ideas for better meshing with FVMtool?

3. It appears that there are no description of the FVMtool and its parameters (relax, upwind etc.)?

4. How do you export the figures optimally? The figures cannot be edited and they are very large. Do you use screen dumps?

A:

```
Here are my answers to your questions:

1. Why does FEMtool notwork? First of all I can assure you that
the solver works. I just tested the T-channel tutorial in Netflow
on our machines and the solver runs and gives the results. This
leads me to believe that there is still something wrong with the
licensing. If you are saying that the FVMTool runs and the FEMTool
doesn't I can conclude the following: You are running
CoventorWare2001.1 using the CoventorWare2001.3 license. This is
ok for most solver EXCEPT "FEMTool". The reason is that our
supplier has merged the licensing of both FVMTool and FEMTool into
1 single license "server" and therefor the FEMTool "server" as it
existed before doesn't exist anymore. The only way to solve this
problem is to upgrade your software version to CoventorWare2001.3.
Your colleges should be able to point you to the right
directories.

2. Can we use Ideas for better meshing with FVMtool? I am not sure
what you mean exactly with this question but if you are asking if
you can use Ideas to create meshes for the solver the answer is
yes. In additio I have included a few meshing tips in the attached
PDF file. In addition you can say about the FVMTool and FEMTool:
* FVM seems to enjoy an advantage in memory use and speed for very large
problems, higher speed flows and source term dominated flows (like
combustion)
* FEM solutions can be very accurate using generally smaller grids

3. It appears that there are no description of the FVMtool and its
parameters (relax, upwind etc.)? I have also included some more
information on this in the attached PDF file. You can also find
some more information in the reference section of the MemCFD and
Netflow tutorials that come on the CD

4. How do you export the figures optimally? The figures cannot be
edited and they are very large. Do you use screen dumps? There are
many options in the visualizer to export pictures you have created
on your screen. I would like to refer you to the MEMS Analyzer
Reference Guide ,section 5.3.5 on the print function in the
visualizer. There are also options to export MPEG files.

5. We have also tried to use Free meshing which also works though
it is very slow and inaccurate. Is this typically or is  his type
of mesh generally not suitable for FVMtool. We assume that FVMtool
is an abrevation for Finite Volume Method? You are right that FVM
stands for Finite Volume Method. You will find that the brick
meshes (or structured meshes as they are sometimes called) are
more accurate with less elements. It is very difficult to give
general guidelines but you usually need a lot of free-meshed
elements to get good results.
```

Q:

```
When LMTOOLS is opened and we in "server status" perform a "status
enquiry" we among other messages find the following:
 Users of MTI_MemCFD:  (Total of 7 licenses available)
 Users of MTI_NetFlow: (Total of 7 licenses available)
However, if we try to run more than one simulation, the following
message is written in the LOG-file:

***FLUENT LOG FILE START *** Welcome to Fluent 5.6.1
Copyright 1999 Fluent Inc.      All Rights Reserved Loading
```

```
"C:\Coventor\CoventorWare2001.1\runtime\fluent\NT40\fluent5.6\lib\fl_s11
95.dmp" Done. Current fluent usage:   1. frh@ggstpc3          Fri
Nov 30 10:21 ggstpc3 License for fluent expires 29-oct-2003. All
licenses for fluent are currently in use. All licenses for fluent
are currently in use. ***FLUENT LOG FILE END ***
```

A:

```
This is a very good question and I appologize that I did not
notice it myself. I already got into contact with our licensing
department and asked them to sort out this mistake.

I looked further into the matter of fluent solver licenses and you
were absolutely right. Our third party software supplier who
supplies the Fluidic license made a mistake in cutting only a
license for 1 seat while the payment had been made for 7 seats. We
have contacted them and requested the new license. I am afraid
this will take a few days probably. Thank you for your patience.
```

Q:

```
 How does the Add List function
work? In the manual I have found following:
----------------
Add List...: Enables a fileDialog window that displays directory
file paths. The user can point to a file with a listing of mbif
files. This mbifList file is created by the user, and may be
located in any arbitrary directory. It contains lines of file
paths to mbif files for the Visualizer to read. This function
provides a way to load multiple mbifs at one time.
----------------
How do the user create the mbifList file? When making a time
dependent simulation it is to my knowlegde not created
automatically, i.e. there are no *.mbiflist files anywhere on the
computer.
```

A:

```
AddList: Here is how AddList works. You make a text file which
contains the files you would like to list. As an example I have
made a list of mbif files m1.mbif through m5.mbif. You save this
file and give it the .mbifLIST extention. I personally use emacs
on both Unix and Windows2000, it is freeware and is maintained by
the GNU project. It is very usefull for looking into files and
editing them. Now you place this file in a directory where the
mbif files are located. Now you can browse to this list file and
import the complete list in one go. The "Visualize List" command
that you are used to does not use this .mbifLIST function. Instead
it looks at the other .value files for the files to list that are
in the result directory. The .value files are binaries.
```

Q:

```
Is it possible to save the settings in the Visualizer? Say, I wish
to have Mass Fraction 1, Pressure and Velocity as default Active
Fields instead of Mises and Displacement.
```

A:

```
Visualizer settings: Unfortunately it has not been possible to
save the settings of the visualizer. We understand that especially
for fluidic customers the fact that the visualizer always opens
with the Von Mises Stress and displacement is very inconvenient.
We are working on this issue and you should see improvements in
the next releases.
```

Appendix E

Curve Fitting

Rewriting the relations $\mu = A_1 \exp(B_1/T)$ and $D = A_2 T \exp(B_2/T)$ yields

$$\ln(\mu) = B_1 \frac{1}{T} + \ln(A_1), \tag{E.1}$$

$$\ln(D/T) = B_2 \frac{1}{T} + \ln(A_2). \tag{E.2}$$

Hence plotting $\ln(\mu)$ and $\ln(D/T)$ as function of $1/T$ yields a straight line with the slope B_1 and B_2, respectively, and the ordinate axis intercept equals $\ln(A_1)$ and $\ln(A_2)$, respectively. Linear regression to the table values have been made using MatLab. Figure E.1 shows the linear regression.

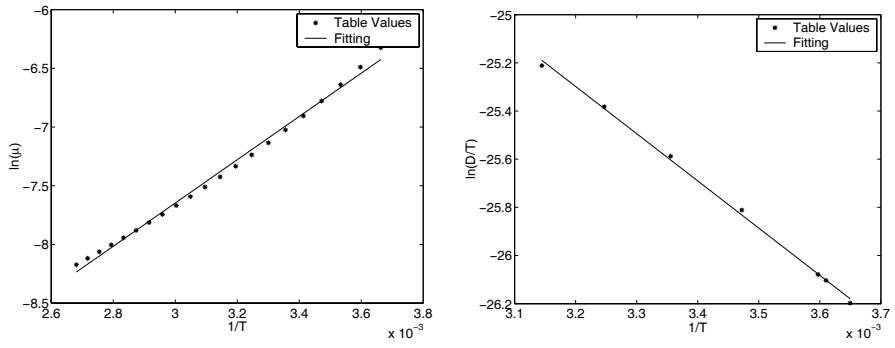

(a) (b)

Figure E.1: Linear regression to table values.

Appendix F

Grid Dependency Analysis

In the following Excel sheets simulation results from a grid dependency analysis are presented.

Grid Dependency Analysis

CHART: 1.

Simulation of a 180 degree turn with a rectangular cross section. Inner radius: 150μm, width: 50μm, depth: 25μm. Pressure driven flow, with a pressure drop of 1e-6 from inlet to outlet.

MatLab calculation based on analytical derivation

FlowRate	Max Vel	grid
8,13E+04	1,302E+02	100x100
8,13E+04	1,302E+02	50x50
8,09E+04	1,300E+02	25x25

Mesh: turn2510res Cell size is in average: 5 micron

Res File	Sol. Tol.	Flowrate	Max Vel.	FlowRate deviation:
turn2510res3	1,00E-02	8,472E+04	1,332E+02	4,21 %
turn2510res	1,00E-04	8,765E+04	1,344E+02	7,81 %
turn2510res2	1,00E-06	8,770E+04	1,344E+02	7,87 %

Mesh: turn2515res Cell size is in average: 3,33 micron

Res File	Sol. Tol.	Flowrate	Max Vel.	FlowRate deviation:
turn2515res1	1,00E-04	8,378E+04	1,293E+02	3,05 %
turn2515res2	1,00E-06	8,417E+04	1,300E+02	3,53 %
turn2515res3	1,00E-08	8,418E+04	1,300E+02	3,54 %

Mesh: turn2520res Cell size is in average: 2,5 micron

Res File	Sol. Tol.	Flowrate	Max Vel.	FlowRate deviation:
turn2520res1	1,00E-04	8,428E+04	1,288E+02	3,67 %
turn2520res2	1,00E-06	8,317E+04	1,301E+02	2,30 %
turn2520res3	1,00E-08	8,318E+04	1,301E+02	2,31 %

Mesh: turn2525res Cell size is in average: 2 micron

Res File	Sol. Tol.	Flowrate	Max Vel.	FlowRate deviation:
turn2525res1	1,00E-04	8,135E+04	1,288E+02	0,06 %
turn2525res2	1,00E-06	8,246E+04	1,308E+02	1,43 %
turn2525res3	1,00E-08	8,247E+04	1,309E+02	1,44 %

Mesh: turn2530res Cell size is in average: 1,67 micron

Res File	Sol. Tol.	Flowrate	Max Vel.	FlowRate deviation:
turn2530res1	1,00E-04	8,060E+04	1,277E+02	-0,86 %
turn2530res2	1,00E-06	8,217E+04	1,306E+02	1,07 %
turn2530res3	1,00E-08	8,219E+04	1,307E+02	1,09 %

Figure F.1: Excell.

CHART: 2.

Simulation of a 180 degree turn with a rectangular cross section. Inner radius: 150μm, width: 50μm. The depth is 50μm for the simulation results above the thick line and 75μm for the results below the thick line. Pressure driven flow, with a pressure drop of 1e-6 from inlet to outlet.

MatLab calculation based on analytical derivation

FlowRate	Max Vel	grid
3,99E+05	3,347E+02	100x100
3,99E+05	3,347E+02	50x50
3,98E+05	3,341E+02	25x25

Mesh: turn5010res Cell size is in average: 5 micron

Res File	Sol. Tol.	Flowrate	Max Vel.	FlowRate deviation:
turn5010res1	1,00E-04	4,098E+05	3,329E+02	2,71 %
turn5010res2	1,00E-06	4,121E+05	3,348E+02	3,28 %
turn5010res3	1,00E-08	4,121E+05	3,348E+02	3,28 %

Mesh: turn5015res Cell size is in average: 3,33 micron

Res File	Sol. Tol.	Flowrate	Max Vel.	FlowRate deviation:
turn5015res1	1,00E-04	4,003E+05	3,309E+02	0,33 %
turn5015res2	1,00E-06	4,052E+05	3,354E+02	1,55 %
turn5015res3	1,00E-08	4,053E+05	3,355E+02	1,58 %

Mesh: turn5020res Cell size is in average: 2,5 micron

Res File	Sol. Tol.	Flowrate	Max Vel.	FlowRate deviation:
turn5020res1	1,00E-04	3,942E+05	3,269E+02	-1,20 %
turn5020res2	1,00E-06	4,026E+05	3,348E+02	0,90 %
turn5020res3	1,00E-08	4,026E+05	3,349E+02	0,90 %

MatLab calculation based on analytical derivation

FlowRate	Max Vel	grid
8,32E+05	4,569E+02	100x100
8,32E+05	4,569E+02	50x50
8,29E+05	4,564E+02	25x25

Mesh: turn7510res Cell size is in average: 5 micron

Res File	Sol. Tol.	Flowrate	Max Vel.	FlowRate deviation:
turn7510res1	1,00E-04	8,470E+05	4,652E+02	1,80 %
turn7510res2	1,00E-06	8,534E+05	4,600E+02	2,57 %
turn7510res3	1,00E-08	8,533E+05	4,600E+02	2,56 %

Mesh: turn7515res Cell size is in average: 3,33 micron

Res File	Sol. Tol.	Flowrate	Max Vel.	FlowRate deviation:
turn7515res1	1,00E-04	8,279E+05	4,491E+02	-0,49 %
turn7515res2	1,00E-06	8,420E+05	4,579E+02	1,20 %
turn7515res3	1,00E-08	8,421E+05	4,580E+02	1,21 %

Mesh: turn7520res Cell size is in average: 2,5 micron

Res File	Sol. Tol.	Flowrate	Max Vel.	FlowRate deviation:
turn7520res1	1,00E-04	8,140E+05	4,420E+02	-2,16 %
turn7520res2	1,00E-06	8,379E+05	4,575E+02	0,71 %
turn7520res3	1,00E-08	8,381E+05	4,577E+02	0,73 %

Figure F.2: Excell.

Appendix G

MatLab Code for Velocity Profile in a Turn

```
% Velocity profile in a turn

clear all
close all

global ro ri

vboundary=100; %EO velocity
ro=200; % outer radius
ri=150; % inner radius
h=25;   % channel height
S=(ro-ri)*h;
dpdtheta=-9.2113e-8/pi; % pressure gradient
mu=1.002e-9; %dynamic viscosity
data=[0    0    0    0    0    0    0    0    0    0    0    0    0    0    0    0 0;
      0 16.8 21.5 23.5 24.2 24.2 24.0 23.6 23.2 22.7 22.1 21.2 19.9 17.5 13.1 0;
      0 25.4 33.9 37.5 38.9 38.9 38.8 38.2 37.5 36.6 35.6 34.1 31.8 27.7 19.8 0;
      0 29.3 39.8 44.4 46.2 46.2 46.1 45.4 44.6 43.6 42.3 40.5 37.6 32.5 22.9 0;
      0 29.3 39.8 44.4 46.2 46.2 46.1 45.4 44.6 43.6 42.3 40.5 37.6 32.5 22.9 0;
      0 25.4 33.9 37.5 38.9 38.9 38.8 38.2 37.5 36.6 35.6 34.1 31.8 27.7 19.8 0;
      0 16.8 21.5 23.5 24.2 24.2 24.0 23.6 23.2 22.7 22.1 21.2 19.9 17.5 13.1 0;
      0    0    0    0    0    0    0    0    0    0    0    0    0    0    0    0 0];
M=50+1;
N=25+1;
Ksum=75;
rvec=linspace(ri/ro,1,N);
zvec=linspace(0,1,M);

MtP=zeros(N,M);
Discharge=0;

tic
disp('Finding Roots')
%---------FINDING ROOTS FOR BESSELFUNCTIONS----------------
epsilon=10^-4;
Lmax=1000;
Nmax=90;

%Mt1=zeros(Nmax,1);
%Mt2=zeros(Nmax,1);
%MtP=zeros(Nmax,1);

lamb=linspace(epsilon,100,Lmax);
bes2=bes5(lamb);
gamman=zeros(Nmax,1);
gamman(1)=fzero(@bes5,-0.1);
n=1;
incr=1;
while n<2
```

```
    n=n+1;
    gamman(n)=fzero(@bes5,gamman(n-1)+incr);
    if floor(10^4*gamman(n))==floor(10^4*gamman(n-1))
        n=n-1;
        incr=incr+0.2;
    end
end
while n<Nmax
    incr=gamman(n)-gamman(n-1);
    n=n+1;
    gamman(n)=fzero(@bes5,[gamman(n-1)+0.9*incr gamman(n-1)+1.1*incr]);
end
%------------------------------------------------------------

disp(toc)
disp('Matrix build up')

R0=bessely(0,gamman)-besselj(0,gamman).*bessely(1,gamman)./besselj(1,gamman);
R0riro=bessely(0,gamman*ri/ro)-besselj(0,gamman*ri/ro).*bessely(1,gamman)./besselj(1,gamman);
R2=bessely(2,gamman)-besselj(2,gamman).*bessely(1,gamman)./besselj(1,gamman);
R2riro=bessely(2,gamman*ri/ro)-besselj(2,gamman*ri/ro).*bessely(1,gamman)./besselj(1,gamman);
integral2=(R0riro-R0)./gamman;
D=1/2*(1/2*(R0-R2)).^2-1/2*(ri/ro)^2*(1/2*(R0riro-R2riro)).^2;

for i=1:N
r=rvec(i);
%r=1.3;
%for j=1:M
%z=zvec(j);
%z=0.9;
if i/5==round(i/5)
    disp(toc)
    i
end

R1r=bessely(1,gamman*r)-besselj(1,gamman*r).*bessely(1,gamman)./besselj(1,gamman);

for n=1:Nmax
for k=1:Ksum
    Enk=-4/(D(n)*(2*k-1)*pi)*(gamman(n)^2+(ro*(2*k-1)*pi/h)^2)^(-1)*integral2(n);
    MtPtemp=Enk*sin((2*k-1)*pi*zvec)*R1r(n);
    MtP(i,:)=MtP(i,:)+MtPtemp;
    Discharge=Discharge+Enk*integral2(n)*2/((2*k-1)*pi);
end %for
end %for

%end %of zvec(i)
end %of rvec(i)

%figure(1)
%plot(zvec,Mt1)
%mesh(rvec,zvec,MtP')
%axis([ri/ro 1 0 1 min(min(MtP)) max(max(MtP))])
%axis equal

%figure(2)
rdim=ro*rvec;
zdim=h*zvec;
udim=MtP*dpdtheta*ro/mu;
Discharge
Qdim=Discharge*dpdtheta*ro^2*h/mu

f2m=(1-ri/ro)*(sum(MtP)-(MtP(1,:)+MtP(N,:))/2)/(N-1);
Discharge0=((sum(f2m)-(f2m(1)+f2m(M))/2)/(M-1))
Qdim0=Discharge0*dpdtheta*ro^2*h/mu

f2m=(ro-ri)*(sum(udim)-(udim(1,:)+udim(N,:))/2)/(N-1);
Discharge2=h*((sum(f2m)-(f2m(1)+f2m(M))/2)/(M-1))

%mesh(rdim,zdim,udim')
%axis([ri ro 0 h min(min(min(udim)),0) max(max(udim))])

%figure(4)
%mesh(rdim,zdim,data)
```

```
%axis([ri ro 0 h min(min(min(data)),0) max(max(data))])

%disp('Discharge (micro-m/s):')
%disp(Qdim)

subpl=1;
if subpl==1
rdim=ro*rvec;
zdim=h*zvec;
udim=MtP*dpdtheta*ro/mu;
figure(1)
subplot(1,2,1), mesh(rvec,zvec,MtP')
axis([ri/ro 1 0 1 min(min(MtP)) max(max(MtP))])
title('Non-dimensional velocities.')
subplot(1,2,2), mesh(rdim,zdim,udim')
axis([ri ro 0 h min(min(min(udim)),0) max(max(udim))])
title('Velocities (\mu m/s)')
%subplot(2,2,3), mesh(rdim,zdim,data)
%axis([ri ro 0 h min(min(min(data)),0) max(max(data))])
%title('Coventor')
%subplot(2,2,4), mesh(rdim,zdim,(udim'-data))
%axis([ri ro 0 h min(min(min((udim'-data))),0) max(max((udim'-data)))])
%title('Error')
end

converge=0;
if converge==1
figure(3)
subplot(2,3,1), plot(Bn)
axis([1 length(C0nr) min(C0nr)-1e-4 max(C0nr)+1e-4])
title('Bn')
subplot(2,3,2), plot(Gnz)
axis([1 length(C0nr) min(C0nr)-1e-4 max(C0nr)+1e-4])
title('Gnz')
subplot(2,3,3), plot(C0nr)
axis([1 length(C0nr) min(C0nr)-1e-4 max(C0nr)+1e-4])
title('C0nr')
subplot(2,3,4), plot(D)
axis([1 length(D) min(D)-1e-4 max(D)+1e-4])
title('D')
subplot(2,3,5), plot(Mt1)
axis([1 length(Mt1) min(Mt1)-1e-4 max(Mt1)+1e-4])
title('Mt1')
subplot(2,3,6), plot(Mtemp1)
axis([1 length(Mtemp1) min(Mtemp1)-1e-4 max(Mtemp1)+1e-4])
title('Mtemp1')
Mt1(length(Mt1))
end

%subplot(2,2,1), plot(Ckr)
%axis([1 length(Ckr) min(Ckr) max(Ckr)])
%title('Ckr')
%subplot(2,2,2), plot(Ckro)
%axis([1 length(Ckro) min(Ckro) max(Ckro)])
%title('Ckro')
%subplot(2,2,3), plot(Mt)
%axis([1 length(Mt) min(Mt) max(Mt)])
%title('Mt')
%subplot(2,2,4), plot(Mtemp)
%axis([1 length(Mtemp) min(Mtemp) max(Mtemp)])
%title('Mtemp')
```